THE FUNCTIONAL ROLE OF MIR-210 IN HYPOXIA-INDUCED ANGIOGENESIS

A DISSERTATION

SUBMITTED TO THE FACULTY OF

THE UNIVERSITY OF MINNESOTA

BY

ERICA K. SCHNETTLER

IN PARTIAL FULFILLMENT OF THE REQUIREMENTS FOR THE

DEGREE OF DOCTOR OF PHILOSOPHY

ADVISOR: SUNDARAM RAMAKRISHNAN

FEBRUARY 2017

Acknowledgements

Foremost, I would like to express my sincere gratitude to my advisor, Dr. Sundaram Ramakrishnan, for his thoughtfulness and support over the last four and a half years. He is truly an inspiring teacher, academic, and research scientist. I am fortunate to have been trained under his guidance and care. I could always count on Ramki to be there when I ran into problems and he always pushed me to always question and explore further. He has absolutely transformed the way I think as a scientist. I will miss his friendly smile and constant optimism!

I am also very grateful to the many members of our lab that have come and gone over the years. I especially thank Dr. Colleen Rivard and Dr. MiHae Song for teaching me the medical side of gynecologic oncology and for connecting me to the importance of patient driven research. I also thank Dr. Manju Saluja, Dr. Devika Kir, and Annaporna Venkatachalam for their helpful advice, constructive criticism, openness, and companionship during my years in the Ramki lab. I additionally thank our many interns and summer students for helping me to discover my love for teaching.

For their significant contributions to my thesis work, I thank Dr. Goutam Ghosh – FGFRL1-Luc constructs, Dr. Yan Zeng – miR-210 knock-out mice, and Dr. Alexey Benumov – zebrafish work. I would also like to thank my committee members: Dr. Timothy Walseth, Dr. Jill Siegfried, Dr. Cheuk Leung, Dr. Kaylee Schwertfeger, and Dr. Subree Subramanian, for their suggestions and thoughtful advice during my graduate career. Finally, I am very glad to have been supported by the PharmacoNeuroImmunology (PNI) training grant, and thank Dr. Sabita Roy, Dr. Thomas Molitor, and Yorie Smart for their funding and guidance.

I dedicate this work to my parents.

Abstract

MicroRNAs (miRNA) are involved in fine-tuning cellular responses to hypoxia. miR-210, a hypoxia-induced miRNA, has been shown to play an important role in angiogenesis. miR-210 is known to target key players in mitochondrial metabolism, DNA repair, cell cycle regulation, and cell survival. Such targets may broadly affect endothelial cell homeostasis and angiogenesis. One of the highly ranked targets of miR-210 is fibroblast growth factor receptor-like protein 1 (FGFRL1). We confirmed this by luciferase reporter assays that demonstrated FGFRL1 is a direct target of miR-210. Although FGFRL1 binds Fibroblast Growth Factor (FGF) ligands, it is not a typical FGF receptor because it lacks an intracellular receptor tyrosine kinase domain. In the present study, we investigated the role of FGFRL1, on regulating bFGF signaling in endothelial cells. Our studies suggest that during hypoxia miR-210 inhibits FGFLR1, a dominant negative or “decoy” receptor, leading to increased FGF signaling in endothelial cells. We show that transfection with either miR-210 duplex or FGFRL1 siRNA can sensitize human umbilical vein endothelial cells (HUVECs) to bFGF induced proliferation. Cells treated with miR-210 or siFGFRL1 also show increased fibroblast growth factor receptor-1 (FGFR-1), Protein Kinase B (AKT) and Mitogen-activated protein kinase (MAPK) phosphorylation after treatment with bFGF.

To corroborate our *in vitro* finding in endothelial cells, we next investigated the role of miR-210 and FGFRL1 on angiogenesis using *in vivo* models. In a transgenic zebra fish model, we found that injection of miR-210 caused a 30% increase in angiogenesis at the caudal vein plexus after 36-hours. Injection of FGFRL1 siRNA showed similar results and increased angiogenesis compared to control. miR-210 knock-

out (KO) mice were subsequently generated to further understand the role of miR-210 on angiogenesis. Interestingly, miR-210 KO mice showed increased the levels of FGFRL1 in mouse endothelial cells and other tissues, further demonstrating that miR-210 can regulate FGFRL1 levels *in vivo*. In the matrigel plug assays, miR-210 KO mice showed decreased angiogenesis in the presence of bFGF compared to wild-type (WT) mice. In the aortic ring assays, miR-210 KO aortas showed decreased vessel sprouting in the presence of FGF and hypoxia compared to WT. In a subcutaneous tumor model, miR-210 KO mouse also showed decreased vascular recruitment to the tumor compared to WT mice. Overall, our *in vivo* experiments show that miR-210 plays a critical role regulating in pathological angiogenesis. Together these findings provide insight that miR-210 sensitizes endothelial cells to bFGF signaling by targeting the dominant-negative receptor, FGFRL1, during hypoxia. Furthermore, modulation of miR-210 or FGFRL1 expression or activity is a viable strategy to regulate angiogenesis, either positively during ischemia or negatively during cancer progression and metastasis.

Table of Contents

List of Figures

List of Tables

Abbreviations

α-SMA: alpha-smooth muscle actin

aa: amino acid

AKT: protein kinase B

ANG1: angiopoietin-1

ANGPTL4: angiopoietin-related protein 4

AV: arteriovenous

BSA: bovine serum albumin

bFGF: basic-fibroblast growth factor

Ca: calcium

CBP: CREB-binding protein

CD31: cluster of differentiation 31

cPHD: collagen prolyl hydroxylase

CMV Pro: cytomegalovirus promoter

CTGF: connective tissue growth factor

CUL-2: cullin-2

CVP: caudal vein plexus

DAPI: Hoescht-33342, 4', 6-diamidino-2-phenylindole

DMEM: dulbecco's modified eagle's medium

DNA: deoxyribonucleic acid

EBM-2: Endothelial Growth Basal Medium

EC: endothelial cell

ECM: extracellular matrix

EMT: epithelial-mesenchymal transition

EFNA3: ephrin-A3

EGF: epidermal growth factor

EPO: erythropoietin

Erb-2: receptor tyrosine-protein kinase erbB-2

ERK: extracellular-signal-regulated kinase

FACS: fluorescence-activated cell sorting

FBS: fetal bovine serum

FF luc: firefly luciferase

FGF: fibroblast growth factor

FGFR: fibroblast growth factor receptor

FGFRL1: fibroblast growth factor receptor-like 1

GI: gastrointestinal

GLUT: glucose transporter type

GFP: green fluorescent protein

HBSS: hank's buffered saline solution

HEK: human embryonic kidney cells

Hg: mercury

HGF: hepatocyte growth factor

HIF: hypoxia inducible factor

Hpf: hours post fertilization

HRE: hypoxia response element

HUVEC: human umbilical vein endothelial cells

Ig: immunoglobulin

IGF2: insulin-like growth factor 2

IgG: immunoglobulin G

IL: interleukin

IP: intraperitoneal

ISCU1/2: iron-sulfur (Fe-S) cluster scaffold proteins

IV: intravenous

KD: knockdown

KO: knockout

LLC: lewis lung cell carcinoma

MAPK: mitogen activated protein kinase

miRNA: microRNA

MMP: matrix metalloproteinases

MO: morpholino

mRNA: messenger RNA

mTOR: mammalian target of rapamycin

Neo: neomycin

NLS: nuclear localization signal

NOS: nitric oxide synthase

O/N: over-night

ODDD: oxygen-dependent degradation domain

ORF: open reading frame

P53: tumor protein p53

PBS: phosphate buffered saline

PCR: polymerase chain reaction

PHD: prolyl hydroxylase

PTP1B: phospho-tyrosine phosphatase-1B

PDGF: platelet-derived growth factor

PML NB: promyelocytic leukemia nuclear bodies

pO_2: partial pressure of oxygen

qPCR: quantitative polymerase chain reaction

RISC: RNA-induced silencing complex

RNA: ribonucleic acid

ROS: reactive oxygen species

SD: standard deviation

SDS-PAGE: sodium dodecyl sulfate polyacrylamide gel electrophoresis

SE: standard error

shRNA: short hairpin RNA

siRNA: short interfering RNA

SUMO: sumoylation

TKI: tyrosine kinase inhibitor

TPEN: N,N,N′,N′-Tetrakis(2-pyridylmethyl)ethylenediamine

Ub: ubiquitin

UTR: untranslated region

VEGF: vascular endothelial growth factor

VEGFR: vascular endothelial growth factor receptor

VHL: von-hippel lindau protein

WNT: wingless-type MMTV integration site family

WT: wild type

CHAPTER I:

Background

The Tumor Microenvironment

What is the tumor microenvironment?

The tumor microenvironment is the cellular and structural environment in which the tumor exists. It plays an important role in tumor physiology, structure and function (1, 2). The tumor microenvironment involves a fundamental relationship between the tumor and surrounding cells that is essential for tumor cell growth, progression, and development of metastasis. Immune cells, stromal cells, and extracellular matrix (ECM) molecules are some of the key neighbors that help to interact and support the growing malignant cells (Fig. 1) (3). Tumors can in turn influence the surrounding microenvironment by releasing extracellular signals promoting blood vessel growth and peripheral immune tolerance. Over the last few decades research interest involving the tumor microenvironment has dramatically increased. Scientists now hope to develop diverse therapies that not only target the tumor cells, but also target key components of the microenvironment in order to better treat cancer patients (4).

A great pioneer in understanding the role of the tumor microenvironment was Dr. Judah Folkman who introduced the idea that solid tumors could secrete stimulatory factors that would attract local blood vessels (angiogenesis) for nourishment and growth (5). He first proposed this idea in 1971 and would describe tumors as “hot and bloody.” The discovery of these stimulatory factors, one of which is known as vascular endothelial growth factor (VEGF), would not be discovered until over a decade later (6). Due to his ground breaking research, Dr. Folkman is credited with founding the field of angiogenesis research, which has led to the discovery of a number of therapies based on inhibiting local vascular supply near the tumor site (7-9). In addition to Dr. Folkman’s

research, many other leaders have made ground-breaking discoveries in understanding the components of the tumor microenvironment (10).

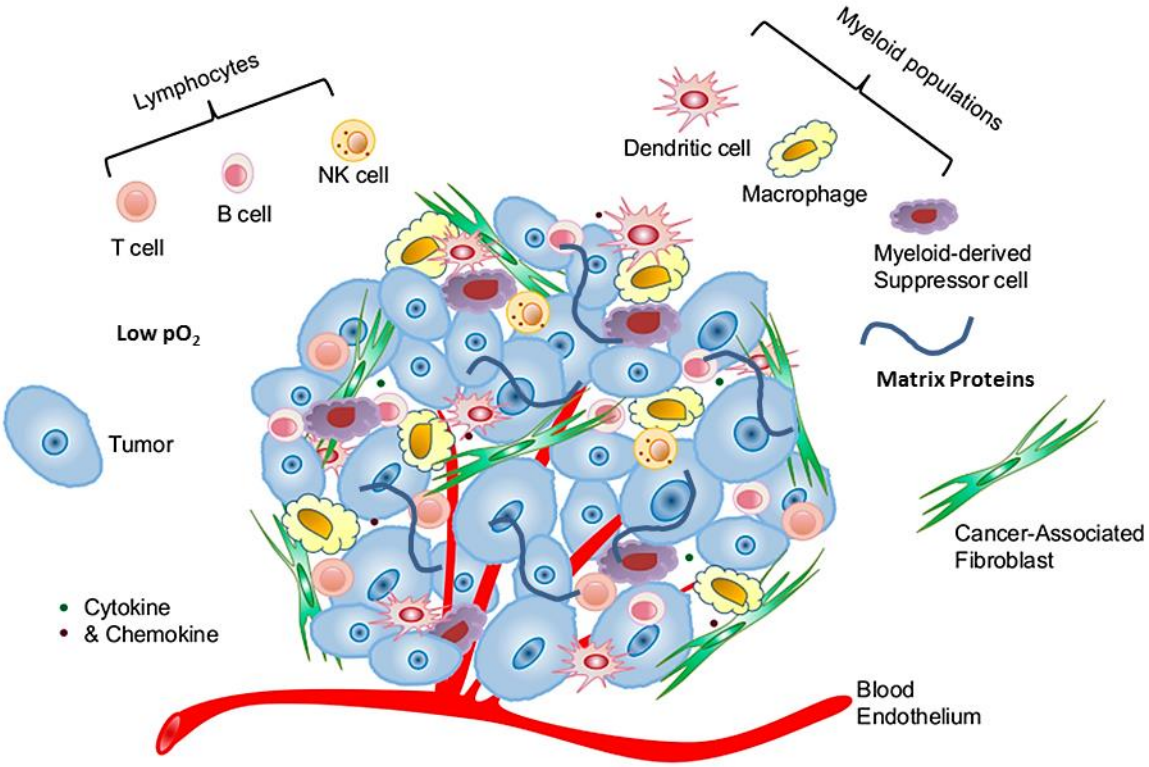

Figure 1 – The tumor microenvironment. The tumor microenvironment consists of a variety of cellular and molecular components that help to shape the tumor landscape and promote growth and metastasis. The cellular constituents consist of immune cells, stromal cells, normal and transformed cells. The molecular components consist of matrix proteins, growth factors, matrix remodeling enzymes, and cytokines. The chemical status of the tumor microenvironment can also include low oxygen tension and low pH. These cellular and molecular components compromise the proper balance of host immunity by promoting chronic inflammation and tumor progression. [Image modified from (11). No permission required for educational use (CC BY-NC-SA 4.0)]

Key cellular components

The tumor microenvironment is a highly complex and heterogeneous environment that is comprised of both cellular and chemical components that can promote a cancerous phenotype (1, 2). The most well characterized cellular components

of the tumor microenvironment include fibroblasts, endothelial cells (ECs), pericytes, lymphatic ECs, immune cells, bone marrow-derived stromal stem and progenitor cells,

Cellular Components	Role in the Tumor Microenvironment
Adipocytes	• Actively recruit cancer cells by secreting adipokines • Promote cancer cell growth by providing fatty acids as fuel
B Lymphocytes	• B cell infiltration is associated with good prognosis • IL-10 producing B cells, such as B_{reg}, may be tumor promoting
Endothelial Cells	• Growth factors released by the tumor stimulate EC sprouting • Blood vessels supply O_2 and nutrients for tumor growth
Fibroblasts	• Produce GFs, cytokines, ECM proteins and remodeling enzymes • Contribute to an immunosuppressive environment
Lymphatic Endothelial Cells	• Tumors can stimulate lymph vessel sprouting by releasing GFs • Lymph vessels provide an exit from the primary tumor site
Macrophages	• Tumor associated Macrophages can be tumor promoting • Immunosuppressive, release GFs and IL-10
NK & NKT Cells	• Usually found outside the tumor • For some cancers they can predict good prognosis
Pericytes	• Provide structure for tumor vasculature • Low pericyte coverage correlates to poor prognosis
Stem Cells	• Tumor stem cells provide a source of relapse after chemotherapy • Mesenchymal stem cells recruited from the bone marrow
T Lymphocytes	• Can be either pro- or anti- tumor. • T_{regs}, TH17, CD4+ Th2 helper T cells associated w/ poor prognosis
Molecular Components	**Role in the Tumor Microenvironment**
Fibrous Proteins	• Collagens, Fibronectin, Elastin, Laminin • ECM stiffening, reduced elasticity
Proteoglycans	• HA, Heparin Sulfate • Increased stromal cell production, release of growth factors
Growth Factors	• VEGF, FGF, PDGF, EGF • Promote vessel growth and inflammation
Enzymes	• MMP, Collagen Crosslinking Enzymes • Break down and build up ECM
Chemical Components	**Role in the Tumor Microenvironment**
Hypoxia	• Promotes angiogenesis, ECM degradation, glycolysis, tumor cell proliferation and migration • Treatment resistance
Low pH	• Stimulates metastatic potential, alters drug efficacy • Treatment resistance

Table 1 – Components of the tumor microenvironment and their function (3, 12).

and the surrounding extracellular matrix (ECM) that is produced by these cells (13). Table 1 summarizes a list of key cells and molecules and a partial list of their functions within the tumor microenvironment (3). Many of these cells reside in the stroma of the carcinoma, which is the connective tissue below the basal lamina (14). The stroma surrounding a tumor often reacts to intrusion via inflammation, similar to how it might respond to a wound. Inflammation around the tumor cite can encourage angiogenesis, increase cancer cell growth, and prevent cell death (15). Studies have shown that tumor microenvironment associated cells, such as fibroblasts, can also contribute to tissue remodeling that allows the tumor to expand and metastasize by secreting matrix remodeling enzymes (16). The tumor microenvironment may also promote or initiate epithelial-mesenchymal transition (EMT), a process required for cancer cell invasion and metastasis (17).

Some of the unique molecular and chemical properties that make up the tumor microenvironment include growth factors, fibrous proteins, proteoglycans, matrix remodeling enzymes, small molecules (e.g. NO), metabolites (e.g. glucose), acidic pH level, and oxygen level ($P0_2$) (12). These molecular properties of the tumor microenvironment and their pro-tumor functions are highlighted in table 1. Of these properties, research has found that low oxygen tension, or hypoxia, is a hallmark of the neoplastic microenvironment (18). Hypoxia within the microenvironment results as tumors grow at a faster rate that the existing blood supply can support. Hypoxia has been identified in many cancer types to contribute to tumor development and progression (19, 20). Hypoxia drives cells of the tumor microenvironment into a survival state that promotes recruitment of local vasculature, ECM remodeling, genetic instability, and metabolic transition towards glycolysis. Hypoxia orchestrates these survival tactics

under low oxygen by increasing protein levels of a transcription factor, Hypoxia-inducible factor 1 alpha (HIF1-α), which will be discussed in the next section (21).

Role in drug resistance

While we often think resistance to chemotherapy is caused by genetic alterations within the tumor cells that confer survival and drug resistance, studies have shown that the tumor microenvironment plays an additional role in chemotherapy response (22). The tumor microenvironment can lead to anticancer drug resistance by limiting the ability of drugs to penetrate tumor tissue and to reach all of the tumor cells at a lethal concentration. To reach all viable cells in the tumor, anticancer drugs must be delivered efficiently through the tumor vasculature, cross the vessel wall, and traverse the tumor tissue (23). As we will discuss in the angiogenesis section, tumor blood vessels are often abnormal and greatly contribute to problems with drug delivery. Additionally, heterogeneity within the tumor microenvironment can lead to marked gradients in the rate of cell proliferation and to regions of hypoxia and acidity, which all can influence the sensitivity of the tumor cells to drug treatment (24). pH can also play a major role in the ionization state, efficacy, and chemical properties of certain chemotherapies (25). Absent or dysfunctional lymphatics may cause an increase in interstitial fluid pressure which can additionally inhibit drug delivery (26).

Therapeutics targeting the tumor microenvironment

Although traditional anti-cancer therapies have been focused on specifically targeting the cancer cell, there has been a flood of new research and drug design based on understanding and targeting the unique components of the tumor microenvironment

(27). Other research has looked closely at how to solve issues involving tumor microenvironment impedance on drug delivery (28). Summarized in table 2, is a list of tumor microenvironment cellular targets, a targeting strategy for anti-tumor response, and drug example (29).

Microenvironment Target	Strategy	Drug Example
Immune Cells	Promote T cell activation and enhance immune response	Ipilimumab, Sipuleucel-T
Tumor – Associated Macrophages	Inhibit recruitment to the tumor and metastatic sites	Inhibitors of chemokines such as CCL2, CSF-1R
Endothelial Cells	Inhibit blood vessel growth into the tumor	Bevacizumab, Aflibercept (VEGF inhibitors)
Tumor Hypoxia	Increase tissue O_2 levels, decrease HIF1-α	HIF1-α inhibitors
Cancer Associate Fibroblasts	Regulate production of growth factors and ECM proteins	FGF and PDGF pathway inhibitors
Extracellular Matrix (ECM)	Inhibit ECM degradation	MMP inhibitors
Signaling Molecules	Inhibit receptor kinase activity	Tyrosine kinase inhibitors: Gefitinib, Sunitinib,

Table 2– Drug targets in the tumor microenvironment.

Monoclonal antibodies have been a recent success in targeting various components of the tumor microenvironment (30). Shown in the table above, Ipilimumab is a monoclonal antibody that binds cytotoxic T lymphocyte-associated antigen 4 (CTLA-4), a receptor of T lymphocytes that dampens their cytotoxic activity (31). By administering an antibody to CTLA-4, this immune dampening effect can be blocked and T lymphocytes may become cytotoxic and destroy the cancer cells. Another class of drugs that have been extensively studied and developed to inhibit the pro-tumor effects of the tumor microenvironment includes small molecule kinase receptors that

preferentially block the receptors that bind growth factors such as VEGF, PDGF, or EGF (32). Kinase inhibitors such as Sunitinib, work to make the cancer cells “deaf” to much of the paracrine signaling produced by tumor associated fibroblasts and macrophages. Another recent therapy that has shown some efficacy against tumor resistance is the development of liposome formulations that encapsulate anti-cancer drugs for selective uptake to tumors via the enhanced permeability and retention (EPR) effect (33). Examples include, Doxil and Myocet which are liposome preparations that encapsulate Doxorubicin aimed at better penetrate the tumor tissue (34).

While there is still much to be elucidated about the complex interactions between the tumor cell and its microenvironment, continued research on this dependent relationship will surely lead to more successful evidence based therapies to better treat patients with cancer. Certainly, the most effective approaches will combine therapies to not only kill the cancer cell, but also block the supportive nature of the tumor microenvironment. The main goal of this work is to better understand the molecular mechanisms of this symbiotic relationship, so that we may inhibit them and prevent cancer from progressing.

Hypoxia

What is hypoxia?

Hypoxia is a transient situation in which a given mass of tissue cells does not receive enough oxygen from the blood vessels (35). In other terms, hypoxia can be described as a low or suboptimal level of oxygen compared to what is normal for a given tissue. Hypoxia can result from a failure at any stage in the delivery of oxygen to cells. This can include decreased partial pressures (pO_2) of oxygen, problems with diffusion of

oxygen in the lungs, insufficient available hemoglobin, problems with blood flow to the end tissue, and problems with breathing rhythm (35). Hypoxia and “normoxia” (normal or physiologic tissue oxygen level) are relative terms. For example, while pO_2 of skeletal muscle is 20-30 mm Hg, brain tissue pO_2 level is much higher at 45-65 mm Hg (36, 37).

Although the terms are similar, hypoxia should not be confused as ischemia. Ischemia is defined as insufficient blood flow to a tissue, which can result in hypoxia (38). This is often called 'ischemic hypoxia,’ which can include an embolic event, a heart attack that decreases overall blood flow, or trauma to a tissue that results in damage. While physiological hypoxia is an important factor in processes such as development and embryogenesis, this section will focus primarily on pathological hypoxia. More specifically for the scope of this work, we will describe tumor hypoxia and its role in driving tumor progression.

The role of hypoxia inducible factor 1

In order to survive a low oxygen environment, mammalian cells rely on a transcription factor known as hypoxia inducible factor 1 (HIF1) to upregulate hypoxic adaptation genes (39). HIF1 has been described as the master regulator of the cellular hypoxic response and is important for normal physiology as well as pathophysiology and ischemic disease. HIF1 is a heterodimer composed of two subunits known as HIF1-α and HIF1-β. These HIF1 subunits are both constitutively translated primarily through the PI3/AKT/mTOR and MAPK/ERK pathways (40). However regulation at the protein level is quite different between the two subunits. Unlike HIF1-β, HIF1-α’s stability is drastically dependent on the level of oxygen available within the cell (41).

In Figure 2, we summarize the canonical pathway of HIF1-α degradation in normoxia and activation in hypoxia (42). To briefly review, in the presence of

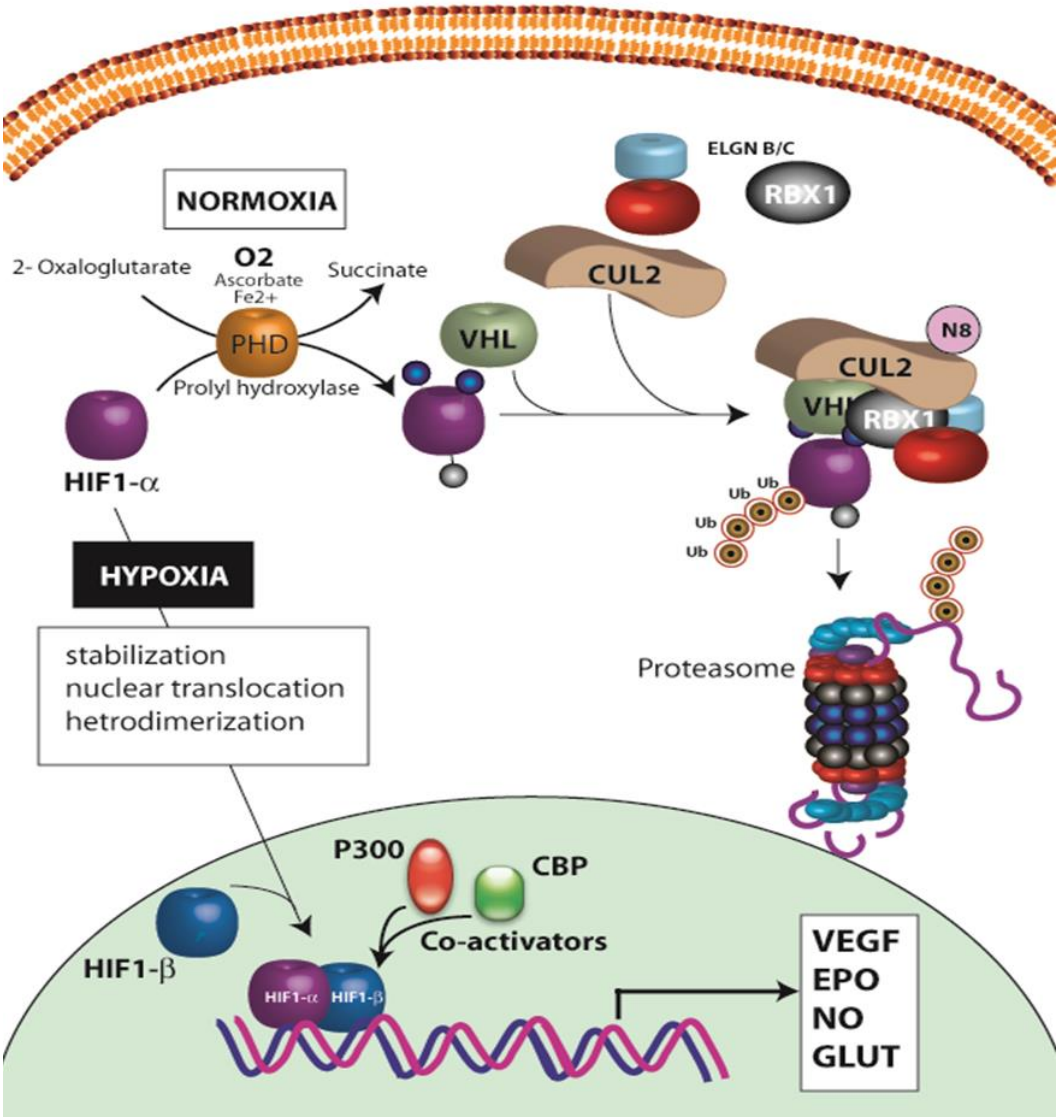

Figure 2 – Regulation of HIF1-α. Under normal oxygen conditions HIF1a is degraded. Oxygen sensing enzyme, prolyl hydroxylase (PHD) begins the process of degradation by hydroxylating HIF1-α at proline residues 402 and 565. Hydroxylated HIF1-α is recognized by Von Hippel–Lindau (VHL) protein and incorporated into the VCB-CUL2-E3 ligase complex. HIF1-α is then polyubiquitinated, leading to degredation by the 28S proteasome. Under hypoxic conditions PHD enzyme activity is inhibited, allowing HIF1-α to accumulate and stabilize in the cytoplasm. HIF1-α will then translocate into the nucleus and bind to HIF1-β to form HIF1. Through interaction with CBP/p300, HIF1 transactivates a multitude of genes necessary for cellular hypoxic adaptation. [Image modified from (43). Courtesy of S. Ramakrishnan]

normal oxygen levels, HIF1-α is degraded. However in hypoxia the protein becomes stabilized and translocates to the nucleus where it heterodimerizes to HIF1-β (44). At this point, HIF1 can combine with other transcription-related proteins to bind hypoxia response elements (HRE) within the DNA and upregulate genes appropriate for cell survival during hypoxia (45). A partial list of the genes upregulated by HIF1 is described in table 3. Overall, HIF1 is responsible for a large shift in several molecular pathways that will allow cells to adapt under low oxygen conditions (46).

Hypoxic Adaptation: Genes Upregulated By HIF1	
Function	**Genes**
Glucose Metabolism	• Aldolase-A,C (ALDA,C) • Adenylate Kinase-3 • Carbonic anhydrase-9 • Enolase- (ENO-1) • Glucose Transporter-1,3 (GLU1,3) • Glyceraldehyde Phosphate Dehydrogenase (GAPDH) • Hexokinase 1, 2 (HK1,2) • Lactate Dehydrogenase-A (LDHA) • Pyruvate Kinase M (PKM) • Phosphofructokinase L (PFKL) • Phosphoglycerate Kinase 1 (PGK1)
Proliferation/Survival	• Cyclin G2 • Insulin-Like Growth Factor-Binding Protein 1, 2, 3 • Transforming Growth Factor Receptor a (TGF-a) • Insulin-Like Growth Factor 2
Iron/Erythropoiesis	• Erythropoietin (EPO) • Transferrin (Tf) • Transferrin Receptor (Tfr) • Ceruloplasmin
Angiogenesis	• Vascular Endothelial Growth Factor (VEGF) • VEGF Receptor • Endocrine-Gland-Derived VEGF • Leptin (Lep) • Transforming Growth Factor Receptor B3 (TGF-B3)

Vascular Tone	• Nitric Oxide Synthase (NOS2) • Heme Oxygenase-1 • Endothelin 1 (ET1) • Adrenomedulin (ADM)
Matrix Remodeling	• Matrix Metalloproteinases (MMPs) • Plasminogen Activator Receptors and Inhibitors (PAIs) • Collagen Prolyl Hydroxylases • Collagen Type V (a1) • Fibronectin (FN1)
Apoptosis	• Bcl-2/adenovirus EIB 19kD-interacting protein 3 (BNip3) • Nip3-like Protein X (NIX)
Invasion/Metastasis	• Vimentin (VIM) • Urokinase receptor (UPAR) • Autocrine Motility Factor (AMF) • hepatocyte growth factor receptor (c-MET)

Table 3 – Partial list of genes regulated by HIF1-α (46).

Tumor hypoxia

Hypoxia is involved in many pathophysiological processes such as ischemic disease, diabetes, atherosclerosis, inflammatory disorders, and chronic obstructive pulmonary disease (47). In these particular disease states, hypoxia can often play a beneficial role. For example, hypoxia can drive the development of new vasculature to increase oxygen delivery in the myocardium of patients with coronary artery disease (48). On the other hand, hypoxia driven angiogenesis can have a deleterious effects for patients in the context of cancer (49). In addition to stimulating tumor angiogenesis, hypoxia can alter cancer cell metabolism, increase cell migratory and metastatic behavior, and promote extracellular matrix remodeling (50).

Cancer cells are often characterized by uncontrolled proliferation (2). As a result, solid tumors can form and grow at a rate that rapidly outpaces the ability of local vasculature to supply sufficient levels of oxygen (Figure 4) (51). A tumor mass that

expands to the size of $1mm^3$ must recruit local vasculature or risk starving itself as a result of chronic hypoxia. At this point, the tumor has reached a critical stage and to survive, and the cancer cells must initiate rescue mechanisms such as HIF1-α activation in order to save themselves (51).

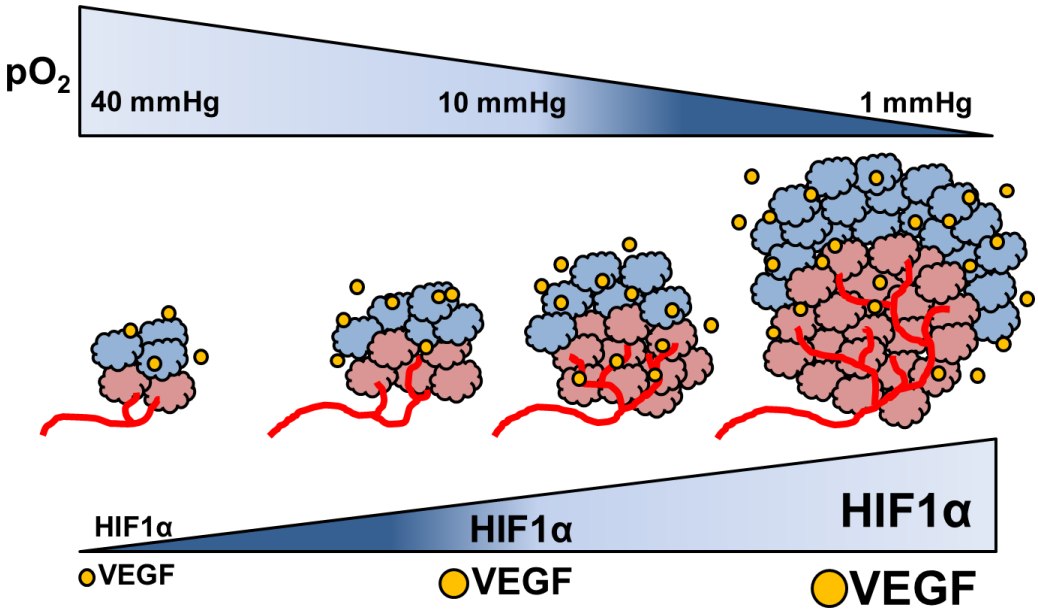

Figure 4 – Pathogenesis of tumor hypoxia. Rapidly dividing tumor cells quickly outgrow their blood vessel and oxygen supply. As growth continues the tumor microenvionment becomes hypoxic (low pO_2). Under hypoxia, transcription factor HIF1-α becomes stabilized and activated to form HIF1 which upregulates a variety of genes that will temporarily aid the cancer cells to survive with little oxygen availability. Cellular adaptations include metabolism alterations, activating angiogenesis, and remodeling the surrounding matirx. (51)

Some of the most significant cellualr alterations driven by HIF1 is the modification of cell metabolism to utilize more energy-efficient pathways and the activation of vascular endothelial growth factor (VEGF) driven angiogenesis (52). If successful in initiating these apdaptations, the tumor may have satisfied its need for oxygen in the short term. However, hypoxic states may still persist heterogeneously in various regions of the tumor microenvironment (53). This effect may also be enhanced as tumor blood

vasculature is often irregular, unevently distributed and leaky, which will be discussed more in the following section (54).

Tumor hypoxia also enhances the Warburg effect, the dependence of tumor cells on glycolytic pathways over normal oxidative mechanisms (55). Another effect of hypoxia is the acidification of tumor cells, primarily as a result of the shift from aerobic to anaerobic metabolism that results in lactic acid accumulation (56). Low pH withhin the tumor microenvironment poses a significant threat to the efficacy of certain chemotherapy drugs as described previously (57). In addition to increasing tumor cell survival, hypoxia promotes genomic instability (58). For example, inhibition of DNA repair mechanisms, increased number of point mutations, and increase in telomerase activity have all been associated with hypoxia (58, 59). HIF1 also promotes extracellular matrix remodeling by upregualting MMPs, fibronectic, and collagen prolyl hydozylase, to name a few (18). Finally, in certain cancer cell types hypoxia was found to induce dedifferentiation and development of stem-cell like features, such as EMT (60). Overall, these cellular alterations induced by hypoxia truly compound the aggressive phenotype of malignant cells and contribute to their progression. As summarized in table 5, a hypoxic tumor microenvironment also can lead to the development of chemotherapy resistance (24).

Tumor Hypoxia and Treatment Resistance to Chemotherapy	
Hypoxic Effect	**Treatment Response**
1. Decreased generation of free radicals	A. Reduced DNA damage by radiation and chemotherapy
2. Tumor hypoxia promotes abnormal, leaky vasculature with variable perfusion capacity.	B. Unpredictable intratumor pharmacokinetics. Tumor blood vessels can have impaired and uneven drug delivery.
3. Hypoxia increases glycolysis leading to the formation of extracellular acidosis.	C. Low pH can alter chemotherapy transport across cell membranes, drug

	activation and accumulation.
4. Hypoxia can slow proliferation kinetics and also elevate levels of glutathione and DNA enzymes.	D. Chemotherapies that target these mechanisms (rapidly dividing cells, DNA damage) can have reduced efficacy in hypoxic tumors.
5. Hypoxic areas in a tumor can lead to increased tumor heterogeneity .	E. Heterogeneity can lead to resistant clonal variants following chemotherapy.
6. Hypoxia can protect and maintain the properties of cancer stem cells.	F. These cancer stem cells may provide a source of recurrence after chemotherapy treatment.

Table 4 – Tumor hypoxia and acquired treatment resistance in human cancers (24)

For all its pro-tumor effects, it comes at little surprise that tumors with measured hypoxia correlate with patient morbidity and mortality (61). For example, cervical tumors with a pO_2 measured at less than 10mm Hg resulted in a significant decrease in progression-free and overall survival (62). Similar results can be seen across many types of cancer including, head and neck, breast, pancreatic, and ovarian cancer (63). Overall, these cases further highlight the need to develop targeted therapies that reduce the beneficial relationship between the tumor microenvironment and the cancer cells.

Angiogenesis

Mechanisms of angiogenesis

Endothelium is a specialized form of mesenchymal tissue that divides the circulating blood from the inner linning of the vascular system (64). It is composed endothelial cells (ECs) connected by adherent and tight junction molecules, such as VE-cadherin and Occludin. Surrounding the ECs is the basement membrane and pericytes (65). Pericytes are contractile cells that wrap around endothelial cells. They regulate capillary blood flow, the clearance and phagocytosis of cellular debris, and the permeability of the blood–brain barrier. Pericytes also stabilize and monitor the maturation of endothelial cells by means of direct communication between the cell membrane as well as through paracrine signaling (65).

Angiogenesis is formation of new blood vessels from existing vasculature (66). It can also be referred to as sprouting angiogenesis which is characterized by the extension and branching of endothelial cells to form blood vessels (Fig. 4) (67). There are several other mechanisms of new vessel formation that are distinct from sprouting angiogenesis. These include vasculogenesis, intussusception, vessel co-option, vascular mimicry, and tumor to endothelial cell differentiation (67). These mechanisms are all highlighted and described in Figure 4. Unless induced by the appropriate stimuli from the local environment, endothelial cells remain largely quiescent during their life span (68).

When receptors in a quiescent vessel bind secreted growth factors, pericytes and ECs become activated and loosen cell junctions and detached from the basement membrane via matrix remodeling (69). This initial process results in vasodilation and increased vessel permeability, which allows plasma proteins such as fibronectin and

fibrinogen to extravasate and form ECM. This matrix provides a new source of growth factors, such as VEGF and FGF, and also provides scaffolding for ECs to migrate. Next

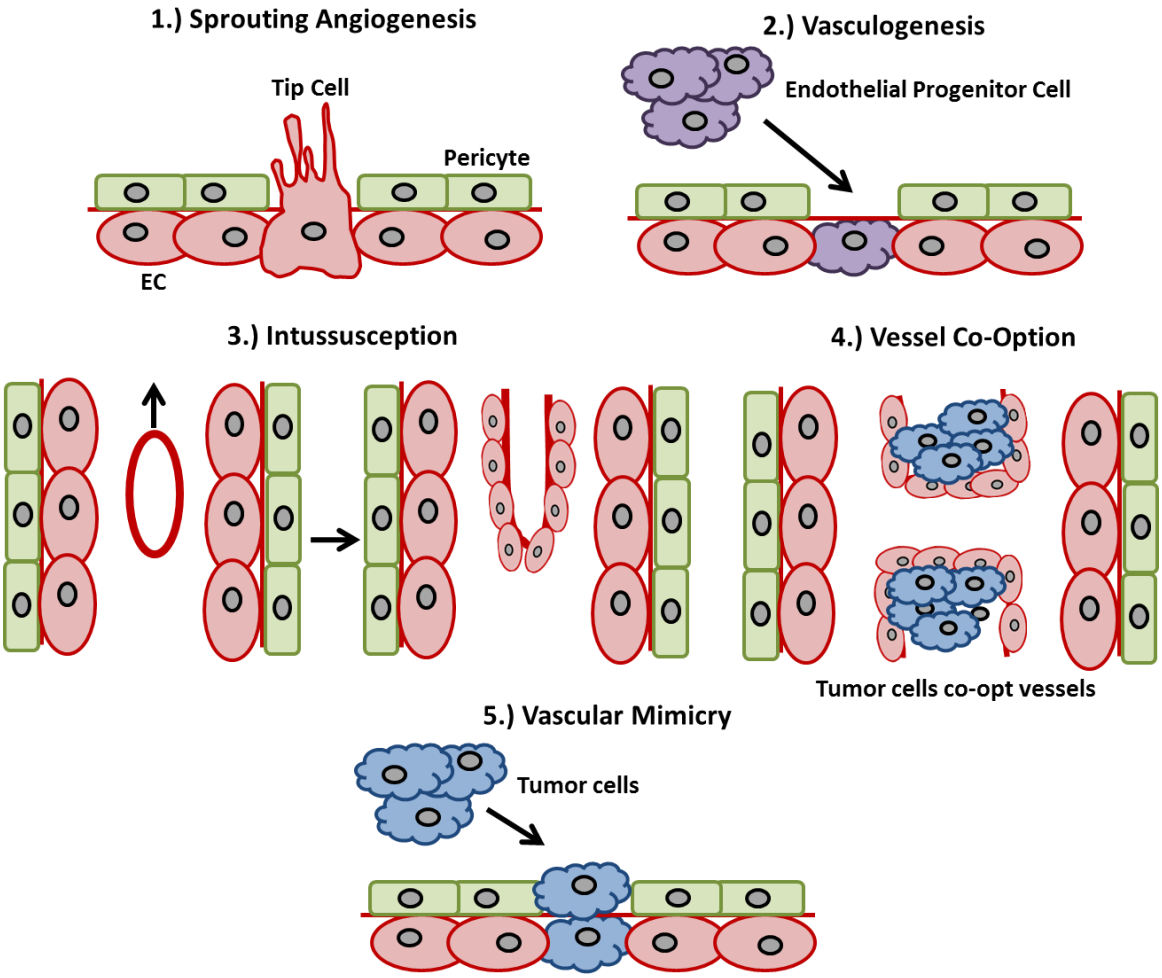

Figure 4 – Mechanisms of new blood vessel formation. (1) Sprouting angiogenesis occurs when endothelial cells from existing vasculature push through the basement membrane towards a stimulus. (2) Vasculogenesis is the generation of new blood vessels from circulating endothelial progenitor cells. (3) Intussusception occurs when an existing vessel splits to form two vessels. (4) Vessel co-option occurs when tumor cells surround and utilize an existing blood vessel. (5) Tumor cells may form vascular like structures in the process of vascular mimicry. (6) Certain tumor cells with stem-like properties may dedifferentiate into endothelial like cells to form new blood vessels.

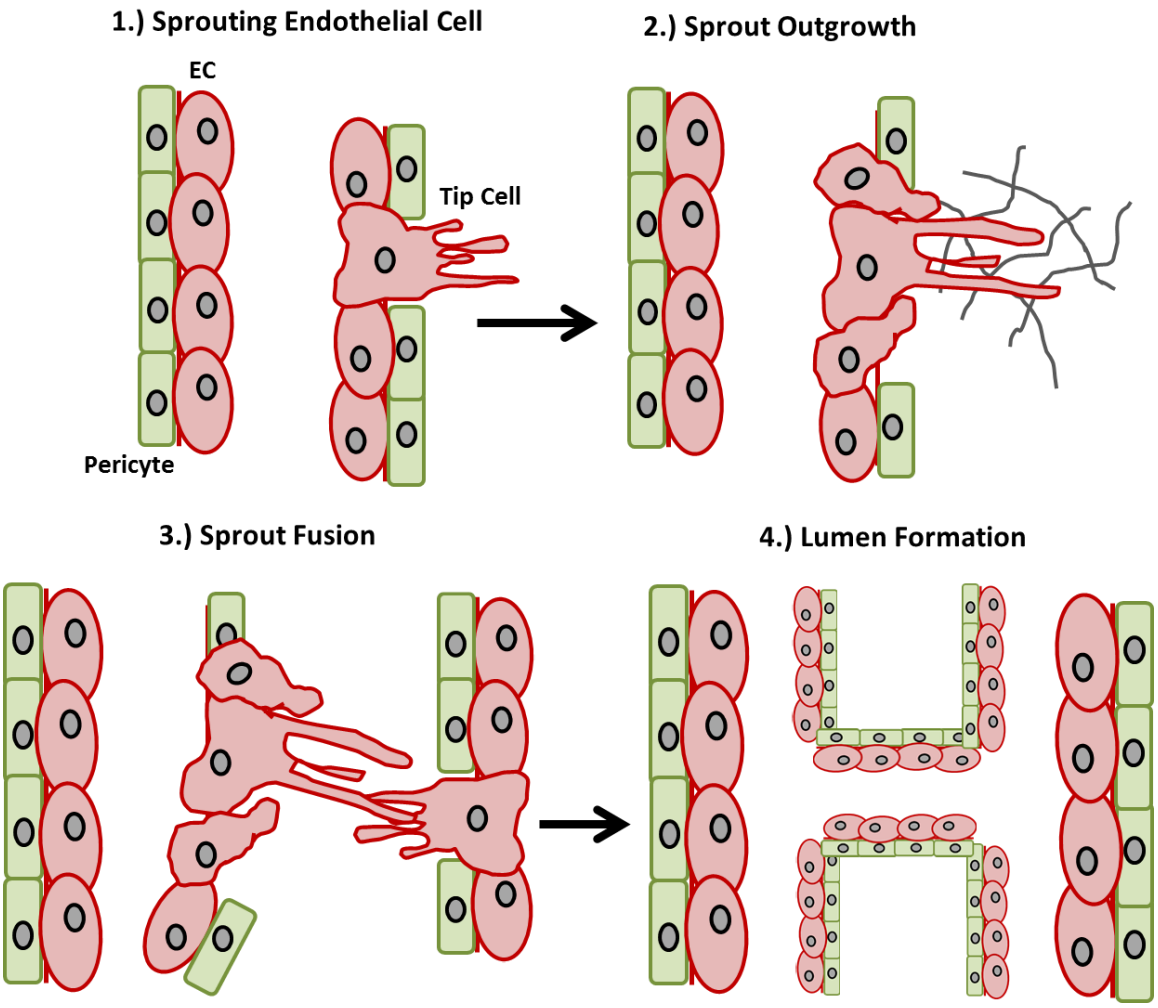

Figure 5 – Key factors and mechanisms involved in angiogenesis. Vessel sprouting is controlled by the balance between pro- and anti- Angiogenic factors. First, a growth factor stimulus must initiate the branching process. These growth or angiogenic factors cause vasodilation, degradation of the basement membrane and surrounding matrix, followed my pericyte detachment. The selected endothelial cell will begin to migrate through the degraded ECM and become the leading cell, also known as the "tip" cell. Initially, the surrounding endothelial cells will remain quiescent. As the tip cell continues its forward migration towards a guidance stimulus, the connected lagging cells will begin to proliferate. When sufficient number of cells have sprouted, tubular structure will begin to form. These sprouting vessels will begin to fuse and recruit pericytes. In the final stages a lumen will form allowing blood to flow. In the final stages tight junctions are reestablished and the vessel becomes mature and quiescent.

a single endothelial cell, or tip cell, receiving the appropriate signal will lead a path along the newly secreted ECM in the direction of the stimulus. Following behind are the stalk cells that begin to divide and elongate the nascent vessel. Next, myeloid cells aid in fusing the neovessels to initiate blood flow, which is required to prevent vessel regression. Finally to complete maturations, the vessel returns to a quiescent state. This process including some of the key stimulatory factors is summarized in Figure 5 (69).

The key growth factors and their receptors involved in regulating angiogenesis are summarized in table 5 (9).

Angiogenic Factors and Their Role in Angiogenesis	
Ligand-Receptor	**Role in EC Physiology**
VEGF-VEGFR1 **VEGF-VEGFR2**	• Induce proliferation, sprouting, and tube formation. • Increase vascular permeability and suppress apoptosis
VEGFC-VEGFR3-NRP2	• Lymphatic development
Notch Pathway	• Negative feedback for VEGF-mediated vessel sprouting. • Vessel fate determination (artery vs. vein).
bFGF-FGFR1	• Chemoattractant for ECs • Induces proliferation
Ephrin-B2-EPHB4PDGF-BB-PDGFRB	• Arterial EC determination • Guides vessel branching
PDGF-BB-PDGFRB	• Promotes migration, recruitment, and proliferation of mural cells
ANGPT1-TIE2	• Facilitates EC matrix interaction for vessel stabilization. • Suppresses EC apoptosis
ANGPT2-TIE2	• Induces apoptosis in the absence of VEGF • Involved in lymphatic patterning
TGFB1-TGFBRII	• Promotes ECM and protease production

Table 5 – Angiogenic factors and their roles in angiogenesis (9).

Angiogenesis in cancer

In non-malignant tissue, vessels are largely quiescent (68). During vessel quiescence, a balance exists between pro- (VEGF, bFGF, PDGF) and anti- (angiostatin, endostatin, thrombosopodin) angiogenic factors (Figure 7) (70). This balance is thought to maintain the equilibrium of quiescent vessels. However, if quiescent vessels are nearby a growing tumor in need of oxygen, the tumor may secrete HIF1-mediated growth factors and tip the balance toward a proangiogenic response (Figure 6) (70). In addition the hypoxic microenvironment may also promote matrix remodeling that is critical for new vasculature sprouting (71). Hypoxia and HIF1 are key contributors of triggering the "angiogenesis switch."

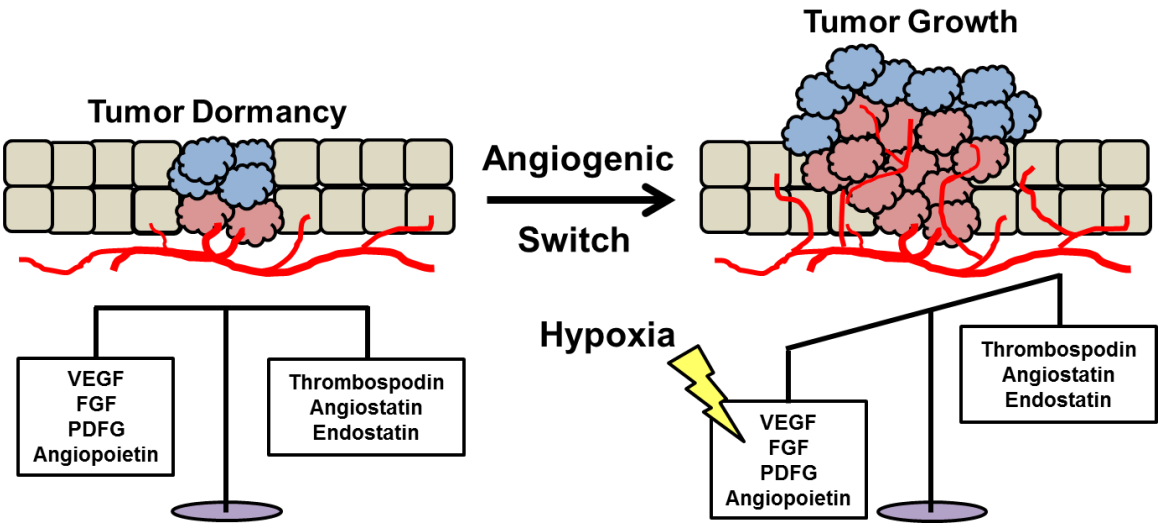

Figure 6 – Activation of the angiogenic switch. Quiescent blood vessels are able to remain in a stable equilibrium by balancing the levels between pro- and anti- angiogenic factors. If the balance is tipped towards favoring proangiogenic molecules an "angiogenic switch" will be activated leading to vessel sprouting and angiogenesis. In the tumor microenvironment, hypoxia can push the balance to favor the increase of proangiogenic factors such as VEGF. This switch can recruit local vasculature to the tumor and enhance tumor growth and survival. Due to this dysregulation and increase in growth factors, tumor vasculature is often structurally abnormal and leaky, which can promote tumor intravasation. (70)

Although angiogenesis increases in a hypoxic tumor microenvironment, the blood vasculature that supplies oxygen to the tumor is often irregular (Figure 7) (72). These vessels are recruited rapidly to the tumor site and are structurally and functionally distinct from vessels borne of physiological angiogenesis. In particular, tumor vessels tend to demonstrate increased vasodilation, permeability, and irregularities of the endothelium, basement membrane and pericyte coverage (72). Tumor vasculature is often characterized as disorganized and includes a mix of characteristics associated with capillaries, arteries, and venules (73). These irregularities are largely believed to be a result of abundant VEGF within the ECM that stimulates vessels via a paracrine fashion versus more controlled autocrine signaling. A major consequence of the deformed tumor vasculature is high interstitial pressure created by leaky vessels. This also causes a maldistribution of blood flow and resources across the tumor. Accordingly, oxygen

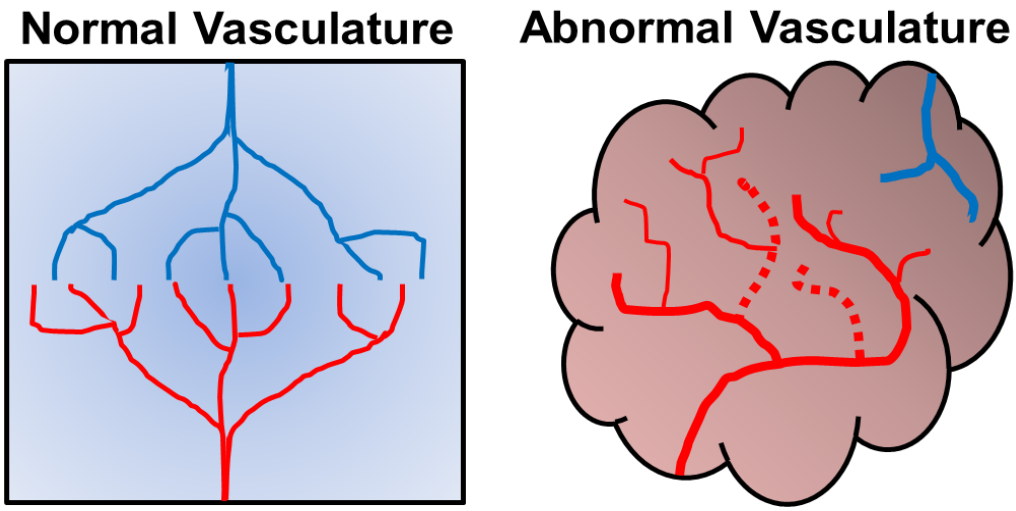

Figure 7 – Physiologic versus tumor vasculature. In normal tissue, blood vessels are well organized and arranged with clear branch points and junctions. Normal vasculature can be distinctly identified as artery, vein, or capillary. In contrast, tumor vasculature is disorganized and arbitrarily branched. Blood vessels in the tumor can be difficult to distinguish between arterial, venous and capillary features. Compared to normal vessels, tumor vasculature is irregular, dilated, and leaky. These abnormal vessels have a loosely bound basement membrane and

inconsistent pericyte coverage. For these reasons partial pressure of the tumor can vary drastically, which can in turn affect delivery of chemotherapeutic agents. Overall, these abnormal attributes contribute to the survival and metastasis of tumor cells. (72)

nutrients, and even chemotherapy will be distributed heterogeneously. Vascular fenestrations can also provide an escape route for metastatic cancer cells to distal sites. In this way tumor vasculature enables tumors to survive, proliferate, and metastasize (72).

Antiangiogenic therapies

Due to its important role in the progression of malignancy, tumor angiogenesis has been focus of several anti-cancer therapies (67). Typically these therapies are combined with traditional chemotherapies to maximize the anti-tumor effect (74). Two recently developed classes of drugs used to inhibit tumor angiogenesis include antibody-based therapies and small molecule inhibitors. VEGF and its receptor VEGFR are the two primary targets of these new types of anti-cancer therapies (75). A summary of FDA approved antiangiogenic therapies is summarized in table 6 (7). For the most part, many of these drugs may extend patient life expectancy for several months (76). However, due to the redundancy and existence of multiple angiogenic pathways, simply blocking VEGF stimulation has proven not to be as successful as hoped in terms of eradicating the cancer (76).

Drug	Target	Indication
Antibody-based therapies		
Bevacizumab (Avastin)	Anti-VEGF antibody	Glioblastoma, metastatic colorectal cancer, metastatic RCC, some non-small cell lung cancers
Aflibercept (Eylea)	VEGF-trap recombinant fusion protein of VEGF-binding domains from VEGFR	Metastatic colorectal cancer
Ramucirumab (Cyrazma)	Human monoclonal VEGFR2 antibody inhibits VEGF binding	Advanced gastric or gastro-oesophageal junction adenocarcinome
Small molecule inhibitors		
Axitinib (Inlyta)	VEGFR1-3, PDGFRB, c-KIT	Advanced RCC
Cabozantinib (Cometriq)	VEGFR1-3, MET	Metastatic medullary thyroid cancer
Everolimus (Afinitor)	mTOR	RRC, neuroendocrine tumors
Pazopanib (Votrient)	VEGFR1-3, PDGFR, c-KIT	RCC
Regorafanib (Stivarga)	VEGFR1-3, PDGFRB, TIE2	Metastatic colorectal cancer
Sorafenib (Nexavar)	VEGFR1-3, PDGFR, RAF	Hepatocellular carcinoma, RCC
Sunitinib (Sutent)	VEGFR1-3, PDGFR, c-KIT, FLT3, RET, CSF-1R	RCC, neuroendocrine tumors
Vendatanib (Caprelsa)	VEGFR1-3, EGFR, RET	Medullary thyroid cancer in patients with unresectable locally advanced or metastatic disease

Table 6 – FDA-approved antiangiogenic therapies

Recently, two strategies have emerged that aim to target tumor angiogenesis by using seemingly contradictory approaches. The first aims to starve the tumor by blocking angiogenesis, while the other looks to “normalize” the vasculature to be more like physiological blood vessels (77). The strategy behind vessel normalization is that the vessels will then distribute blood, as well as anti-cancer agents, more uniformly to all regions of the tumor tissue. This strategy seems counter intuitive, however, may be a

good way to increase chemotherapy uptake and efficacy inside the tumor. VEGF antibody, Bevacizumab has been shown to induce vessel normalization, while still retaining anti-cancer properties in certain types of tumors (78). While we have made great strides in targeting tumor angiogenesis, additional research of the molecular mechanisms between endothelial cells, cancer cell and the tumor microenvironment will help to further elucidate better strategies and therapies for targeting the tumor vasculature.

Fibroblast Growth Factor Signaling

Key cellular components

Fibroblast growth factors (FGFs) are a family of growth factors, with members involved in angiogenesis, wound healing, embryonic development and endocrine signaling pathways (79, 80). They are also key players in the processes of proliferation and differentiation in of wide variety of cells and tissues. FGF ligands are small polypeptides with a partially conserved core of 120–130 amino acids (81). In humans, 22 members of the FGF family have been identified, all of which are structurally related. FGFs are heparin-binding proteins that interact with heparin sulfate proteoglycans, shown to be essential for FGF signal transduction (82). FGF ligands have a variety of unique functions and can either activate or inhibit FGF-receptors (FGFRs) (83). Some FGF molecules are secreted while other have been show to act intracellularly (84). FGF subfamilies and their target receptors are summarized in table 7 (85).

FGFs and Target FGFRs		
FGF subfamilies	**FGF**	**FGFR**
FGF1 (secreted or intracellular)	FGF1 (aFGF) FGF2 (bFGF)	FGFR1-4, Not FGFRL1 (RL1) FGFR 1c, 3c > 2c, 1b, 4, RL1
FGF4 (secreted)	FGF4, FGF5, FGF6	FGFR 1c, 2c > 3c, 4, RL1
FGF7 (secreted)	FGF3, FGF7, FGF10, FGF22	FGFR 2b > 1b, RL1
FGF8 (secreted)	FGF8, FGF17, FGF18	FGFR 3c > 4, > 2c > 1c > 3b, RL1
FGF9 (secreted)	FGF9, FGF16, FGF20	FGFR 3c > 2c > 1c, 3b > 4, RL1 (weak)
FGF19 (secreted)	FGF19, FGF21, FGF23	FGFR 1c, 2c, 3c, 4 (weak)
FGF11 (intracellular)	FGF11, FGF12, FGF13, FGF14	Not known

Table 7 – FGF Receptors and their corresponding ligands (85).

In mammals, the FGFR family has 5 members, FGFR1, FGFR2, FGFR3, FGFR4, and FGFRL1 (or FGFR5) (80). FGFR1-4 consists of three extracellular immunoglobulin-type domains (Ig1-Ig3), a single-span trans-membrane domain and an intracellular split tyrosine kinase domain (86). FGFs interact with the Ig2 and Ig3 domains, with the Ig3 interactions primarily responsible for ligand-binding specificity. Heparan sulfate binding is mediated through the Ig3 domain. An extracellular 'acid box' motif interacts with the heparan sulfate binding site to prevent receptor activation in the absence of FGFs. When FGF binds to the extracellular domain of an FGFR, its dimerization is triggered with other adjacent FGFRs (80). Dimerization leads to a rapid activation of the protein's cytoplasmic kinase domains. The activated receptor as a result then becomes autophosphorylated on multiple specific intracellular tyrosine residues (84).

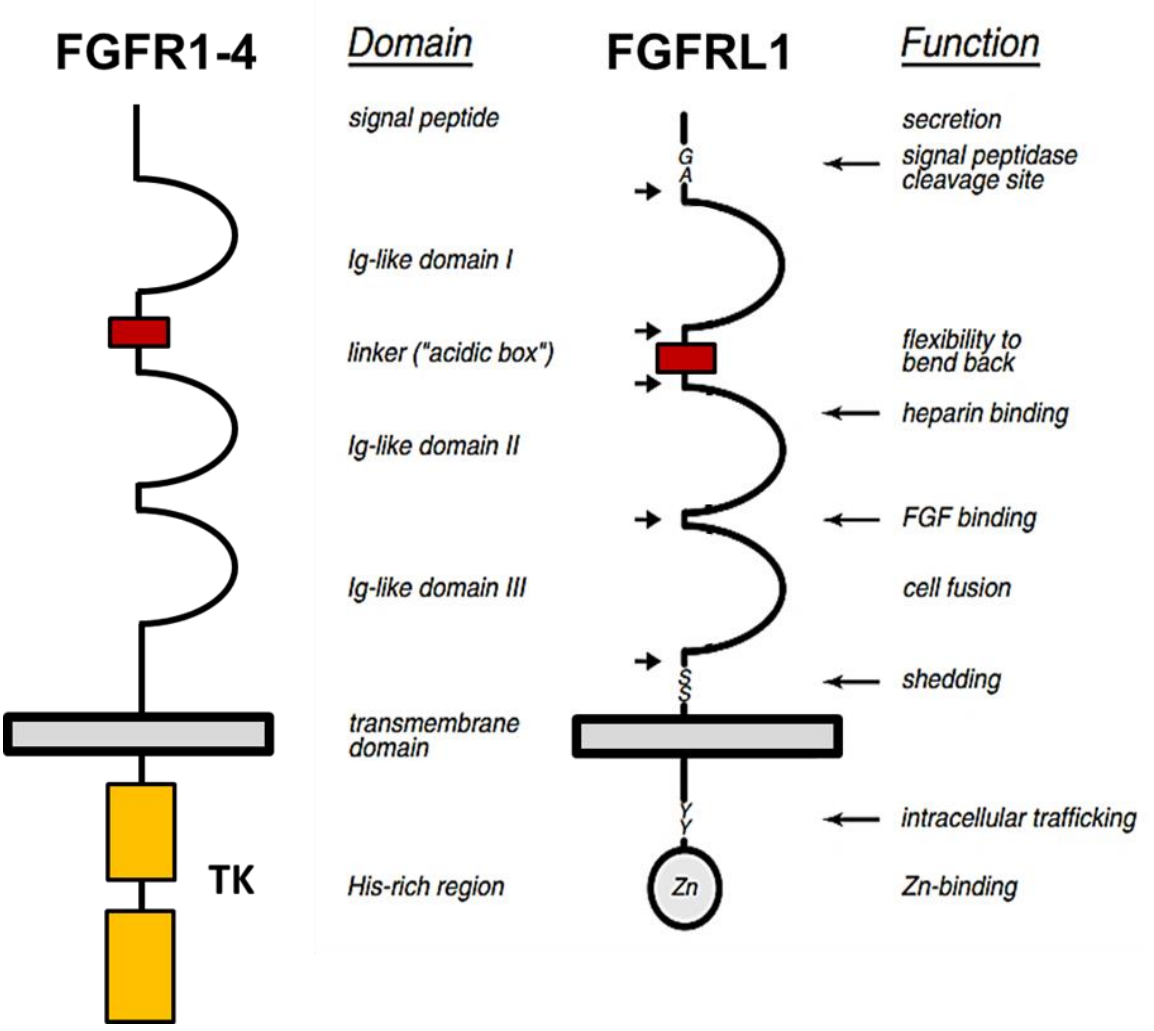

Figure 8 – FGFRL1 structure and functions. FGFRL1 is the newest member of the FGFR family. It shares significant sequence homology with FGFR1-4. However, unlike its family members, FGFRL1 does not contain a cytoplasmic tyrosine kinase domain. Instead, FGFRL1 contains a short c-terminal tail important for intracellular trafficking and zinc-binding. The FGF-receptors share a similar extracellular domain composed of three immunoglobulin-like domains and a single hydrophobic membrane-spanning segment. Additionally, FGFRL1 is able to bind a variety of FGF ligands, including bFGF. FGFRL1 is smaller in size at 504 aa and it is unknown whether or not it can dimerize with FGFR1-4. Multiple alternatively spliced transcript variants encoding the same isoform have been found for this gene. The receptor plays a role in development, differentiation, cell proliferation, and cell adhesion. (87)

FGFRL1 (FGFR5) is the newest member of the FGFR family (Figure 8) (87). FGFRL1 binds several FGF molecules (including bFGF, but not aFGF) and has a similar extracellular domain as its family members. However, its distinguishing feature is that it does not contain an intracellular tyrosine kinase domain. FGFRL1's structure is further described in Figure 8 above (87). Due to its lack of a tyrosine kinase domain, researchers have hypothesized and demonstrated experimentally that FGFRL1 may act as a dominant negative, or decoy receptor by sequestering FGF molecules (87-89). Other studies have shown that FGFRL1 participates in processes such as cell proliferation, cell adhesion, cell fusion, and is capable of some intracellular signaling activity (87, 90-97). Studies with FGFRL1 knock-out mice have demonstrated that the gene plays an important role during embryonic development (98, 99). FGFRL1 deficient mice die at birth due to a malformed diaphragm and lack metanephric kidneys. While the protein is conserved across species, the intracellular domain is barely conserved, with the exception of three motifs, namely a dileucine peptide, a tyrosine-based motif YXXΦ, and a histidine-rich sequence (100). These sequences are thought to be important for intracellular trafficking.

Molecular Pathways

Figure 9 summarizes the key signaling transduction pathways activated by FGF-FGFR (101).

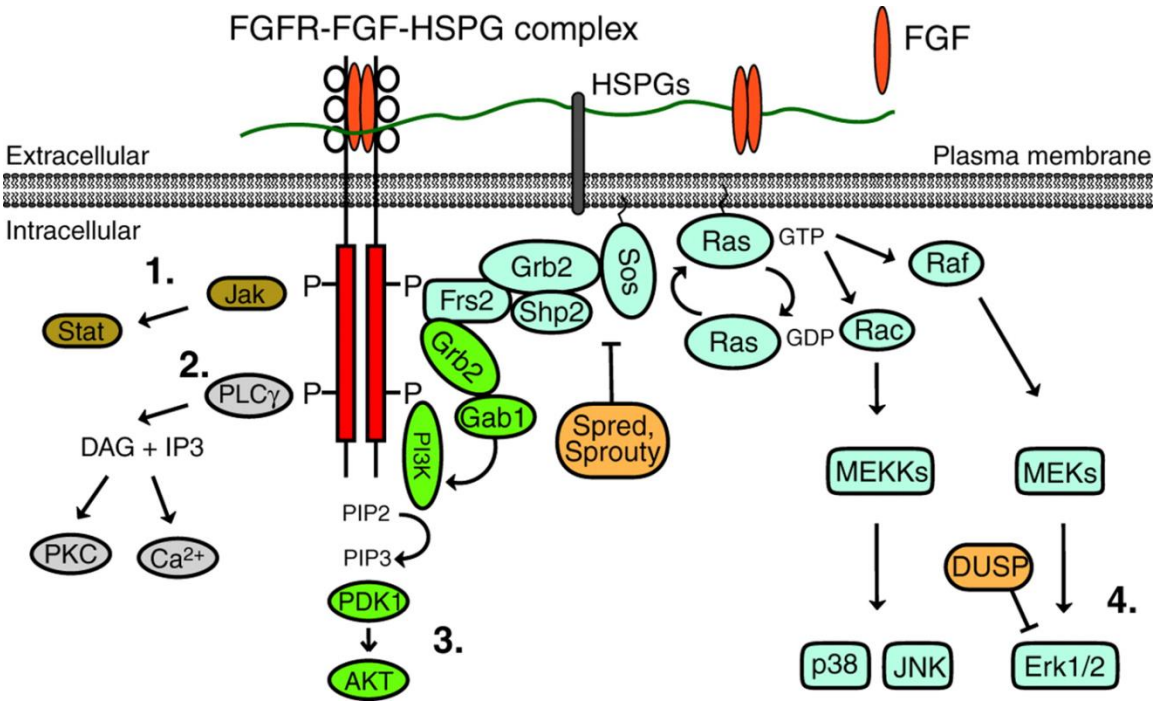

Figure 9 – FGF signaling pathway. Following FGF ligand and heparin binding, FGF-receptors dimerize at the plasma membrane. The kinase domains of these receptors will transphosphorylate each other, leading to recruitment of adaptor proteins and activation of four main intracellular pathways. (1) signal transducer and activator of transcription (STAT). (2) phospholipase Cγ (PLCγ). (3) PI3K–AKT. (4) RAS-RAF-MAPK. These pathways can lead to cellular alterations in proliferation, survival, and motility. [Image from (101). Copyright from Company of Biologists. No permission required for educational use.]

Role in Angiogenesis

Along with embryogenesis, angiogenesis was one of the first areas where FGF signaling was shown to be important (102). In particular, FGF1 and FGF2 were found to be significant for new blood vessel growth in wound healing models (103). FGF2 is a very potent inducer of angiogenesis (104). In a preclinical model of microvascular endothelial cells grown on a 3-dimensional collagen gel, VEGF and FGF2 were able to induce cells to invade the underlying matrix to form capillary-like microvessels (105). FGFs exert their effects by modulating proliferation and migration of endothelial cells,

production of proteases, and promotion of integrin and cadherin receptor expression (106). FGF1 and FGF2 also affect tumor angiogenesis by promoting the cellular proliferation of endothelial cells. In the tumor microenvironment FGFs may exert their effects through either autocrine or paracrine signaling, and stimulate a variety of cells, including ECs (107). A significant amount of cross-talk is thought to exist between members of the VEGF family and FGF-2 during angiogenesis. FGFR1 and FGFRL1 are the most commonly expressed FGFR in endothelial cells, followed by FGFR2 (108). Unlike FGFR1, FGFRL1 remains largely uncharacterized in endothelial cells and in the tumor microenvironment.

Emerging evidence has suggested that upregulation of FGF and FGFR may serve as a mechanism of resistance to anti-VEGF therapy (102). Clinical evidence in colon cancer and glioblastoma supports the role of FGF-2 in resistance to bevacizumab-containing regimens (109, 110). There are several pharmacologic agents that have been or are being developed for inhibition of FGFR/FGF signaling (111). These include both highly selective inhibitors as well as multi-kinase inhibitors. Only four agents (ponatinib, pazopanib, regorafenib, and recently lenvatinib) are FDA-approved for use in cancer, although the approval was not based on their activity against FGFR.

MicroRNA

microRNA (miRNA) are short, ~22 nucleotide RNA that suppress protein synthesis (112). miRNAs do this by binding to the 3' untranslated regions (UTRs) of a target mRNA. miRNAs are well conserved in both plants and animals, and are thought to be a vital and evolutionarily component of gene regulation (113). The human genome contains thousands of miRNAs that appear to target about 60% of the genes in humans and other mammals (114). A single miRNA may repress the production of hundreds of proteins, but this repression is often relatively mild (> 2-fold). miRNA research has further revealed different sets of miRNAs expressed in different cell types and tissues (115). Aberrant miRNA expression is also implicated in variety of disease states (116). For this reason, many miRNA-based therapies are under investigation (117).

<u>miRNA synthesis</u>

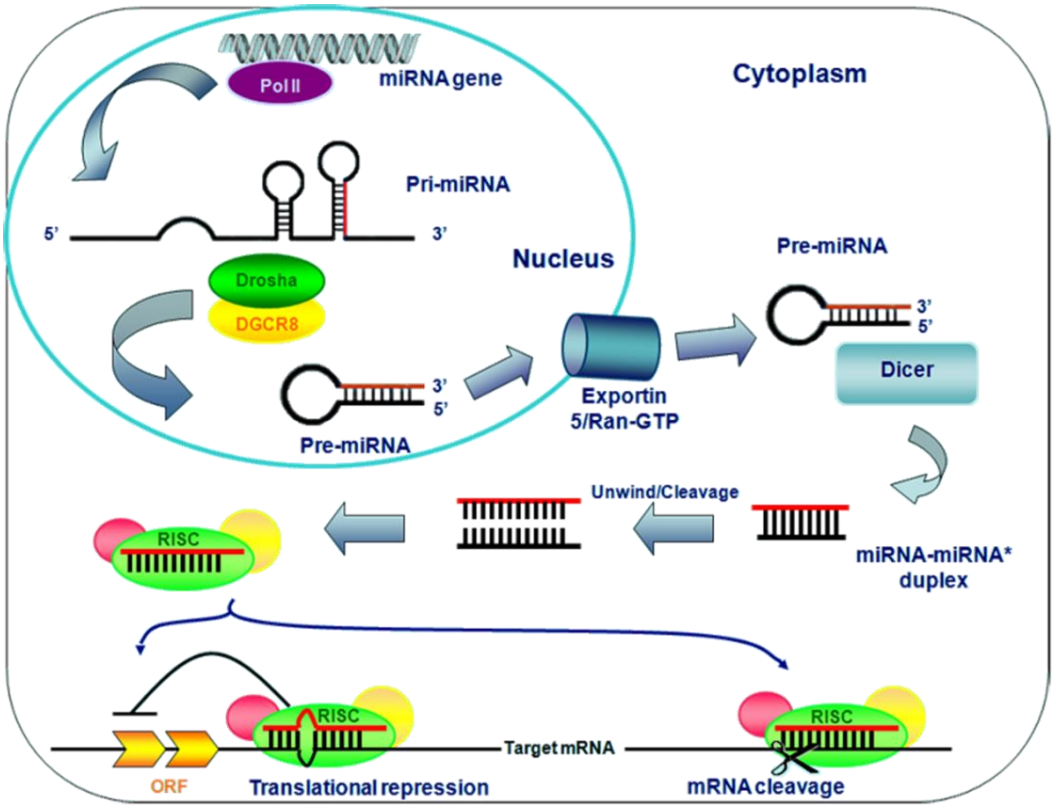

Figure 10 – microRNA synthesis. miRNA gene sequences are transcribed by Pol II into a pri-miRNA sequence that will fold into a hairpin structure. While still in the nucleus, the pri-miRNA is stabilized by DGCR8 and then cleaved into a shorter hairpin pre-miRNA sequence by the ribonuclease, Drosha. The pre-miRNA is transferred to Exportin-5 and exported out of the nucleus and into the cytoplasm. There, it is cleaved by endoribonuclease, Dicer in a complex involving regulatory and stabilizing proteins, TRBP and PACT. This intermediate pre-miRNA form is further processed by Dicer and Aargonaute. Dicer, Argonaute, and TRBP form the RISC loading complex, which facilitates assembly of the RISC and incorporation of the mature miRNA duplex. Once assembled the miRNA duplex is degraded and the functional strand is guided to its 3'UTR target. The miRNA must pair with its target in order to inhibit translation. [Image from Calore F., Fabbri M. MicroRNAs and Cancer. *Atlas Genet Cytogenet Oncol Haematol.* 2012;16(1):51-69. No permission required for educational use (CC BY-NC-ND 2.0 FR)]

miRNA synthesis is summarized in Figure 10, including the figure legend (118).

Mechanism of action

Within the RISC, the mature miRNA provides specificity for mRNA silencing (112). As shown in Figure 11, miRNAs do not perfectly basepair with the target mRNA (119). However, there are some areas of this interaction that must complement. The criteria for miRNA-mRNA 3' UTR interaction are highlighted in Figure 11.

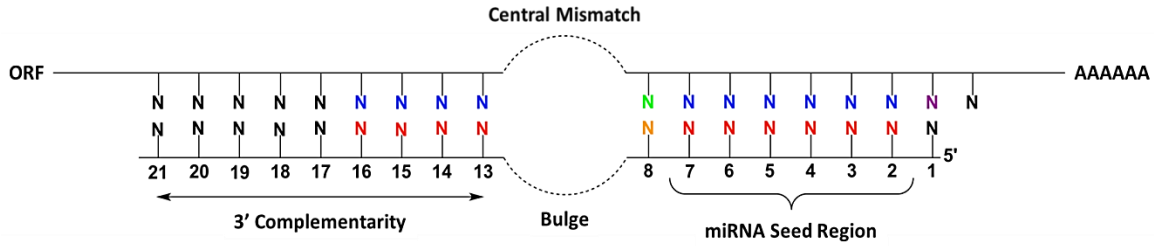

Figure 11 – Criteria for miRNA-mRNA 3'UTR interaction. miRNA interact with their corresponding mRNA target via base pairing. As shown in the figure, these pairings are not perfect matches between bases. Bulges or mismatched bases must be present in the central region of the miRNA-mRNA duplex. In the miRNA "seed" region, represented by nucleotides 2-8, base pairing by be complementary and contiguous. GU pairs or mismatches in the seed region

greatly affect mRNA repression. Additionally, there must be reasonable 3' complementarity to stabilize the interaction with the mRNA (120).

Binding of the mature miRNA and RICS to the mRNA 3' UTR initiates interference of protein translation (121). Blocking of protein synthesis occurs by multiple mechanisms. These are summarized in Figure 12 (122). Silencing may occur by deadenylation of the target mRNA leading to mRNA degradation, interference with ribosome or cofactor recruitment causing inhibition of translation initiation, impairment of ribosomal activity resulting in arrest or slowing of peptide elongation, and recruitment of protease to cleave of nascent peptide (121).

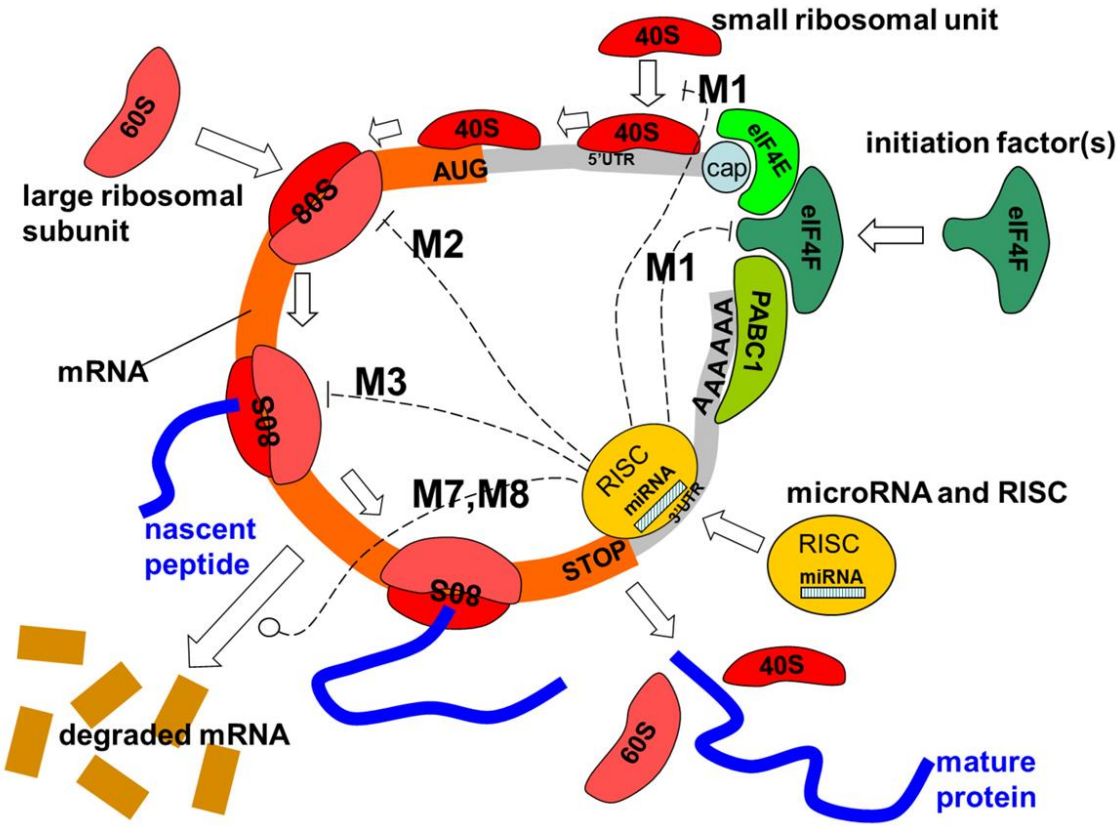

Figure 12 – miRNA interference of protein translation. miRNA associated with the RISC complex for micro-ribonucleuoprotein (miRNP) complexes. Several mechanisms of mRNA translation repression by miRNA have been identified. (M1) Prevention of the initiation process

and assembly of the initiation complex, (M2) Recruitment prevention of the 40S ribosomal subunit on the ribosome assembly, (M3) Prevention of the translation process, (M7,M8) Degradation of the mRNA. Additional mechanisms include miRNP mediated recruitment of deadenylation machinery to remove or “decap” the poly A tail from target mRNAs causing degradation. The miRNP may also recruit proteases (X) that can cleave the nascent peptide as it is produced. [Image from (122). No permission required (CC BY 3.0).]

miRNAs in cancer and angiogenesis

Reports have demonstrated that specific mRNAs are involved in the hypoxic response and contribute to the repression of biologically important genes by low oxygen tension (123, 124). As mentioned previously, hypoxia is a dominant driver in the development of tumor angiogenesis, and recent reports have shown that miRNAs are key players in mediating this process (125, 126). First, miRNAs can modulate HIF1 signaling through both direct and indirect mechanisms (127). Second, growth factor and proangiogenic factor secretion by the tumor has also been shown to be regulated by miRNAs (128). And finally, tumor miRNAs can play a major role in modifying and/or degrading the ECM in order to enhance the angiogenic response (129). Table 9 summarizes miRNAs that have been implicated in both physiological and pathological angiogenesis (130). These miRNAs are sometimes referred to as angiomiRs. While dozens of miRNAs have been implicated in regulating angiogenesis, the molecular mechanisms of these processes remain largely understood. Further effort is needed to identify novel targets and show experimentally how miRNA can orchestrate the angiogenic response.

AngiomiR	Confirmed Target/s in Vascular Cells	Biological Function in Vascular Cells
miR-126	SPRED1, PIK3R2, VCAM1, SDF-1/CXCL12	Proangiogenic, vascular integrity

miR-17-92 cluster	Tsp-1, CTGF, TIMP1, HIF1a, TSR, VEGFR2, VEGF, ITG-a5	Proangiogenic, neovascularization, proliferation and motility, response to hypoxia
miR-210	Ephrin A3	Response to hypoxia, pro-angiogenic
miR-424	CUL2	Response to hypoxia, pro-angiogenic
miR-21	RhoB, PPARa, PTEN, Bcl2, SPRY2, PDCD4	Antiangiogenic/Proangiogenic, inflammation, proliferation, anti-apoptotic, migration
miR-15a/16	Bcl-2, VEGFR2, FGFR1, VEGF, FGF2	Antiangiogenic, anti-survival
miR-221/222	c-kit, eNOS, p27	Antiangiogenis, suppression of proliferation and migration, pro-apoptosis
Let7	THBS1, THBS2, TIMP1, Nrp-2, c-Met, AGO1	Proangiogenic, sprout formation, proliferation, migration, response to hypoxia
miR-155	CCN1, AT1R, eNOS, Ets-1	Vascular inflammation, cell proliferation and migration
miR-23a/b	Rb-p, CCNH	Anti-proliferative
miR-24	GATA2, PAK4, NDST1, LIMK2, PAK4, HMOX-1	Antiangiogenic, anti-survival, proapoptotic, decreased response to VEGF, decreased motility
miR-26a	SMAD1, GSK3B	Proangiogenic
miR-27a/b	SEMA6A. Sprouty, VE-Cadherin	Proangiogenic, neovascularization
miR-130a	GAX, HOXA5, RUNX3	Proangiogenic, vascular integrity
miR-31	E-selectin	Vascular Inflammation
miR-200b/c	Ets-1, ZEB1, Flk1	Antiangiogentic, response to hypoxia, growth arrest
miR-503	CCNE1	Antiangiogenis, anti-proliferation/migration
miR-199a-5p	FLAP, Ets-1	Response to hypoxia, antiangiogenic
miR-143/145	Klf4, myocardin, Elk-1, KLF5, TGFBR2	Differentiation, proliferation of smooth muscle cells
miR-101	EZH2, mTOR, CUL3	Antiangiogenic, endothelial cell homeostasis, Proangiogenic, response to hypoxia
miR-93	VEGF-A	Antiangiogenic
miR-218	Robo1, Robo2, GLCE	Regulates vascular patterning

miR-22	AKT3	Induces EPC senescence
miR-107	Dicer-1, HIF-1β	Inhibits EPC differentiation
miR-204	SHP2, RUNX2, angiopoietin-1	Pulmonary arterial hypertension, Corneal neovascularization
miR-124	NFATc1, CAMTA1, PTBP1	proliferation of pulmonary artery smooth muscle cells
miR-34a	SIRT1, Foxj2	EC cellular senescence, stress resistance, differentiation
miR-217	SIRT1, FOXO3A	EC cellular senescence, stress resistance
miR-146a	NOX4, SMAD4, HuR, IRAK1,TRAF6, RhoA, IL-1 receptor-associated kinase 1, and TNF receptor-associated factor 6	Proangiogenic, Cell proliferation, Inflammation
miR-181a	NOX5, Prox1	Cell proliferation, vascular development and neo-lymphangiogenesis
miR-125	RTEF-1, VE-Cadherin	Antiangiogenic

Table 9 – Key miRNAs in Hypoxia and angiogenesis (130).

Aims of the Research

Low oxygen tension, or hypoxia, is a hallmark of the neoplastic microenvironment and a well-documented source of therapeutic failure in solid tumors. Numerous studies have consistently linked tumor hypoxia with poor prognosis and resistance to conventional therapy. Under low oxygen tension, malignant tumors rapidly adapt to their environment by modifying cell metabolism, activating angiogenesis, and allowing for increased survival and metastasis. Because these hypoxia-driven cellular adaptations directly contribute to the survival of cancers, it is an important consideration for new therapeutic strategies.

Although historically differentially induced genes by low oxygen, and in particular by Hypoxia Inducible Factor 1 (HIF1), has dominated hypoxia research, recent studies of gene repression promoted by low oxygen tension have received increased attention. Reports have demonstrated that specific microRNAs (miRNA) are involved in “fine-tuning” the cellular response to hypoxia. Studies have consistently established that miR-210 induction is a feature of the hypoxic response in both normal and transformed cells. miR-210 is trans-activated by HIF1, and its overexpression has been detected in cardiovascular diseases and cancers. High miR-210 levels in solid tumors have also been consistently associated with poor clinical outcome. **The focus of this research is on miR-210 and its role in mediating angiogenesis and tumor microenvironment under hypoxic conditions.**

A spectrum of miR-210 targets have been identified, with roles in mitochondrial metabolism, angiogenesis, DNA repair, and cell survival. Such targets may broadly affect the progression of tumors and other pathological settings, such as ischemic disorders. However, few of these targets have been validated using *in vivo* animal

models. To this end, there remains a major gap in our understanding of the biological and biochemical roles of miR-210 and its targets. To help close this gap, we generated miR-210 KO mice to characterize its biological role angiogenesis and in the tumor microenvironment. Interestingly, one of the top predicted targets of miR-210, fibroblast growth factor receptor-like protein 1 (FGFRL1), is overexpressed in KO tissue, including endothelial cells. Fibroblast growth factor receptors (FGFRs) play a critical role in angiogenesis, and formation of new blood vessels via activation of tyrosine kinase signaling pathways. In contrast, FGFRL1 contains no tyrosine kinase domain, but still has the ability to bind to FGFs. We hypothesized that FGFRL1 acts as a negative regulator of FGF signaling and is downregulated by miR-210 in hypoxia in order to sensitize cells to FGFs. **The overall goal of this project is to elucidate the role of miR-210 and FGFRL1 on angiogenesis and tumor microenvironment.** We were able to accomplish this by using both genetic and pharmacologic approaches to characterize miR-210/FGFRL1 both *in vitro* and *in vivo*. This work encompasses two specific AIMs:

AIM-1. ***To determine the underlying mechanisms of miR-210 and FGFRL1 mediated angiogenesis in vitro.***

AIM-2. ***To characterize the impact of miR-210 on pathological angiogenesis and tumor microenvironment in vivo.***

In compliment to each other, these specific aims were set to elucidate the role of the miR-210/FGFRL1/FGF-signaling axis in pathological angiogenesis. Understanding the molecular mechanisms of hypoxia induced angiogenesis in the tumor microenvironment is important as these insights may lead to improved response to

therapy, and eventually to better biology-based disease management, thereby improving prognosis and quality of life. In addition to cancer, hypoxia also plays a central role in the pathogenesis of major ischemic disorders. Therefore, a deeper understanding of cellular adaptation to oxygen deprivation has broad and profound implications for translational medicine.

CHAPTER II:

MIR-210 MODULATES bFGF SIGNALING AND ANGIOGENESIS BY DOWNREGULATING FGFRL1 IN HYPOXIC ENDOTHELIAL CELLS

Introduction:

Angiogenesis is a key feature of the hypoxic response, and plays a significant role in vascular ischemic disease as well as tumor adaptation and survival (5, 131-135). While research has highlighted the role of Hypoxia Inducible Factors (HIFs) in mediating angiogenesis during hypoxia, we have seen that miRNAs provide a tertiary level of control in regulating cellular adaptation to hypoxia, including angiogenesis (43, 136-138). Multiple studies have established that miR-210 induction is a feature of the hypoxic response in both normal and transformed cells (139-142). miR-210 is a direct target of Hypoxia Inducible Factor-1a (HIF1a) and its overexpression has been shown to facilitate cellular adaptation to low oxygen conditions. A handful of miR-210 targets have been characterized and demonstrated to participate in cellular processes, including cell cycle regulation, mitochondria function, apoptosis, and cell migration. miR-210 has also been shown to play a role in endothelial cells (ECs) and in hypoxia induced angiogenesis (130, 143-145). As a proangiogenic factor, miR-210 has been implicated in variety of ischemic disorders as well as tumor angiogenesis (141, 146-148).

miR-210-mediated effects on angiogenesis are in part related to its influence on mitochondrial metabolism. During hypoxia, miR-210 has been demonstrated to suppress proteins involved in mitochondrial respiration, including the iron-sulfur (Fe-S) cluster scaffold proteins, ISCU1 and ISCU2 (149, 150). Additionally, miR-210 can control cellular levels of vascular endothelial growth factor (VEGF) through the targeted regulation of receptor tyrosine kinase ligand Ephrin-A3 (EFNA3) and phospho-tyrosine phosphatase-1B (PTP1B) (151, 152). Other than these mechanisms, there remains a major gap in characterizing the role of miR-210 in ECs and in *in vivo* models of angiogenesis. Therefore, miR-210 KO mice were generated to better study these

processes. Overall, our in vivo studies show that absence of miR-210 dampened hypoxia-induced vessel sprouting and tumor cell induced angiogenesis.

Interestingly, we found a target of miR-210, Fibroblast Growth Factor Receptor-Like 1 (FGFRL1), upregulated in KO mouse endothelium. In the present study we identify FGFRL1 as a significant contributor to angiogenesis. Like VEGF signaling, fibroblast growth factor (FGF) signaling plays a critical role in stimulating angiogenesis (102, 107, 153). Several FGFR family members, including FGFRL1, are highly expressed in endothelial cells (108). Unlike FGFR1, the function of FGFRL1 remains uncharacterized in ECs. Studies have previously established that FGFRL1 is capable of binding heparin and FGF ligands, including bFGF (87-89). However, it lacks an intracellular tyrosine kinase domain (98, 100, 154). To this end, researchers have hypothesized and demonstrated experimentally that FGFRL1 may act as a dominant negative, or decoy receptor by sequestering FGF molecules (87-89). Previous work has additionally demonstrated that miR-210 targets and downregulates FGFRL1 in cancer cells (155, 156). Other studies have shown that FGFRL1 participates in processes such as cell proliferation, cell adhesion, cell fusion, and is capable of some intracellular signaling activity (87, 90-97).

This work focuses on uncovering the function of miR-210 and FGFRL1 in primary ECs and in miR-210 KO mice. We hypothesized that FGFRL1 acts as a negative regulator of FGF signaling, and is therefore downregulated during hypoxia by miR-210 in order to sensitize endothelial cells to FGF induced signaling. *In vitro* studies reveal that miR-210 can sensitize human umbilical vein endothelial cells (HUVECs) to bFGF induced proliferation, migration, and tube formation. We found that FGFRL1 played a more specific role in negatively regulating bFGF induced proliferation. Like previous *in*

vitro studies (88), we also identified FGFRL1 excretion from HUVECs into the extracellular matrix and culture media. Intracellularly we found both cytoplasmic and nuclear populations of FGFRL1. Further analysis of nuclear FGFRL1 populations revealed localization to Promyelocytic Leukemia (PML) Nuclear Bodies (NBs). PML nuclear bodies are highly expressed in vascular endothelium and have been reported in the literature as a suppressor of neoangiogenesis (157-159). Although the precise cell function of PML NBs is not clear, they are believed to be nuclear depots that sequester other factors to control cellular processes such as transcription (160-163). Interestingly, hypoxia decreased both FGFRL1 and PML levels in HUVECs, implicating their shared role in cellular adaptation to hypoxia in the nucleus. Overall, both our in vitro and in vivo studies demonstrate the role of miR-210 in modulating FGF signaling in hypoxic endothelial cells by downregulating FGFRL1.

Materials & Methods:

Cell Culture & Hypoxia – Primary Human umbilical vein endothelial cells (HUVEC) were purchased from Lonza (Basel, Switzerland) and Neuromics (Edina, MN). Endothelial cells were cultured in Endothelial cell Growth Media EGM-2™ (Lonza) and used up to passage number 6 (P6). Lewis Lung Carcinoma (LLC) cells were obtained from ATCC (Manassas, VA) and grown in RPMI 1640 medium supplemented with 10% FBS, 2mM L Glutamine, 100units/ml Penicillin-Streptomycin. HEK293T cells were obtained from ATCC (Manassas, VA) and grown in DMEM high glucose media supplemented with 10% FBS, 2mM L Glutamine, and 100units/ml Penicillin-Streptomycin. Hypoxia was achieved by flushing modular incubator chambers (Billups-Rothenberg) with 95% N2, 5% CO2 for 15 min to effect O2 levels of ~3% in the media.

Reagents – bFGF was purchased from Sigma-Aldrich (F0291). Geltrex® Low-growth factor basement membrane matrix (Life Technologies) was used for *in vitro* tube formation assays. Matrigel™ basement membrane matrix (BD Biosciences) was used for plug assay and tumor cell-induced angiogenesis studies. Lipofectamine RNAiMAX reagent (Invitrogen) was used for cell transfections. Antibodies used were: anti p44/42 MAPK (CST#4696S), anti phospho-p44/42 MAPK (CST#4370S), anti AKT (CST#2920S), anti phospho-Ser 473 AKT (CST#3787S), anti Beta-Actin (sc-47778), PE conjugated anti-CD31 (BD Pharminogen-52477), FITC-conjugated anti-αSMA (Sigma-F377) anti FGFRL1 (PA5-21516, sc-50326, and sc-18637), anti phospho Y654 FGFR1 (ab59194), anti FGFR1 (CST#3472), anti PML (sc-966), anti Histone 3 (CST#9715), anti bFGF (sc-1360), Dynabeads sheep anti-Rat IgG (11035). Appropriate secondary antibodies conjugated to horseradish peroxidase (Vector labs) or IRDye® secondary antibodies (LI-COR) were used. Secondary antibodies conjugated to Alexa Fluor 488 or

Alexa Fluor 647 from Molecular Probes (Invitrogen) used for immunofluorescent staining. Isolectin GS-IB4, Alexa Fluor 488 conjugate (Life Technologies) was used for retina assay. miR-210 duplex and scrambled negative control ordered from Pre-miR™ miRNA Precursors and Ambion (Life Technologies). siRNAs and siControls from Santa Cruz Biotechnology. TPEN was ordered form Sigma-Aldrich (P4413). Fluorescent probes- Hoescht-33342, 4', 6-diamidino-2-phenylindole (DAPI) were purchased from Molecular Probes (Invitrogen). Cell Counting Kit-8 (CCK-8) was purchased from Dojindo Molecular Technologies, Inc. Guava Cell Cycle Reagent (Millipore) for Flow Cytometry was used for cell cycle analysis.

Real-Time PCR – Total RNA was isolated using the TRIzol Reagent (Invitrogen) with chloroform extraction, isopropanol and ethanol washes. cDNA was synthesized using the miScript Reverse Transcription Kit (Qiagen) or Superscript Vilo cDNA synthesis kit (Invitrogen). Quantitative real-time PCR was performed to examine the expression of miR-210 or FGFRL1 transcripts using SYBR green (Applied Biosystems) according to manufacturer's instructions. All qPCR experiments were conducted in triplicate with samples from three separate experiments. Results were interpreted by the delta-delta-Ct method with normalization to Beta Actin (mRNA), RNU48 (human-miRNA), or SNORNA (mouse-miRNA) levels.

qPCR Primers –

Target	Forward Primer	Reverse Primer
FGFRL1 (Human)	5'-AACTATGAGCCTCACGGCAC-3'	5'-ATGCACACACAGGTGCAGAT-3'
FGFRL1 (Mouse)	5'- CTCCACTGGGCACTGTAGC-3'	5'-GCTGCTGCTGCTATTGGG-3'
Beta Actin Control (Human)	5′-AGGGCTGCTTTTAACTCTGGT-3′	5′-CCCCACTTGATTTTGGAGGGA-3′
Beta Actin Control (Mouse)	5'-CATGGCCTTCCGTGTTCCTA-3'	5'-CCTGCTTCACCACCTTCTTGAT-3'

miR-210 (Human)	5’-ATGCCTGTGCGTGTGA-3’	UP: 5’- GTGCGTGTCGTGGAGTC-3’
RNU48 Control (Human)	5'-AGTGATGATGACCCCAGGTAACTC-3'	5'-CTGCGGTGATGGCATCAG-3'
miR-210 (Mouse) and **SNORNA202** Control (Mouse) primer sets were purchased from QIAGEN – qPCR miScript primer assay.		

miR-210 Overexpression & siRNA Knockdown – For transient transfection, HUVECs were transfected using lipofectamine RNAiMAX with miR-210 duplex or scrambled control at a concentration of 50nM. siRNA and siRNA control were transfected into HUVECs at a concentration of 20nM. Cells were incubated with the RNAi complexes for a minimum of 8 hours before the media was changed.

Luciferase Assay – Experiments were conducted in HEK293 cells. Cells were co-transfected with either scrambled-miR or miR-210 duplex, luciferase-FGFRL1 3’UTR reporter construct, and pRL-SV40 Renilla luciferase construct. Cells were them incubated in normoxia or hypoxia for 24 hours following transfection. Cell extracts were prepared after 24 hours, and luciferase activity was measured using the Dual-Luciferase Reporter Assay System (Promega).

Cell Viability – After transient transfection with RNAi or appropriate negative control, HUVEC’s were growth factor starved in EBM-2 with 1% serum o/n. HUVEC’s (10,000) were then plated on gelatin (0.2%) coated 96 well plates and incubated in EBM-2 media with 2% FBS was supplemented with bFGF (10ng/ml). Appropriate negative (no bFGF) were used and all treatments were done in triplicates. Cell viability was measured by using WST-8 (CCK-8) assay. Proliferation was then calculated as a percentage of the positive control.

Real-time Cell Proliferation – HUVEC (20,000) were plated on gelatin (0.2%) coated E-plate 16 (ACEA Biosciences) in the presence or absence of bFGF in EBM-2 (2% FBS). Transfection and growth factor starvation were done as previously described. Each experiment was carried out at least twice. Impedance measurement was recorded every 15 minutes for 24-48 hours using the Real-Time Cell Analyzer Dual Plate (RTCA DP) Instrument (ACEA Biosciences).

Cell cycle analysis – HUVEC were plated in gelatin (0.2%) coated 60 mm dishes. Once 75% confluent, they were transfected with either miR-210, siFGFRL1, or siControl and then growth factor starved in EBM-2 with 1% serum overnight to induce G_0 cell cycle arrest. HUVECs were then stimulated to proliferate in EGM-2 in the presence of bFGF and 2% FBS for 8 hours. Cells were fixed with ice-cold 70% ethanol and stained with PI (20 µg/ml) and RNase (200 µg/ml) for 30 min at room temperature. PI labeled cells were then analyzed in BD FACS Canto II using FACS Diva software (BD Biosciences, USA) and 10,000 events were recorded.

Real-time Cell Migration (trans-well migration) - HUVECs were transfected and growth factor starved as previously mentioned. Cells (50,000) were plated in the upper chamber of the CIM Plate-16 (ACEA Biosciences). Migration of cells was monitored in real-time towards a gradient of 10 ng/ml bFGF (lower chamber). Impedance measurement was recorded every 15 minutes for 12-24 hours using the Real-Time Cell Analyzer Dual Plate (RTCA DP) Instrument (ACEA Biosciences).

Scratch-wound migration assay – HUVEC were plated in gelatin-coated (0.2%) 24 well plates, allowed to attach and then transfected with RNAi. Subsequently they were growth factor starved in EBM-2 with 2% serum overnight and a scratch wound

assay was carried out, as previously described (164). The cells were then treated with or without 10ng/ml bFGF in EBM-2 with 2% serum. Zero-hour and twenty four-hour images of the scratch wound were taken at 2.5X and 4X magnification with the Nikon AZ100M Fluorescence Microscope. Closure of the wound area was quantitated using ImageJ software.

Tube formation assay – HUVECs were transfected with either miR-210 or scrambled (sc) control, followed by growth factor starvation in EBM-2 with 1% serum O/N (14 hours). Geltrex® Low-growth factor basement membrane matrix (250ul/well) was added to a 24 well plate. Subsequently, 75,000/well HUVECs were added over the matrix layer to form tubes in the presence or absence of bFGF (10ng/ml). At 12 hours, images were captured at 4X magnification with the Nikon AZ100M Microscope and the tube length, nodes and junctions were quantitated using the ImageJ Angiogenesis Analyzer plugin.

Immunoblotting (bFGF induced signaling) – Endothelial cells were plated on gelatin (0.2%) coated 60 mm dishes. Once 80% confluent, they were transfected with either miR-210, sc, siFGFRL1, or siControl. After overnight growth factor starvation, they were stimulated with 10ng/ml bFGF and lysates were collected at 0, 10, 20 and 40 min on ice. Cells were washed in PBS then lysed with RIPA buffer (Alfa Aesar) containing protease and phosphatase inhibitor cocktail (Thermo Scientific). Lysates were cleared by centrifugation for 30 min at 10,000 rpm at 4°C. Protein concentration was measured using BCA™ Protein Assay Kit (Pierce). The samples were resolved in SDS-PAGE gels and transferred to a nitrocellulose membrane (BIO-RAD). Bolts were blocked with 5% non-fat milk or 5% BSA in TBST (for phospho-proteins) for one hour at room temperature. The membrane was incubated with primary antibody in their recommended

dilutions overnight at 4^{o}C. Membranes were then incubated with anti-mouse, goat or rabbit IgG secondary antibodies (1:2000) conjugated with horseradish peroxidase or anti-rabbit 680 and anti-mouse 800 IRDye® secondaries (1:10,000) at room temperature for one hour. Immunoblots were detected with Clarity™ Western ECL Substrate (BIO-RAD) using enhanced chemiluminescence technique and IR fluorescence was detected using Odyssey Imager. Densitometric analyses and quantification of bands were done using ImageJ software.

Immunofluorescence Staining – Cells were grown on glass coverslips treated with gelatin (0.2%). Cells were fixed in 4% PFA at room temperature for 20 minutes, and then washed twice with PBS. Cells were permeabilized in 0.2% Triton-X-100 and then blocked in 5% BSA in TBS plus 1% Tween 20 for 1 hour at room temperature. Primary antibodies were diluted according to manufacturer instructions and the cells were incubated overnight. After three washes with PSB, secondary antibodies conjugated to Alexa Fluor 488 or Alexa Fluor 647 were applied for 2 hours at room temperature. Cover slips were washed again with PBS then mounted onto glass slides using Prolong Gold plus DAPI (Invitrogen). Fluorescence images were captured using a Leica DM5500 B microscope. Nuclear and cytoplasmic localization was quantified by NIH Image analysis software.

Subcellular Fractionation – HUVECs were lysed on a 10cm plate using 250ul of subcellular fractionation buffer (250 mM Sucrose, 20 mM HEPES, 10 mM KCL, 1.5 mM$MgCl_2$, 1 mM EDTA, 1 mM EGTA, 1 mM DTT, and protease and phosphatase inhibitor cocktail). Lysates were passed through a 25 Ga needle 10 times using a 1ml syringe then incubated on ice for 20 minutes. The nuclear pellet was collected by centrifugation and the supernatant (cytosolic fraction) removed. The cytosolic fraction

was centrifuged again, and the supernatant was saved. To wash out any additional cytosolic proteins, the nuclear pellet was resuspended in subcellular fractionation buffer, passed through a 25 Ga needle, and centrifuged again (this step was repeated twice). After the wash steps, the nuclear pellet was resuspended in non-denaturing lysis buffer (50 mM Tris HCL, pH 8.5, 10% glycerol, 2 mM EDTA, 150mM NaCl, 1% Triton X-100) containing DTT and protease/phosphatase inhibitor cocktail. To release soluble proteins from the nuclei, the resuspended nuclear pellet was briefly sonicated (>3 seconds) once at low amplitude/intensity on ice. The lysate was mixed gently by pipetting up and down. Nuclear and cytoplasmic protein concentration was measured using BCA™ Protein Assay Kit (Pierce).

Immunoprecipitation – For immunoprecipitation, extracts were pre-cleared with appropriate control IgG and A/G PLUS-agarose beads (Santa Cruz) for 30 minutes at 4˚C. Following centrifugation, lysates were incubated with 3 ug of primary antibody for 1 hour at 4˚C. Next, Protein A/G PLUS-agarose beads were added to the lysates and incubated overnight at 4 ˚C on a rocker platform. The beads were then extensively washed (4 times) with buffer, centrifuged, and finally resuspended in sample buffer. Immunocomplexes were separated on a 4-20% SDS-PAGE gel, blotted on PVDF membrane and detected with anti-bFGF or anti-FGFRL1.

Zebrafish Developmental Angiogenesis Assay – Tg(fli1:EGFP) zebrafish embryos were harvested and injected with either miR-210 or miR-210 morpholino, siFGFRL1 or siControl. Thirty-six hours later the caudal vein plexus was imaged using fluorescence microscopy. Changes in developmental angiogenesis were assessed by quantifying the area of the caudal vein plexus. Over 50 embryos were analyzed per group. These experiments were carried out by Dr. Alexey Benumov.

Generation of miR-210 KO mice – Gene inactivation was carried out by using a replacement vector. Only the mature miR-210 sequence was deleted and replaced by a neomycin resistance cassette during homologous recombination. Diphtheria Toxin A (DTA) was used for negative selection. Embryos and Breeding? Genotypes of the mice were identified by PCR and gel electrophoresis. Mice generated by Dr. Yan Zeng.

Whole Mount Immunofluorescence Staining of Neonatal Mouse Retina – Neonatal mouse retina's from P5 WT and miR-210 -/- mice were isolated and prepared for blood vessel analysis as described in (165). Isolectin GS-IB4, Alexa Fluor 488 conjugate (Life Technologies) was used to stain retinal blood vessels. Data pooled from three separate litters containing altogether 6 miR-210 -/- and 8 WT pups. Whole mount images taken at 2X and 4X magnification with the Nikon AZ100M Fluorescence Microscope. 20X and 40X images were taken with Leica DM5500 B microscope. The radius of vascular networks was quantified by measuring the length between the center of the optic nerve and the edge of leading vessels. These measurements were performed in four-five quadrants and then averaged for each retina. Vascular density and branch points were quantified by measuring Isolectin positive vessels in a fixed area. 40X images of the vascular network were processed using NIH Image J software with Angiogenesis Analyzer plugin. The data were expressed as mean ± SD and were statistically analyzed by student t test.

Aortic Ring Assay – The aortic ring assay was performed as previously described in (166). Briefly, the descending thoracic aorta was isolated, growth factor starved, and 1-mm long aortic rings were cut and embedded in growth factor-reduced Geltrex supplemented with 50ng/ml bFGF and 20 U/mL heparin on a 24-well plate. The aortic rings were then cultured in EBM-2 media supplemented with 2% FBS and 10

ng/ml bFGF at 37°C. Aortas were incubated in either normoxic or hypoxia conditions. A hypoxia incubator chamber as described previously was used to house embedded aortic rings during the course of the 12 day experiment. Images of the aortic rings were taken daily starting on day 2 of the experimental course using a 2X objective on the Nikon AZ100M microscope. In order to obtain images, embedded aortas were taken out of the hypoxic chamber (ischemia/reperfusion) for a period of less than an hour daily, and then placed back into the chamber where the oxygen was flushed out with 95% N2, 5% CO2 for 15 min. After 12 days aortas were fixed and representative images were taken. Average sprout length per group was measured.

Matrigel Plug Assay – 400 ul of a 3:1 matrigel (BD Biociences):PBS mix containing 500 ng/ml bFGF or PBS only were injected subcutaneously into the right flank of WT and miR-210 -/- mice. After 10 days animals were sacrificed; matrigel plugs (n=8 WT, n=6 KO) were surgically removed and fixed in either 10% neutral buffered formalin or snap frozen in OCT. Formalin fixed plugs were paraffin embedded, sectioned, and H&E stained. Flash frozen plugs were sectioned (10um) for staining with DAPI and anti-CD31. Images taken using Leica DM5500 B microscope at 20x. Number of CD31 positive vessels per field was quantified and averaged in each group.

Tumor Cell Induced Matrigel Plug Assay – Female, ~4 months old, WT and miR-210 -/- were used for tumor angiogenesis studies. The University of Minnesota Institutional Animal Care and Use Committee approved the protocol. LLC cells ($5.0x10^5$/ plug) (in PBS) were mixed with Matrigel™ (3:1) and 400 ul was injected subcutaneously into the right flank of the mice. LLCs are an approved cell line by the NIH and derived from spontaneous lung tumors of C57BL/6 mice. Tumor volume (mm^2) measurements were obtained every other day starting on day three. After 15 days animals were

sacrificed; matrigel plugs (n=15 WT, n=14 KO) were surgically removed and photographed. Plugs were next snap-frozen in liquid nitrogen or fixed in 10% formalin. Frozen tumor plugs were sectioned (15um), fixed in cold acetone (-20° C) for 10 min, rehydrated and blocked in 1% BSA. Slides were then stained with PE-conjugated anti CD31 (1:100), FITC-conjugated anti α-SMA (1:500) and counterstained with DAPI. Random areas (5-20) were imaged at 20X magnification using Leica DM5500 B microscope. CD31-positive vessel length and branch points (nodes) were quantified by morphometric analyses, as described below. CD31-positive vessels co-staining with α-SMA were quantified similarly to quantitate mature vessels (morphometric analysis).

Syngeneic ID8 mouse ovarian tumor model – 5 × 10^6 murine ID8 ovarian cancer cells in 0.2 ml of PBS were injected i.p. into female WT C57BL/6 mice (n=10) or C57BL/6 miR-210−/− mice (n=8). When the mice reached an advanced disease state (~2.5 months after injection), both groups were weighed and sacrificed. Malignant ascites was drained and volume was measured. Number of metastatic nodules (over $10mm^3$) was documented on peritoneal organs, peritoneal wall, and diaphragm. Organs and solid tumors were collected and fixed in 10% formalin or flash frozen in liquid nitrogen. Tissue sections were made followed by H&E staining.

Morphometric Analysis of Blood Vessel Density – As previously described (167), Fluorescent digital images were first linearized, binarized, and then skeletonized using the Reindeer Plug-In Functions for Adobe Photoshop before calculating in arbitrary units the relative number of blood vessels (vessel density), the branch-points (vessel branching), and total blood vessel length.

Statistics – Results represent an average of two-four independent experiments. Data are expressed as means ± SD. Statistical analyses were performed using GraphPad Prism® 6. Differences in mean values between the two groups were analyzed using the two-tailed Student's t-test. *P value < 0.05* considered statistically significant.

Results:

FGFRL1 3'UTR is a target for miR-210 – Bioinformatics analyses based on miR-210 sequence complementarity to mRNA 3'UTRs identified FGFRL1 as a top target (Fig. 13A-B). The pre-miR and mature sequences are shown in Figure 13A,B. mircroRNA-data-integreation-portal (mirDIP) was utilized as a search engine to identify miR-210 targets across several miRNA prediction algorithms. Using this robust approach, hundreds of targets were identified. However, we found that FGFRL1 was consistently ranked as a top target across multiple prediction algorithms (Fig. 13C). miRDB, DIANA-microT, and PITA all ranked FGFRL1 within the top 1%, giving us evidence to further pursue miR-210 regulation of FGFRL1. Using miRDP we next generated a FGFRL1 3'UTR sequence map to identify the predicted miR-210 binding sites (Fig. 14A, B). Shown in Figure 14, we identified seven potential miR-210-seed locations. These target sites exhibit both significant base-pairing complementarity as well as G-U wobble pairing.

A

Pre-miR-210 (stem loop)

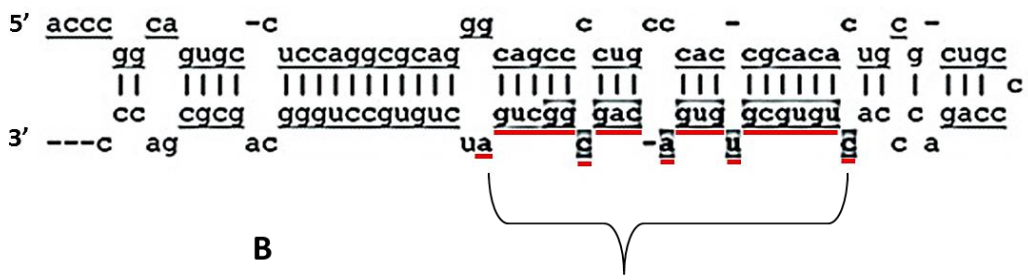

B

miR-210 Mature Sequence:

3’ – AGUCGGCGACAGUGUGCGUGUC – 5’

C

MiR-DIP			
Target	miRNA	Prediction Database	Rank
FGFRL1	miR-210	miRDB	Top 1%
FGFRL1	miR-210	PITA	Top 1%
FGFRL1	miR-210	DIANA-microT	Top 1%
FGFRL1	miR-210	MicroCosm Targets	Top Third
FGFRL1	miR-210	RNA22 3` UTR predictions	Mid Third

***miR-DIP combines microRNA prediction databases to provide control over target prediction searches**

Figure 13 – Sequence analysis predicts FGFRL1 as a top miR-210 target. (A) Diagram of the immature “Pre” miRNA sequence of miR-210. The mature miR-210 sequence is underlined in red in the pre-miRNA stem loop structure. Mature miR-210 arises from the 3’ minus strand. The Pri-miR-210 sequence is 110 base pairs long and is located in an intron on chromosome 11p15.5. miR-210 is located upstream of one of its predicted targets, IGF-2. Unlike IGF-2, miR-210 is not genomically imprinted. miR-210 is a direct target of HIF1a and contains an HRE in its promoter. miR-210 does not appear to be expressed in a miRNA cluster. (B) Diagram of the mature miR-210 sequence. miR-210 is conserved across species. (C) Multiple prediction algorithms and databases identify FGFRL1 as a top predicted target of miR-210. microRNA-Data-Integration-Portal (mirDIP) was utilized as a search engine to identify miR-210 targets across several prediction algorithms. Predictions are based on miRNA and 3’UTR sequence interactions and complementarity. Three algorithms including, miRDB, PITA, and DIANA-microT rank FGFRL1 in the top 1% of predicted miR-210 targets.

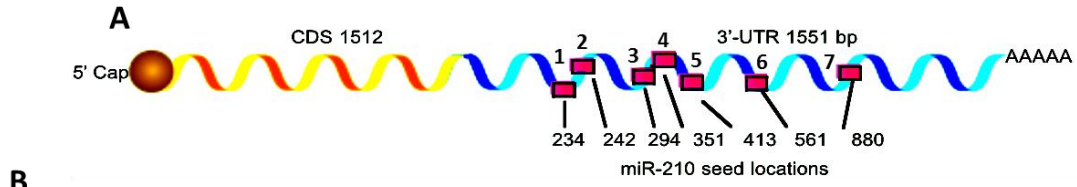

B **FGFRL1 3'UTR - Human**

```
  1 ACGGCACCGT ATCTGCAGTG GGCACGGGGG GGCCGGCCAG ACAGGCAGAC TGGGAGGATG
 61 GAGGACGGAG CTGCAGACGA AGGCAGGGGA CCCATGGCGA GGAGGAATGG CCAGCACCCC
121 AGGCAGTCTG TGTGTGAGGC ATAGCCCCTG GACACACACA CACAGACACA CACACTGCCT
181 GGATGCATGT ATGCACACAC ATGCGCGCAC ACGTGCTCCC TGAAGGCACA CGTACGCACA
241 CACGCACATG CACAGATATG CCGCCTGGGC ACACAGATAA GCTGCCCAAA TGCACGCACA
301 CGCACAGAGA CATGCCAGAA CATACAAGGA CATGCTGCCT GAACATACAC ACGCACACCC
361 ATGCGCAGAT GTGCTGCCTG GACACACACA CACACACGGA TATGCTGTCT GGACGCACAC
421 ACGTGCAGAT ATGGTATCCG GACACACACG TGCACAGATA TGCTGCCTGG ACACACAGAT
481 AATGCTGCCT TGACACACAC ATGCACGGAT ATTGCCTGGA CACACACACA CACACGTGTG
541 CACAGATATG CTGTCTGGAC ACGCACACAC ATGCAGATAT GCTGCCTGGA CACACACTTC
601 CAGACACACG TGCACAGGCG CAGATATGCT GCCTGGACAC ACGCAGATAT GCTGTCTAGT
661 CACACACACA CGCAGACATG CTGTCCGGAC ACACACACGC ATGCACAGAT ATGCTGTCCG
721 GACACACACA CGCACGCAGA TATGCTGCCT GGACACACAC ACAGATAATG CTGCCTCAAC
781 ACTCACACAC GTGCAGATAT TGCCTGGACA CACACATGTG CACAGATATG CTGTCTGGAC
841 ATGCACACAC GTGCAGATAT GCTGTCCGGA TACACACGCA CGCACACATG CAGATATGCT
901 GCCTGGGCAC ACACTTCCGG ACACACATGC ACACACAGGT GCAGATATGC TGCCTGGACA
```

Figure 14 – The FGFRL1 3'UTR contains multiple target sites for miR-210 (A) Schematic diagram of the FGFRL1 mRNA transcript and the miR-210-seed locations in the FGFRL1 3′-UTR. (B) Sequence analysis has revealed 7 seed locations in the FGFRL1 3'UTR that may be important for mRNA translation inhibition by miR-210. These target sites exhibit seed region complementarity as well as significant base pairing and G-U "wobble" pairing.

To validate direct targeting by miR0210, the WT FGFRL1 3'UTR containing the first 5 target sites was cloned downstream of Firefly luciferase reporter construct (Fig. 15A). This construct was then co-transfected into HEK cells along with miR-210 duplex or a scrambled control (Fig.15A). Shown in figure 15B, both hypoxia and miR-210 decreased luciferase activity compared to the normoxia control. Next, 3'UTR seed sequence deletion mutants were prepared to delineate the functional importance of each target site (Fig. 15C). These constructs were co-transfected with miR-210 and luciferase

activity was determined. Transfection efficiency was normalized to Renilla luciferase expressed from IRES. These results are summarized in Figure 15C.

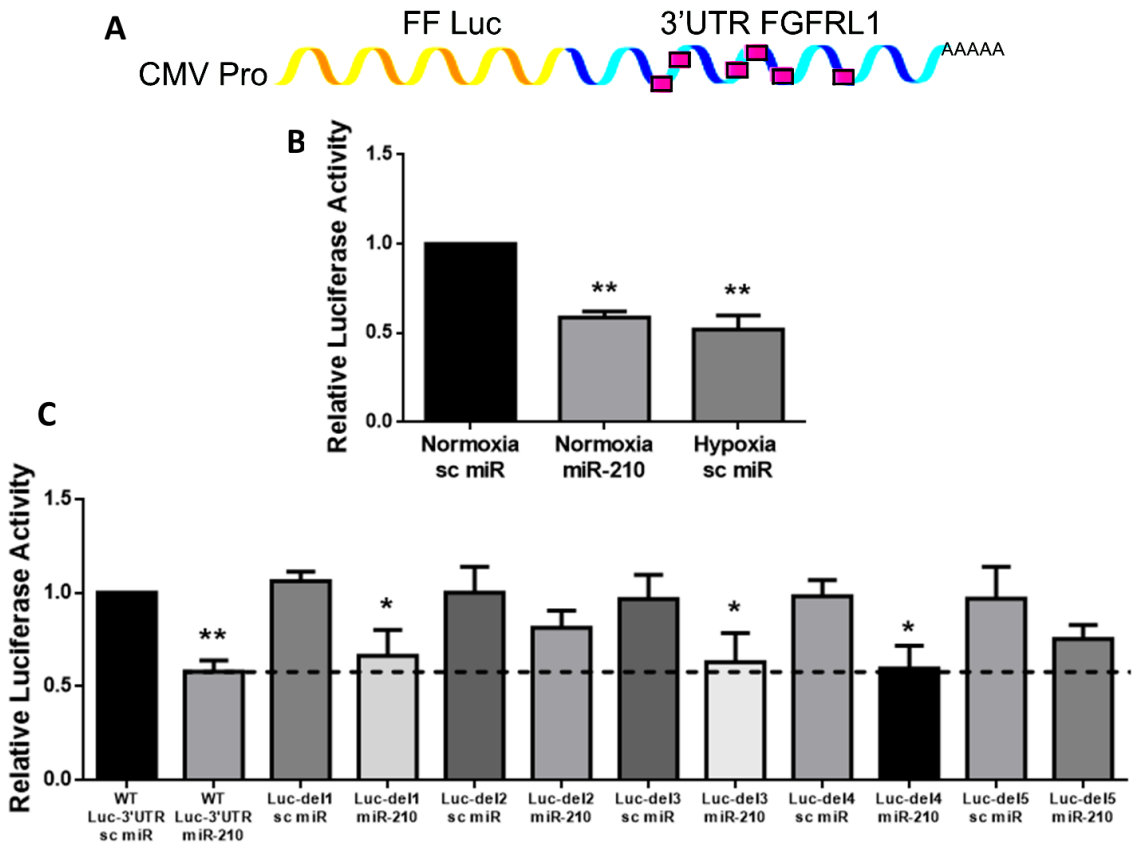

Figure 15 – miR-210 suppresses FGFRL1 3'UTR-dependent protein expression. (A) Schematic diagram of the Luciferase reporter construct containing the FGFRL1 3′-UTR. (B) Graph represents luciferase activity in HEKs co-transfected with sc miR or miR-210, luciferase-FGFRL1 3'UTR reporter construct, and pRL-SV40 Renilla luciferase construct as described in the methods section. Cells were incubated in Normoxia or Hypoxia (sc miR) for 24 hours following transfection. Cell extracts were prepared after 24 hours, and luciferase activity was measured using the Dual-Luciferase Reporter Assay System (Promega). The values are shown relative to the value obtained with Normoxia - sc miR. $n = 3$; **P < 0.01. (C) Luciferase activity (mean +/-SD) using a reporter construct ligated to the 3'UTR of FGFRL1 (wild-type OR individual deletion miR-210 seed sequence sites 1-5) co-transfected with sc miR or miR-210. Data are shown relative to the value obtained with sc miR. $n = 3$; * $p < 0.05$, **p < 0.01.

Hypoxia induced miR-210 decreases FGFRL1 in HUVECs – miR210 induction in HUVECs was confirmed by incubating cells in hypoxia (3% O_2) for 24 and 48 hours. qPCR results illustrate that miR-210 levels increased at both time points when compared to cells treated in normoxic conditions (Fig. 16A). Next, we determined the effects of either hypoxia or miR-210 alone on the expression of FGFRL1 levels in HUVEC. We confirmed in primary endothelial cells that endogenous FGFRL1 transcript and protein levels decreased significantly after treatment with hypoxia or miR-210 duplex (Fig. 16B and 16C).

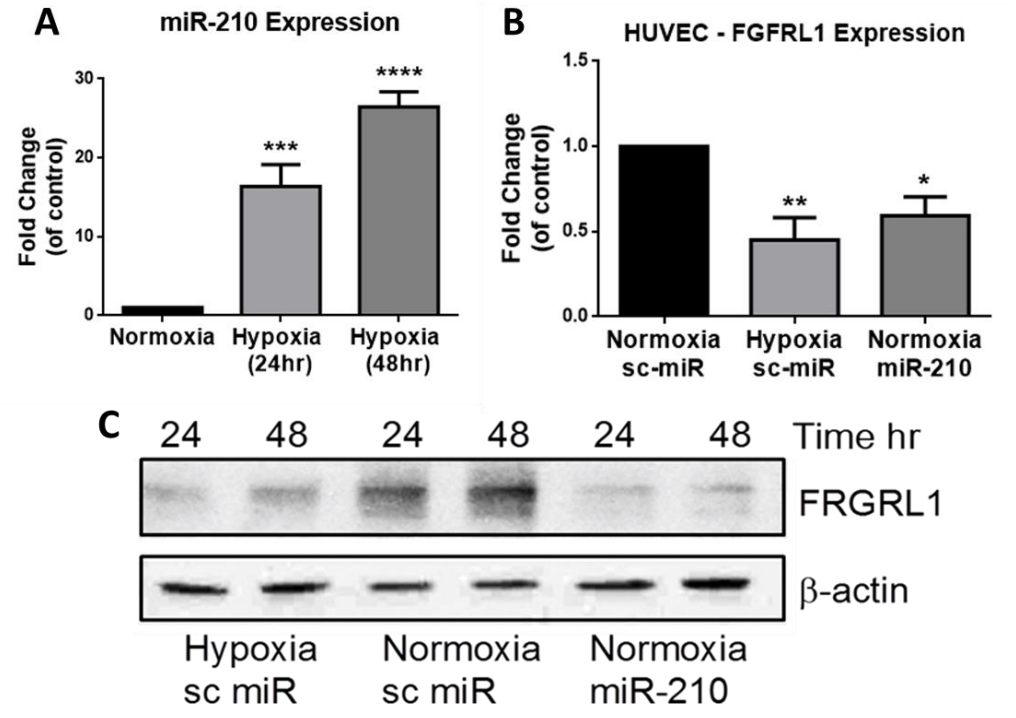

Figure 16 – Hypoxia induced miR-210 decreases FGFRL1 levels in endothelial cells. (A) miR-210 levels (qPCR) in normoxia or hypoxia in HUVEC. Values represent mean +/- SD from three independent experiments. ***P< 0.001, ****P< 0.0001 (B) FGFRL1 transcript levels (qPCR) in HUVECs treated with normoxia, hypoxia, miR-210, or scrambled control (sc). Values represent mean +/- SD from three independent experiments. *P < 0.05, **P< 0.01. (C) Representative western blot shows FGFRL1 levels in normoxia, hypoxia, or treated with miR-210. HUVECs treated with hypoxia or miR-210 for 24 and 48 hours.

miR-210 sensitizes HUVEC to bFGF induced proliferation, migration, and tube formation – Due to the critical role that both hypoxia and FGF signaling play in angiogenesis we wanted to determine if miR-210 had any effect on sensitizing primary endothelial cells to bFGF induced proliferation, cell migration, and tube formation as a result of decreasing FGFRL1 levels. Proliferation of HUVECs was monitored using the xCELLigence Real Time Cell Analysis (RTCA) instrument and compatible E-plate. HUVECs transfected with miR-210 and treated bFGF had significantly increased proliferation (measured by cell index) compared to cells treated with the control scrambled miRNA and the same concentration of bFGF (Fig. 17A).

Figure 17 – miR-210 sensitizes HUVECs to bFGF induced proliferation. (A) Real-time proliferation of HUVEC treated with sc-miR or miR-210. After cell recovery from transfection, HUVECs were serum starved then transferred to an e-plate in the presence or absence of bFGF (10ng/ml) to stimulate proliferation in low (1%) serum EBM-2 media. Cell index indicates electrical impedance measurements. *P < 0.05 at the 24 hour time point.

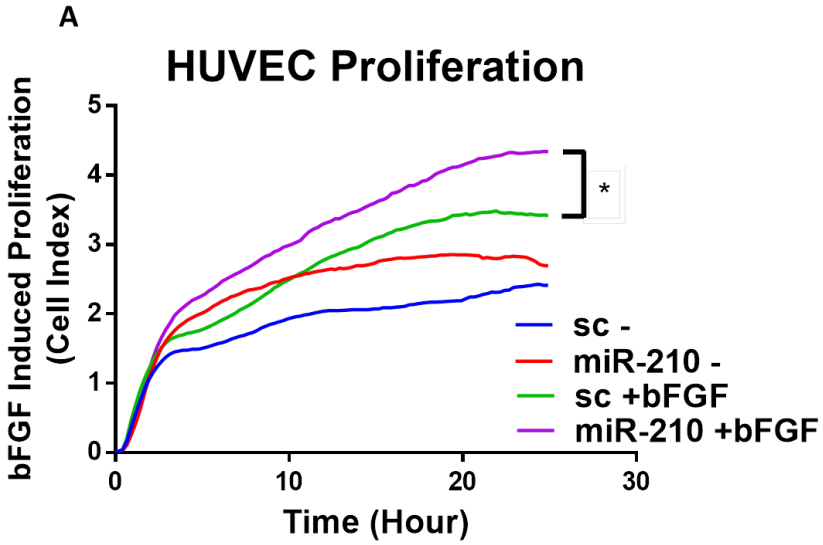

Next, we performed similar experiments to examine bFGF induced migration. HUVEC migration was analyzed by again using the xCELLigence RTCA system as well as the classical scratch-wound technique. Using the xCELLigence CIM plate, cell index

was measured as miR-210 or sc treated cells passed through a membrane from an upper chamber to a lower chamber containing the bFGF stimulus. HUVECs treated with miR-210 showed significantly increased migration towards the bFGF stimulus compared to scrambled control (Fig. 18C). Similar results were found in the scratch wound assay. Cells treated with miR-210 and bFGF showed increased migration into the wound area compared to control (Fig. 18A-B).

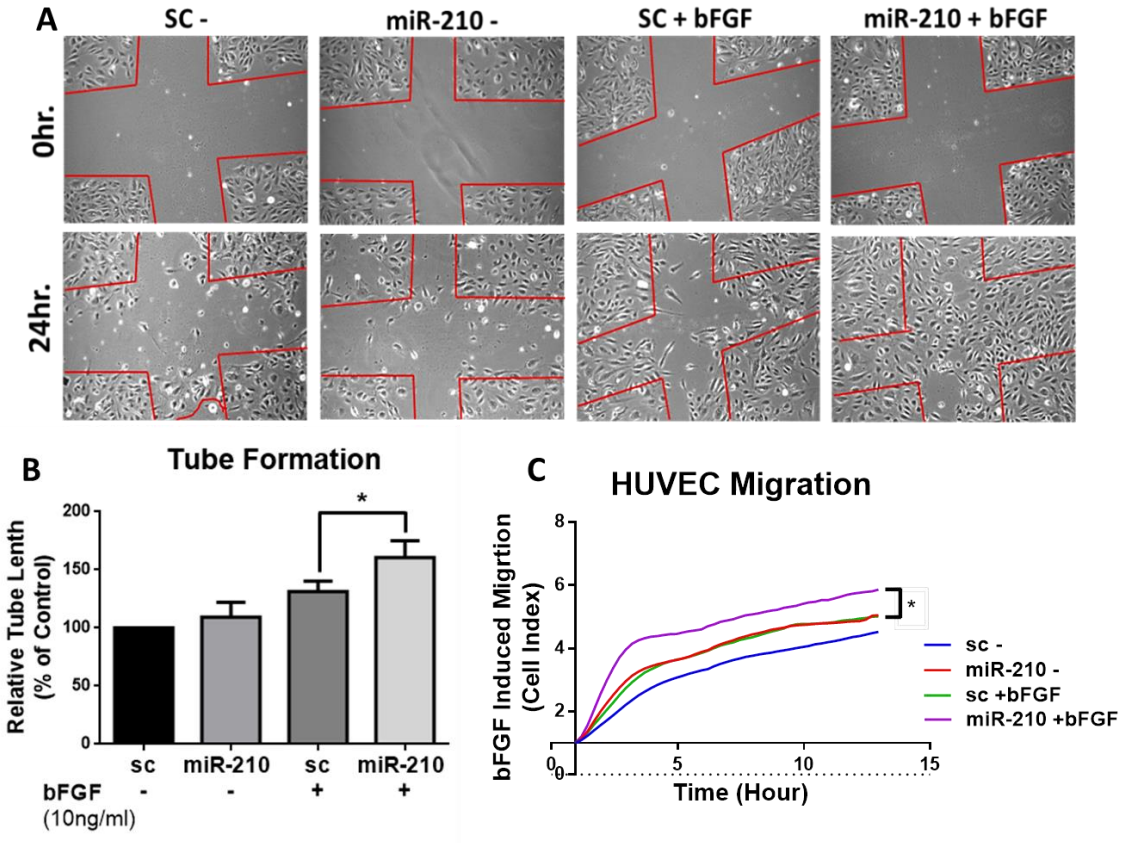

Figure 18 – miR-210 sensitizes HUVECs to bFGF induced migration. (A) Representative images of scratch wound migration assay. HUVECs were transfected with miR-210 or sc-miR, serum starved, then treated with or without bFGF (10ng/ml) as described in the methods section. (B) Quantification of the % cell coverage that migrated into the wound area. Bars represent average +/- SD. *P < 0.05. (C) Real time migration of HUVEC treated with sc-miR or miR-210 in the presence or absence of bFGF (10ng/ml) in the lower chamber. Cell index indicates electrical impedance measurements as cells move from top to bottom chamber. *P < 0.05 at the 24 hour time point.

To evaluate the effect of miR-210 on endothelial cell morphogenesis, tube-forming assays were performed as described in the methods section. Shown in the representative image (Fig. 19A), cells treated with miR-210 and bFGF formed significantly longer tubes with more nodes and junctions, compared to the scrambled miRNA control (quantified in Fig. 19B). Overall, results in Figure 1 conclude that miR-210 is able to sensitize endothelial cells to bFGF which leads to an increase in proliferation, migration, and tube formation compared to control cells.

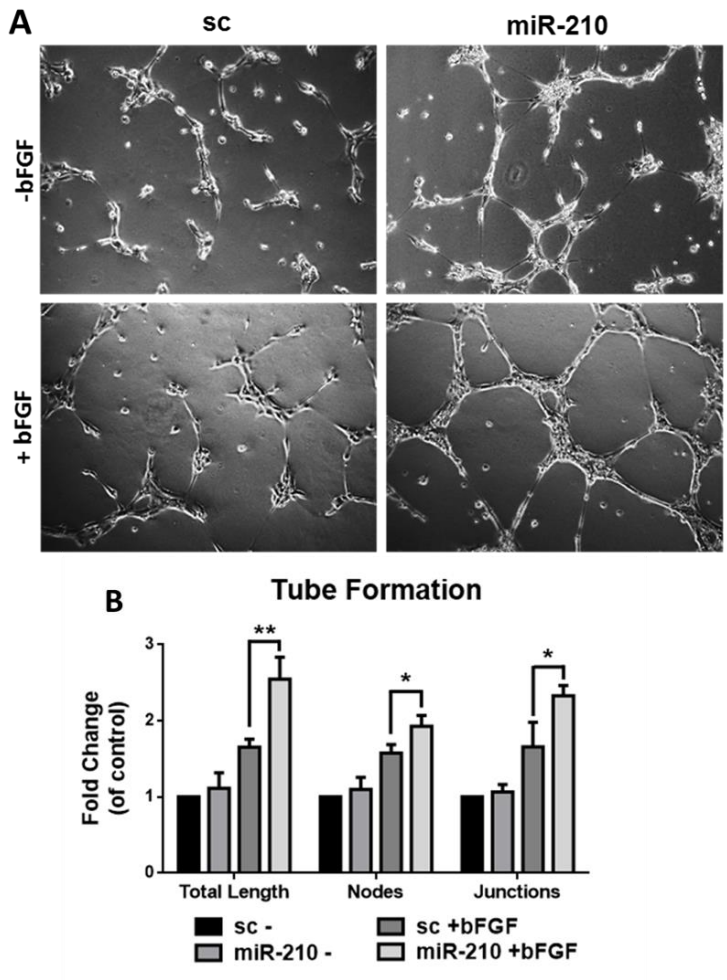

Figure 19 – miR-210 sensitizes HUVECs to bFGF induced tube formation. (A) Representative images of HUVEC tube formation are shown at 10X magnification. Cells were treated with miR-210 or sc-miR, serum starved, and then plated on a Geltrex (reduced growth factor) layer in the presence or absence or bFGF to stimulate tube formation. (B) Histogram represents quantification of total tube length, number of nodes, and junctions in the tube formation assay described in A. Analysis done with ImageJ Angiogenesis Analyzer plugin. Data represent mean +/- SD from three independent experiments. *P< 0.05.

miR-210 sensitizes endothelial cells to bFGF induced signaling – In order to study the mechanisms underlying the ability of miR-210 to sensitize endothelial cells to bFGF, we conducted a series of western blot experiments to evaluate bFGF induced intracellular signaling. We were interested in first looking at levels of FGF-receptor 1 (FGFR1) phosphorylation, followed by further downstream targets such as activated p44/42 Mitogen Activated Kinase (MAPK) and serine/threonine specific protein kinase AKT signaling. Representative blots are shown in supplemental Figure 20A.

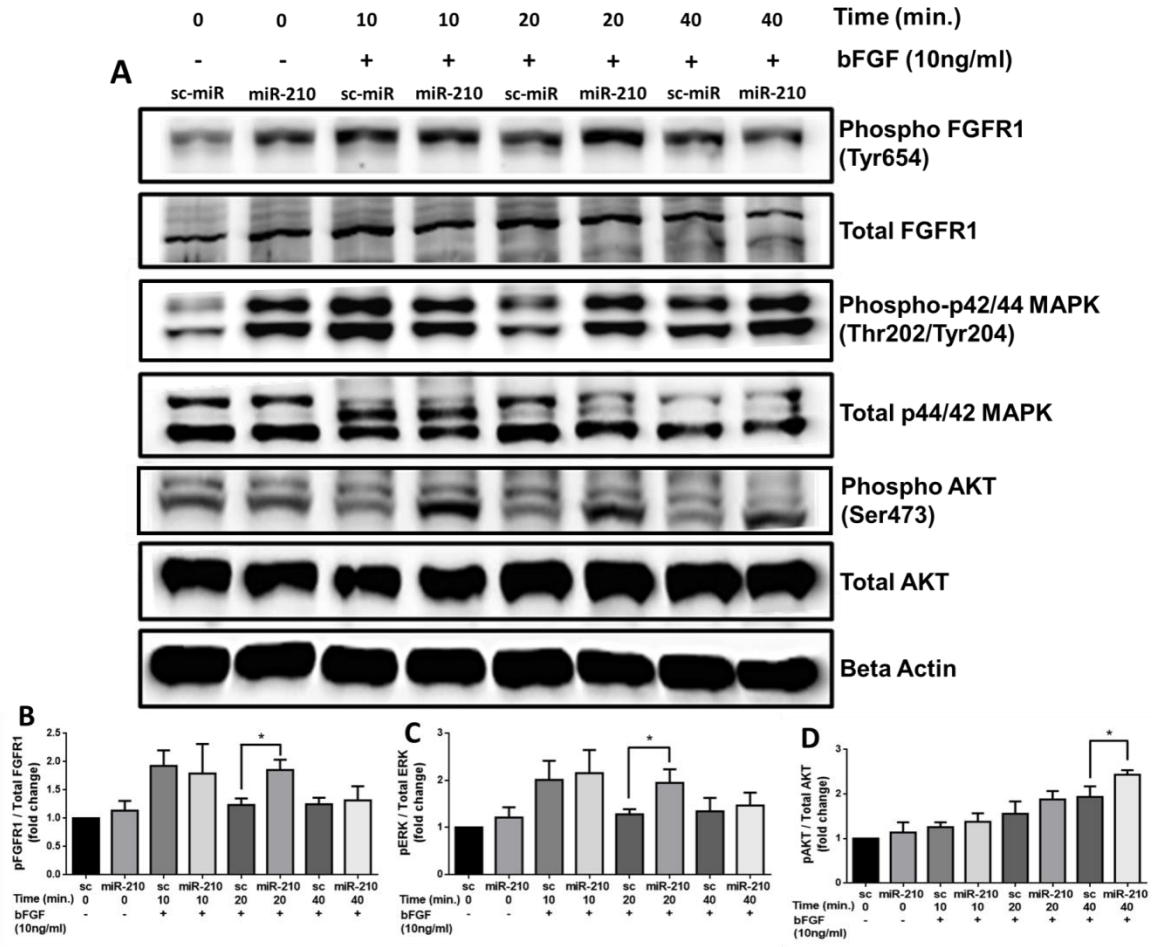

Figure 20 – miR-210 sensitizes HUVECs to bFGF induced signaling. (A) Representative immunoblots of miR-210 or sc-miR treated HUVEC stimulated with bFGF (10ng/ml) for 10, 20, and 40 minutes. pFGFR1/FGFR1, pERK/ERK, pAKT/AKT, and Beta Actin levels were probed. (B-

D) Densitometric quantification of bands is represented in the histograms and data represent mean+/- SD of at least two independent experiments. Relative levels were quantified compared to the sc-miR 0min (bFGF untreated) control. *P < 0.05.

Our studies find that HUVECs treated with miR-210 and bFGF had significantly increased levels of phosphorylated FGFR1 (pTyr654) at the 20 minute incubation time point (Fig. 20B). Similarly, we found an increase in phosphorylation of both p44/42 MAPK and AKT (Ser473), at the 20 minute and 40 minute time points respectively, in miR-210 and bFGF treated cells compared to control (Fig. 20C, D). Overall, these results help us to better understand how miR-210 influences FGF induced signaling pathways.

FGFRL1 regulates HUVEC response to bFGF induced proliferation – Because miR-210 has multiple gene targets, some of which could potentially influence FGF signaling, we wanted to analyze more closely the role that FGFRL1 specifically plays in endothelial cells. Performing similar methods as described in figure one, we utilized FGFRL1 siRNA to test if decreasing endogenous levels of FGFRL1 had any physiological effects and altered response to bFGF in primary endothelial cells. Interestingly HUVECs transfected with siFGFRL1 showed increased bFGF induced proliferation compared to cells transfected with an siRNA control (siC) as measured in real time for 24 hours (Fig. 21A). In order to further characterize FGFRL1's role in proliferation, we next conducted cell viability and cell cycle assays. Both miR-210 and siFGFRL1 in the presence of bFGF increased endothelial cell viability nearly 2-fold over 24 hours compared to control (Fig. 21B). By knocking down FGFRL1 levels using siRNA and miR-210 we were also able to show that the percentage of HUVECs in S and G_2/M increased after 8 hours of bFGF stimulation compared to control using flow cytometry to analyze cell cycle (Fig. 21C).

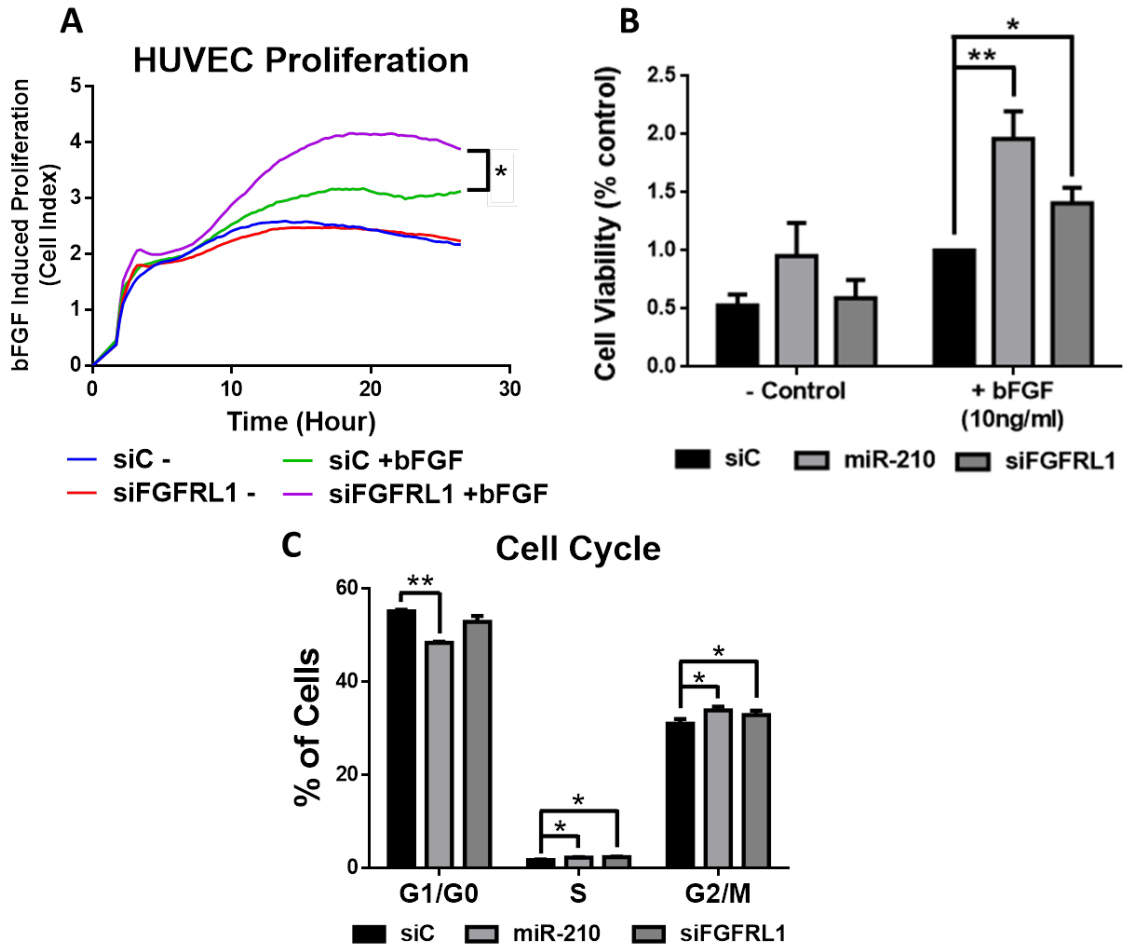

Figure 21 – FGFRL1 regulates HUVEC response to bFGF induced proliferation. (A) Real-time proliferation of HUVEC treated with siControl or siFGFRL1. After cell recovery from transfection, HUVECs were serum starved then transferred to an e-plate in the presence or absence of bFGF (10ng/ml) to stimulate proliferation. Cell index indicates electrical impedance measurements. *P < 0.05 at the 24 hour time point. (B) Cell viability was determined using the Cell Counting Kit-8 (CCK-8) method. HUVECs were transfected with either siC, siFGFRL1, or miR-210. Following serum starvation HUVECs were then plated in low (1%) serum in the presence or absence of bFGF (10ng/ml) and allowed to proliferate for 48 hours. Data represent mean +/- SD from three independent experiments normalized to control (siC +bFGF). *P < 0.05, **P < 0.01. (C) Cell cycle analysis was performed by flow cytometry. Percentage of cells in G0/G1, S, and G2/M are indicated. Histograms represent flow cytometry analysis of HUVECs transfected with siC, siFGFRL1, or miR-210. Cells were serum starved then treated with bFGF for 8 hours prior to flow acquisition. Data represent mean +/- SD from three independent experiments.

Unlike with treatment of miR-210, HUVECs treated with siFGFRL1 did not alter bFGF induced migration compared to control siC (Fig. 22A-C). Additionally, we did not see any significant changes in bFGF induced tube formation in HUVECs with siFGFRL1 (Fig. 23A, B). This suggests that miR-210 may target other factors or pathways that are involved in bFGF induced migration and tube formation.

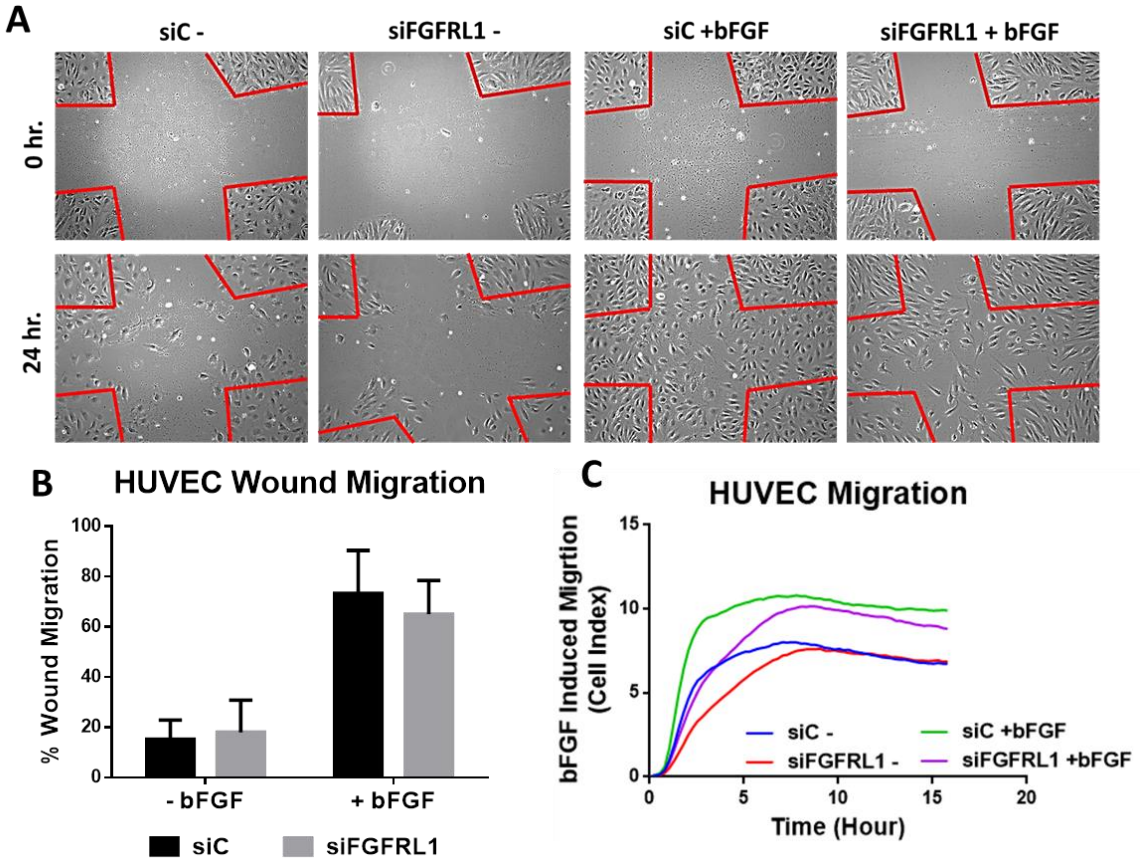

Figure 22 – Suppression of FGFRL1 does not affect bFGF induced migration in HUVEC. (A) Representative images of scratch wound assay. HUVECs were transfected with siFGFRL1 or siC, serum starved, then treated with or without bFGF (10ng/ml) as described in the methods section. (B) Quantification of the % cell coverage that migrated into the wound area. Bars represent average +/- SD. (C) Real time migration of HUVEC treated with siControl or siFGFRL1 in the presence or absence of bFGF (10ng/ml) in the lower chamber. Cell index indicates electrical impedance measurements as cells move from top to bottom chamber.

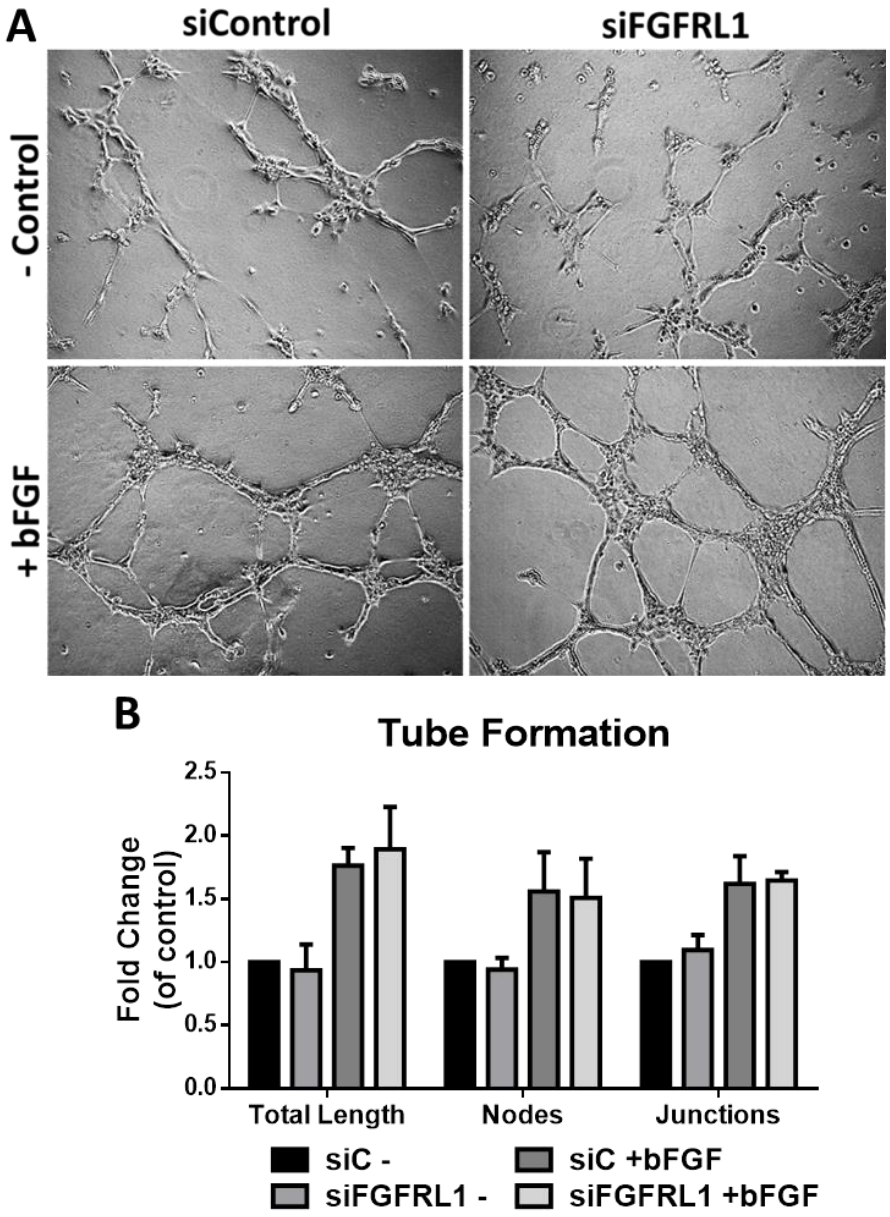

Figure 23 – FGFRL1 does not affect bFGF induced tube formation. (A) Representative images of HUVEC tube formation are shown at 10X magnification. Cells were treated with siFGFRL1 or siC, serum starved, and then plated on a Geltrex (reduced growth factor) layer in the presence or absence or bFGF to stimulate tube formation. (B) Histogram represents quantification of total tube length, nodes, and junctions in the tube formation assay described in F. Analysis done with ImageJ Angiogenesis Analyzer plugin. Data represent mean +/- SD from three independent experiments.

Knock down of FGFRL1 sensitizes endothelial cells to bFGF induced cellular signaling – Because we observed that FGFRL1 primarily played a role in cell proliferation, we wanted to again understand how it was affecting bFGF induced intracellular signaling. Like our previous experiments, we looked at phosphorylated FGFR1, MAPK, and AKT levels. Representative western blot images are shown in Figure 24A. Our studies found that HUVECs treated with siFGFRL1 and bFGF had significantly increased levels of phosphorylated FGFR1 (pTyr654) both at the 0 and 20 minute time points (Fig. 24B) compared to control cells. There was an increase in phosphorylation of both p44/42 MAPK and AKT (Ser473), at the 0 minute and 10 minute time points (Fig. 24C,D). Overall, this data supports that knock down of FGFRL1in HUVEC sensitizes cells to bFGF induced cellular signaling and proliferation.

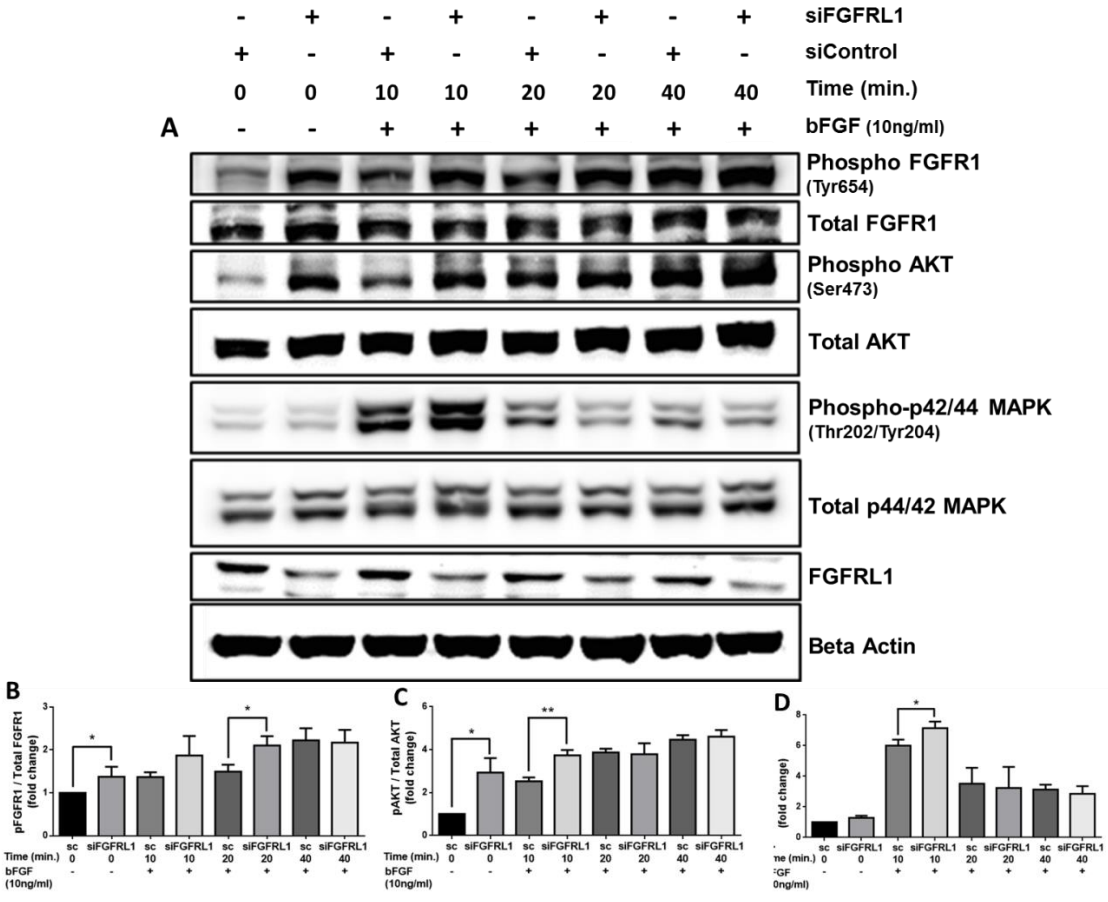

Figure 24 – Suppression of FGFRL1 sensitizes HUVECs to bFGF induced cellular signaling. (A) Representative immunoblots of siControl or siFGFRL1 treated HUVEC stimulated with bFGF (10ng/ml) for 10, 20, and 40 minutes. pFGFR1/FGFR1, pMAPK/MAPK, pAKT/AKT, and Beta Actin levels shown. (B-D) Densitometric quantification of bands is represented in the histograms. Data represent mean+/- SD of at least two independent experiments. Relative levels were quantified compared to the siControl 0-min (bFGF untreated) control. *P < 0.05, **P < 0.01.

Due to the ability of FGF signaling to crosstalk with VEGF pathways, we measured endothelial cell proliferation in response to VEGF after transfection with either miR-210 or siFGFRL1. It has been documented that miR-210 can enhance VEGF signaling, but the role of FGFRL1 is not clear. Results in Figure 25 show that only miR-210 can sensitize endothelial cells to VEGF induced cell proliferation. FGFRL1 had no effect on VEGF induced proliferation in HUVECs.

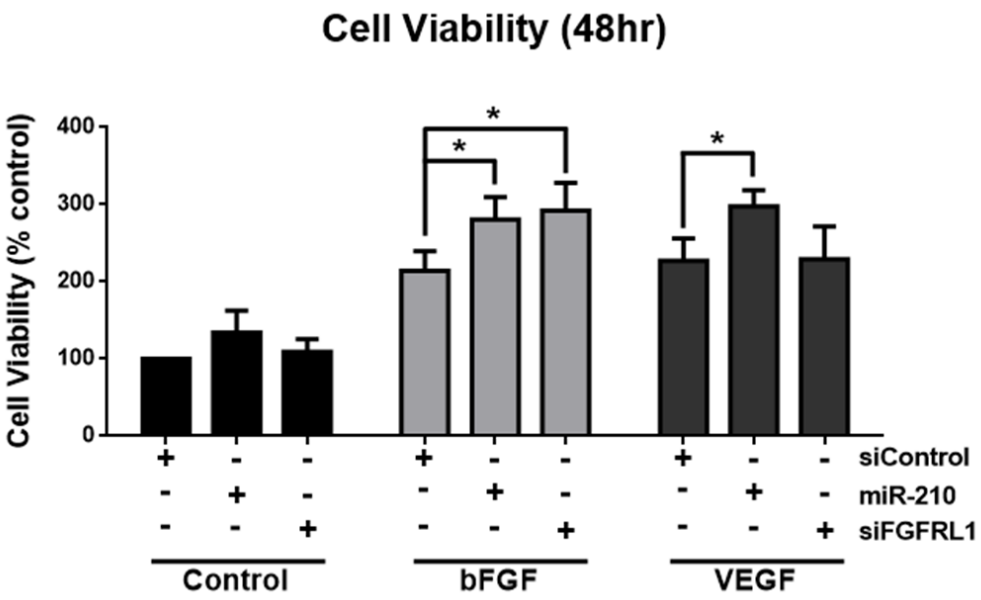

Figure 25 – miR-210 but not FGFRL1 sensitizes HUVEC to VEGF induced proliferation. Cell viability was determined using the Cell Counting Kit-8 (CCK-8) method. HUVECs were transfected with either siC, siFGFRL1, or miR-210. Following serum starvation HUVECs were then plated in low (1%) serum in the presence of bFGF (10ng/ml) or VEGF (100ng/ml) and allowed to proliferate for 48 hours. Data represent mean +/- SD from three independent experiments normalized to control (siC +bFGF). *P < 0.05.

FGFR phosphorylation has been identified to activate JAK/STAT and PLCy1/Ca^{2+} signaling pathways. We wanted to identify if FGFRL1 also played a role in negatively regulating these networks. Data are summarized in Figure 26. We found no evidence that knock-down of FGFRL1 influenced bFGF stimulation of these pathways. Our reports are consistent with other studies that show bFGF does not stimulate calcium signaling in endothelial cells, which is necessary for EC migration (168).

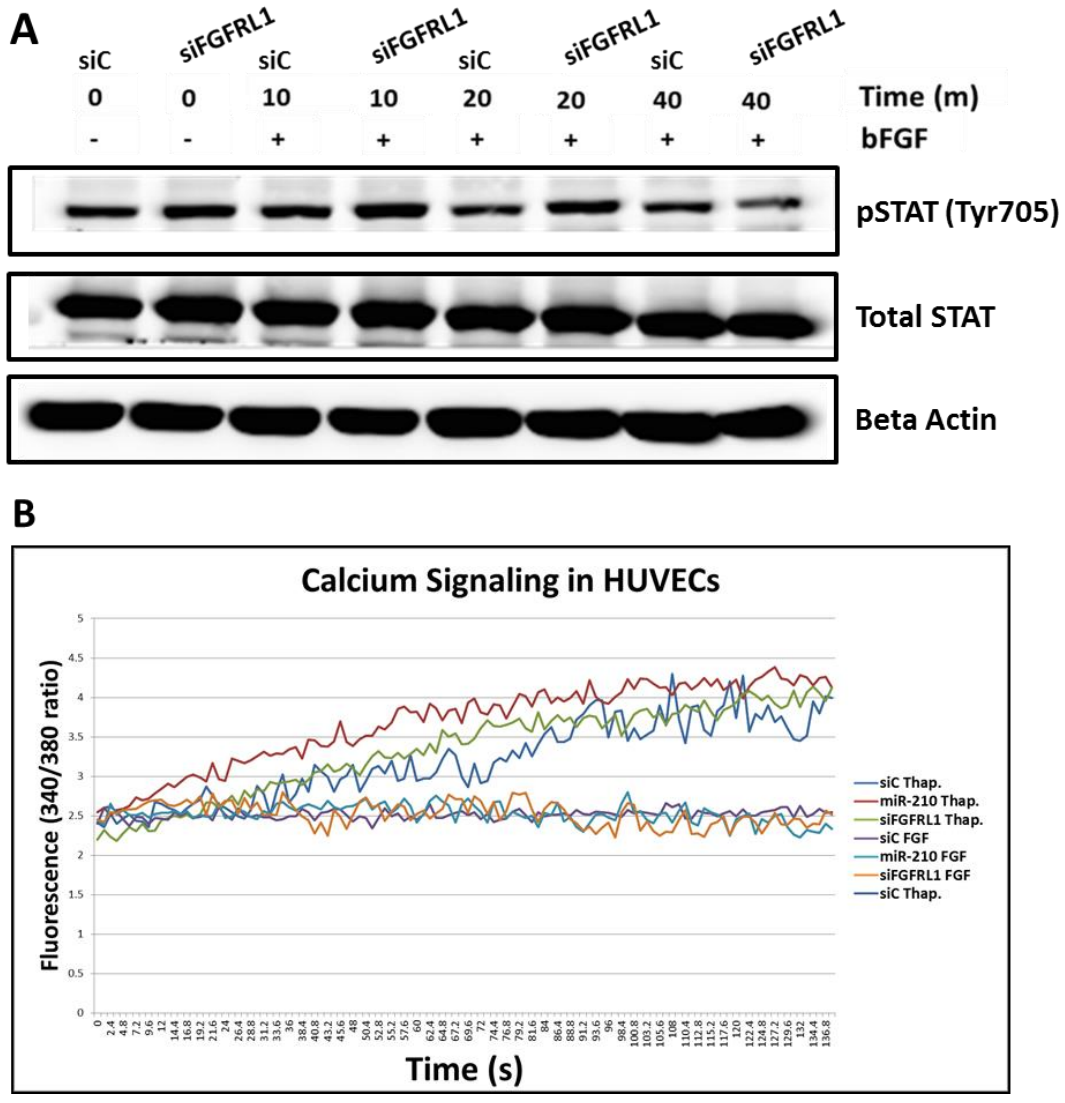

Figure 26 – Suppression of FGFRL1 had no effect on bFGF induced STAT or Calcium signaling. (A) Representative immunoblot of siFGFRL1 or siC treated HUVEC stimulated with

bFGF (10ng/ml) for 10, 20, and 40 minutes. pSTAT1/STAT1 and Beta Actin levels were probed. (B) bFGF does not induce intracellular Ca2+signaling in HUVEC as compared to positive control, Thapsigargin. siRNA treated HUVECs were loaded with fura 2-AM to monitor intracellular Ca2+ concentration as described in the methods section. Upper lines indicated by the arrow represent Thapsigargin treated control. bFGF (10ng/ml) treated cells remained at baseline indicating no calcium release.

FGFRL1 localization in primary endothelial cells – To help us further understand the role that FGFRL1 plays in the endothelial cells, we performed immunofluorescent studies to characterize the localization of FGFRL1 in HUVECs. FGFRL1 protein has unique structural and functional domains that contribute to its function and cellular trafficking (Fig. 27).

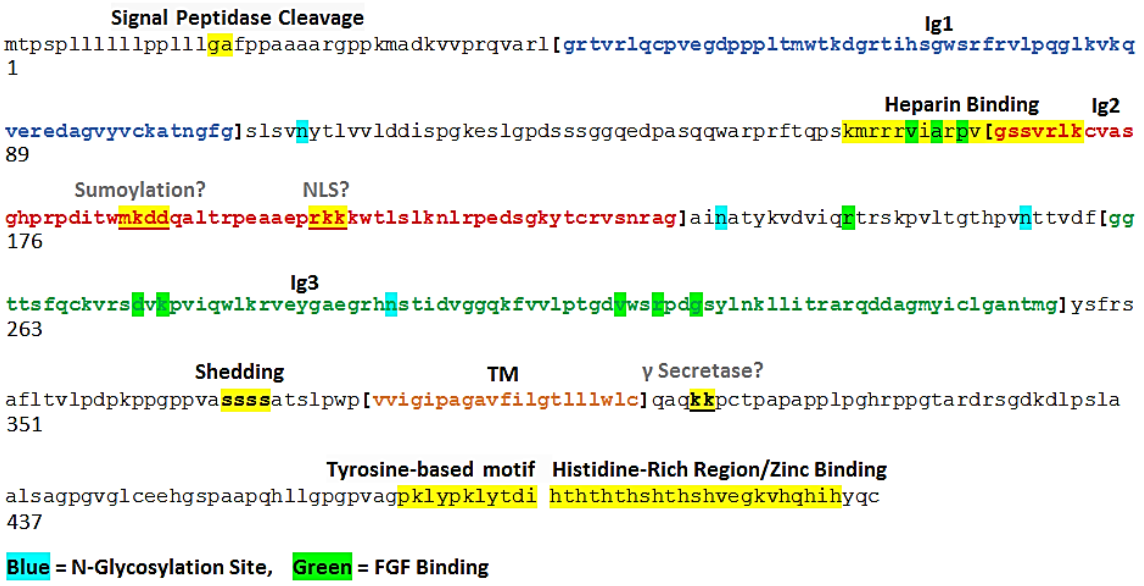

Figure 27 – FGFRL1 amino acid sequence and functional group map. Blue, red, and green amino acids in parenthesis represent the Ig1, Ig2, and Ig3 domains respectively. Orange amino acids represent the transmembrane domain (TM). Asparagine (n) highlighted in blue indicate N-Glycosylation sites. Amino acids highlighted in green are important for FGF binding. FGFRL1 has also been shown to interact with heparin as highlighted in yellow. The S-S-S-S motif upstream of the TM region has been shown to be important for shedding of the receptor. Near the C-terminal end, the Tyrosine-based motif is likely important for intracellular trafficking and the Histidine-rich

region important for zinc binding. In the Ig2 domain, prediction analysis reveals a potential Sumoylation cite (M-K-D-D) and nuclear localization signal (R-K-K). Prediction programs including cNLS, NucPred, and NLStradamus were used to identify the potential NLS. Prediction programs including GPS-SUMO, SUMOplot, and JASSA were used to identify potential Sumoylation consensus sequences. The predicted NLS and SUMO sites are not conserved among other FGFR family members.

Due to its potential to be cleaved, antibodies against the amino-terminal (N') and carboxy-terminal (C') regions of FGFRL1 were used for our immunofluorescence studies to follow up the cleavage products. Interestingly, the staining for endogenous FGFRL1 in HUVECs was primarily localized to the cytoplasm and nucleus, and as predicted FGFR1 localized to the cell membrane (Fig. 28). Both the N' and C' terminus of FGFRL1 was detected in the cytoplasm and nucleus. However, the pattern of localization in the nucleus was quite different between the two, suggesting that a cleavage event may also occur in HUVECs. FGFRL1 C' looked diffuse throughout the nucleus, while FGFRL1 N' was localized to discrete punctate that were approximately 1 μm in size (Fig. 28). In order to help confirm these results, we performed western blot analysis on lysates harvested from HUVEC culture medium, cytoplasmic, and nuclear fractions (Fig. 29A). In addition, these lysates were taken from HUVECs treated in hypoxia and normoxia. We were able to detect large amounts of FGFRL1 secreted into the culture media, and could detect FGFRL1 both in the nucleus and cytoplasm. An antibody against only the FGFRL1 C' (~14kDa) was detected in both the cytoplasmic and nuclear fractions. In addition, we found that the FGFRL1 levels were decreased in hypoxia in each of the cell compartments as indicated by fold change (Fig. 29A). Immunofluorescent staining also confirmed that FGFRL1 levels in the cytoplasm and nucleus were decreased by treatment with either hypoxia or miR-210 (Fig. 29B).

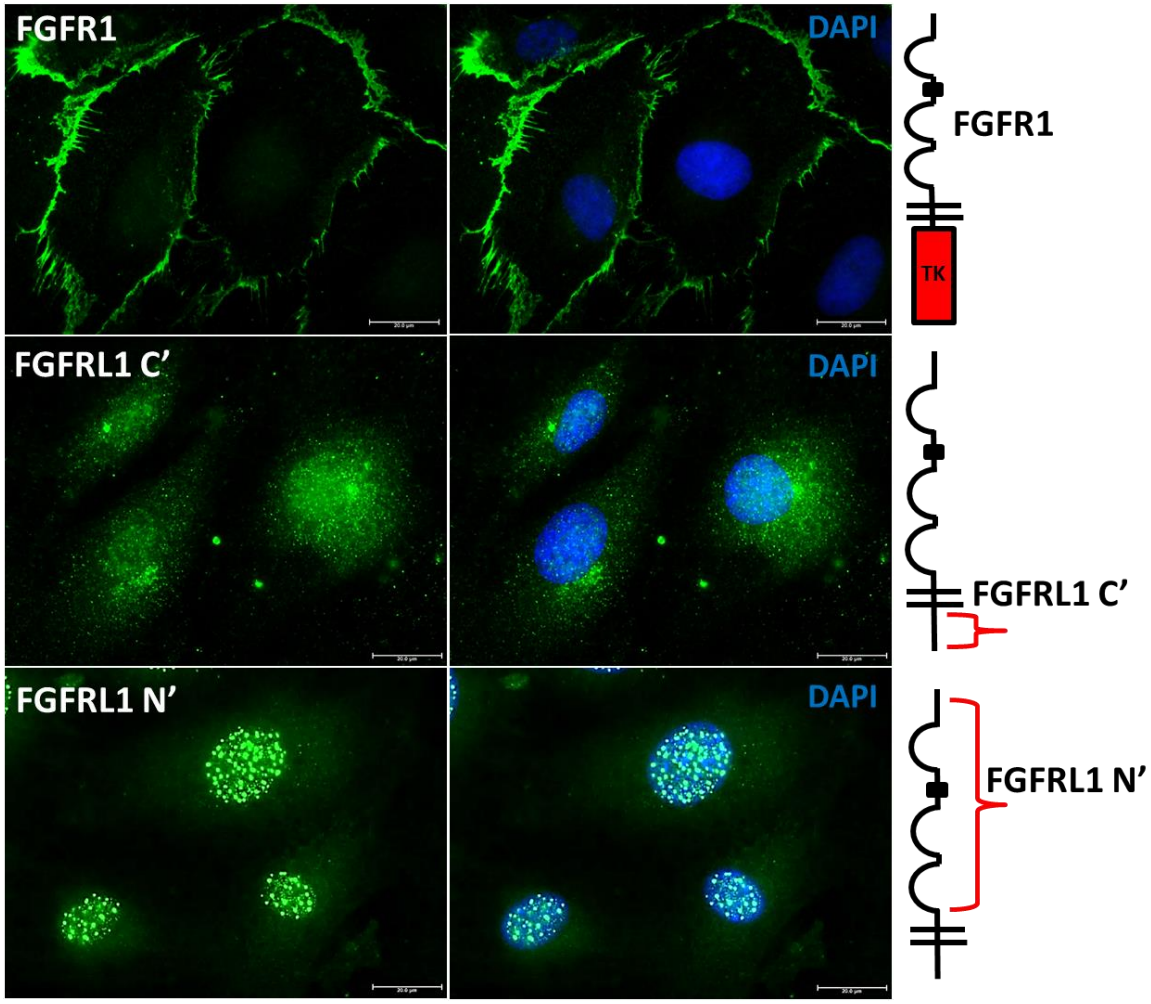

Figure 28 – FGFRL1 N' and C' terminal localization in HUVEC. (A) Immunofluorescence staining of FGFR1, FGFRL1 C-terminus, and FGFRL1 N' terminus in HUVECs (green). Cells were prepared as described in the methods section. Nuclei stained with DAPI. Scales represent 20μm. Images were captured using Leica DM5500 B microscope.

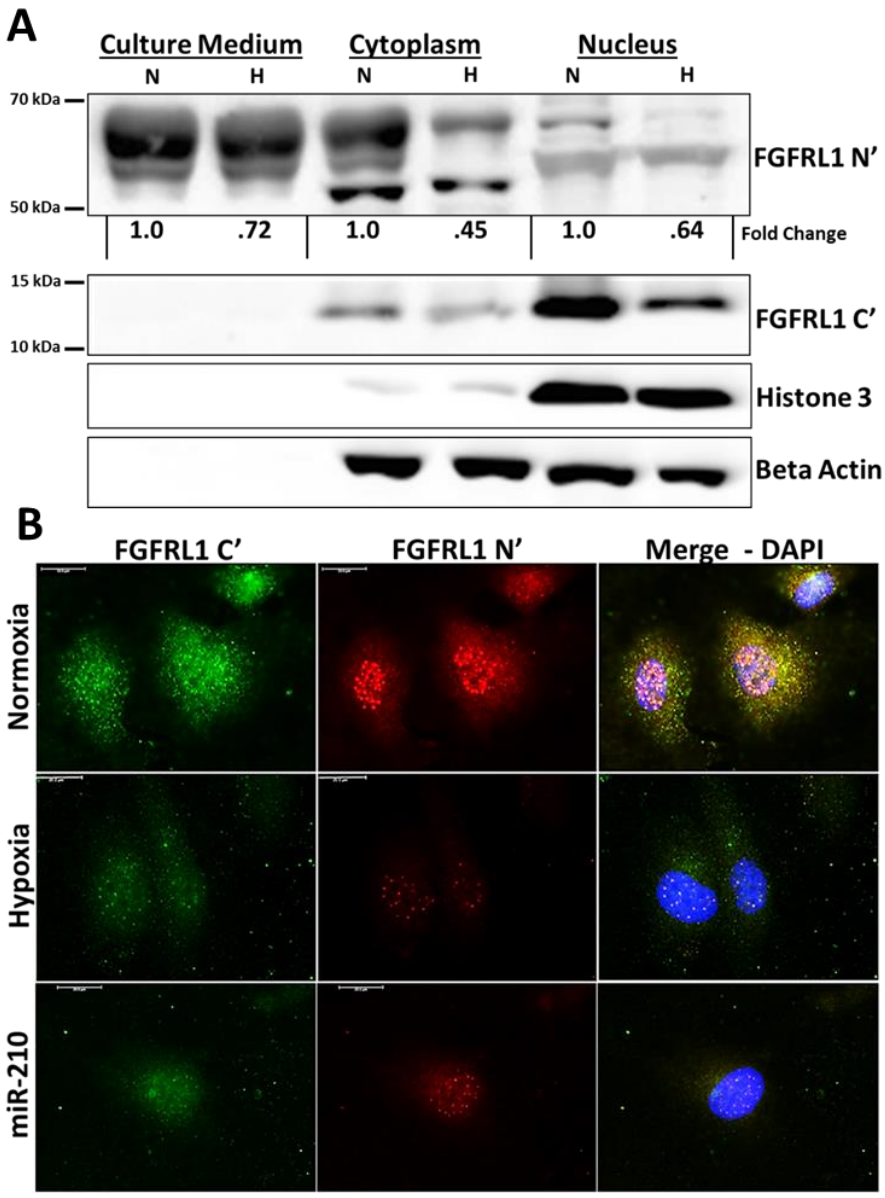

Figure 29 – FGFRL1 compartmentalization in HUVEC. (A) Representative immunoblots of HUVEC culture medium, cytoplasmic, and nuclear fractions. Fractioned lysates collected from cells in normoxia (N) and hypoxia (H) for 48 hours. Blot probed for FGFRL1 N' and C' terminal regions. Fold change of FGFRL1 levels in hypoxia compared to normoxia represented. Levels based on densitometric quantification of bands and normalized to the normoxia protein level. Histone 3 (nuclear) and Beta Actin used as loading controls. (B) Immunofluorescent staining of FGFRL1 N' (red) and C' (green) in HUVECs. Cells cultured in normoxia, hypoxia, or treated with miR-210. Images on the right column are merged with DAPI nuclear staining. Scales represent 20μm.

Because we were able to detect FGFRL1 in different of cellular compartments, we wanted to understand if FGFRL1 from all the fractions sequestered bFGF. After collecting lysates from the culture media, cytoplasmic, and nuclear fractions we used immunoprecipitation to pull down FGFRL1 N' from each of these compartments. Using western blot we probed for bFGF from the immunoprecipitates, and were able to detect bFGF in all endothelial cell compartments including the culture medium (Fig. 30A). Immunofluorescent studies also suggest bFGF-FGFRL1 interaction (Fig. 30B). Overall these results help us to partly elucidate the role of FGFRL1 in endothelial cells. We were able to confirm that FGFRL1 is secreted from HUVEC cells. However, further studies will be necessary to help us understand why and how FGFRL1 is going to the nucleus, and if it has any physiological significance.

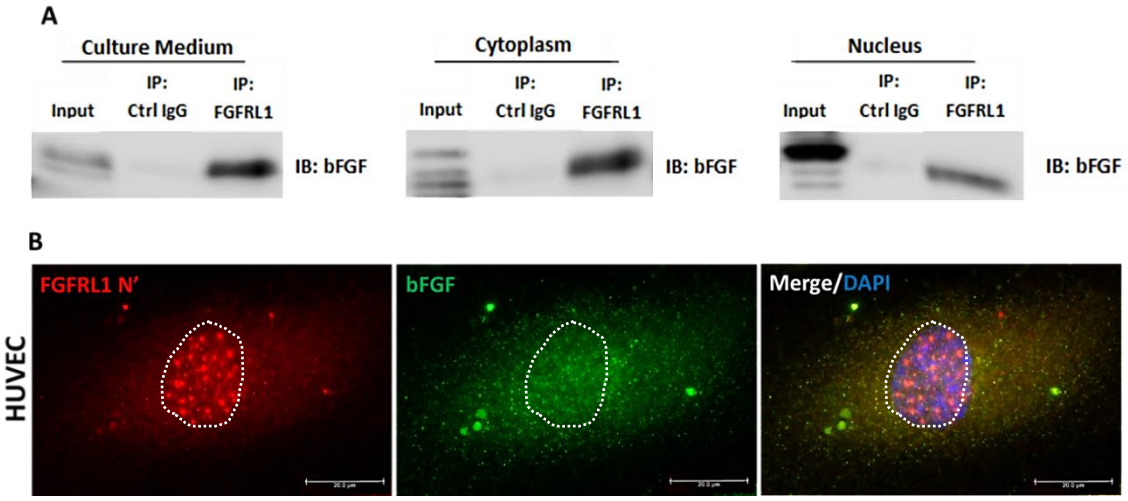

Figure 30 – Co-localization and co-IP of FGFRL1 with bFGF. (A) Co-Immunoprecipitation (IP) of FGFRL1 – bFGF. HUVEC culture medium, cytoplasmic, and nuclear fraction lysates were incubated O/N with FGFRL1 antibody and then with Agarose Plus A/G beads at 4*C, as described in the materials methods section. Immunoblot (IB) analysis was performed using anti-bFGF. Positive control (lane 1) represents input signal from total lysate. Negative control (lane 2) showed as lysate incubated with IgG control. (B) Immunofluorescent colocalization studies of FGFRL1 N' (red) and bFGF (green) staining of HUVECs. Images on the right column are merged with DAPI nuclear staining. Scale represents 20µm.

FGFRL1 localizes to Promyelocytic leukemia (PML) nuclear bodies in HUVECs – After our initial findings, we wanted to investigate where FGFRL1 was localizing in the nucleus. By using immunofluorescence staining we were able to identify the nuclear punctate as Promyelocytic leukemia (PML) nuclear bodies (NBs).

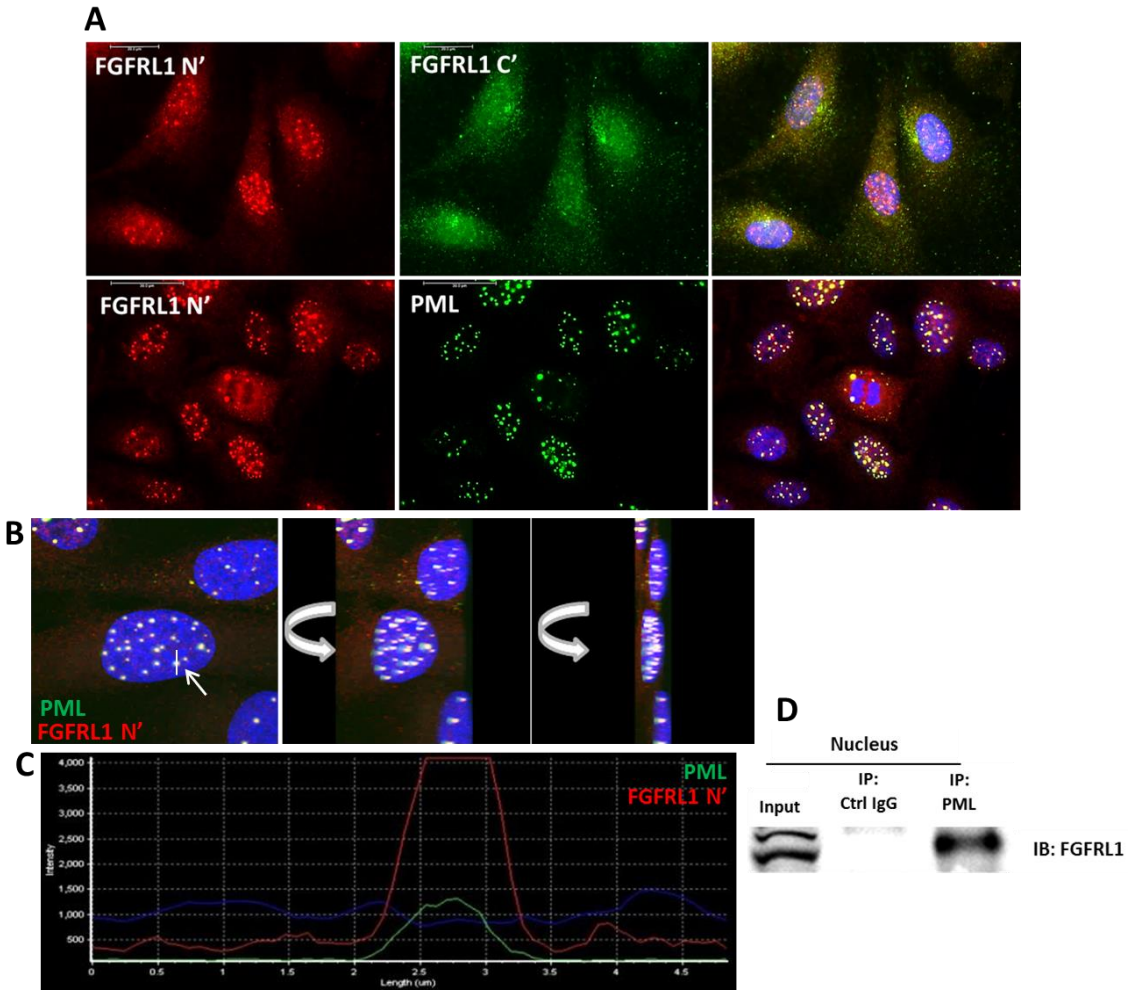

Figure 31 – FGFRL1 localizes to Promyelocytic leukemia (PML) nuclear bodies in HUVECs. (A) Top row: Representative immunofluorescence images of FGFRL1 N' (red) and FGFRL1 C' (green) in HUVEC. Co-localization represented in the merged image on the right. Bottom row: Representative immunofluorescence images of FGFRl1 N' (red) and PML (green) in HUVEC. Images acquired using Leica DM5500 B microscope. White scale bars represent 20um (top) and 30um (bottom). (B) Z-stack images (consisting of flattened image slices superimposed) of nuclei in HUVECs. Images are rotated to show co-localization. Immunofluorescence staining of FGFRL1 N' (red) and PML (green). Intensity of a single NB (as shown by the white arrow) was measured

and is represented in the graph on the below. (C) Green and red peaks represent immunofluorescence signal intensity over a measured distance. (D) Co-Immunoprecipitation (IP) of PML – FGFRL1. Immunoblot (IB) analysis was performed using anti-FGFRL1.

FGFRL1 N' specifically colocalized to PML NB aggregates (Fig. 31A). FGFRL1 N'and C' were both detected in the nucleus, however only FGFRL1 N' could be visualized in discrete nuclear punctate (Fig. 31A). In order to validate our colocalization findings, we utilized confocal microscopy to obtain Z-stack images of HUVEC nuclei co-stained with FGFRL1 N' and PML protein (Fig. 31B). Additionally, immunofluorescent signal intensity from FGFRL1 N' and PML overlapped as the distance of a single NB was measured (Fig. 31C). We further confirmed our results by immunoprecipitating PML protein from HUVEC nuclear lysates, and used western blot to confirm FGFRL1 interaction with PML protein (Fig 31D).

In the next series of experiments, we decreased or disrupted PML body formation in order to gain additional insight on FGFRL1 localization. Like FGFRL1, PML has also been shown to be indirectly downregulated by HIF1a during hypoxia (169). Our studies confirm that HUVECs treated with hypoxia displayed both decreased nuclear FGFRL1 and PML levels (Fig. 32A, top two rows). In addition, HUVECs treated with hypoxia had less PML nuclear bodies compared to cells in normoxia (Fig 32B). PML protein levels were also decreased in hypoxia as measured by western blot (Fig. 32C). Next, we used PML siRNA to decrease the number of PML NBs in HUVECs (Fig. 32A, third row). After decreasing PML, we measured a nearly 2-fold increase in the amount of FGFRL1 in the cytoplasm, and a decrease in the amount in the nucleus (Fig. 32D). These results confirm that FGFRL1 is sequestered to PML NBs. Next, because both PML and FGFRL1 are capable of binding zinc ions, and zinc is important for PML NB structure and formation (154, 170, 171), we used zinc ion chelator, TPEN, to disrupt

FGFRL1-PML localization. Strikingly, we were able to disrupt PML NB formation, however both PML protein and FGFRL1 N' remained at high concentrations in the nucleus in a diffuse pattern (Fig. 32A bottom row and 32D). The exact function of the zinc binding domain of FGFRL1 has yet to be characterized. However, it is possible that the zinc domain is required for some protein-protein interactions in the nucleus.

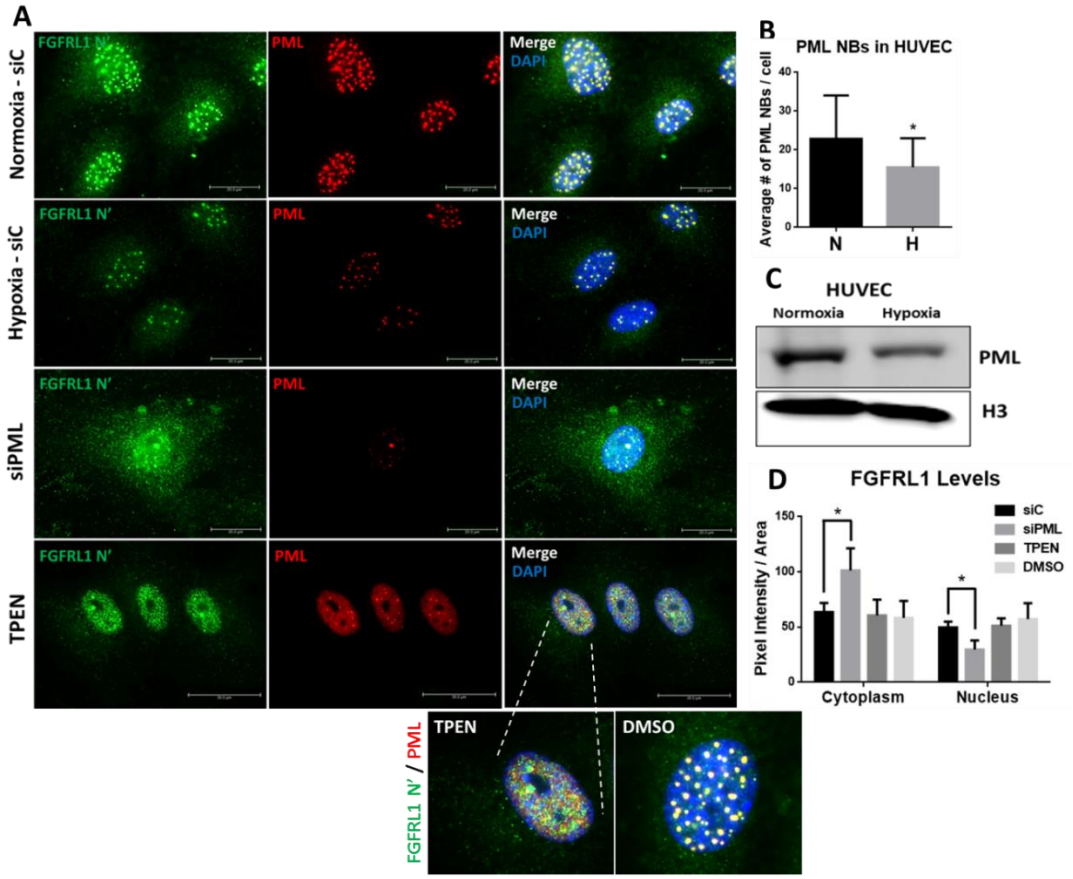

Figure 32 – FGFRL1 is sequestered to PML NBs and both are decreased in hypoxia. (A) FGFRL1 N' (red) and PML (green) immunofluorescent staining on HUVECs treated with normoxia (siC), hypoxia (siC), siPML, TPEN (10uM), or DMSO control (image not shown). (B) Average number of PML NBs per cell in HUVECs treated with normoxia and hypoxia. Error bars show SD. *P < 0.05. (C) HUVEC nuclear lysates were collected from cells treated in N/H. Western blot shows levels of PML protein. (D) Measure of nuclear and cytoplasmic FGFRL1pixel intensity in HUVECs treated with siC, siPML, TPEN, or DMSO. Bars represent average pixel intensity in the cytoplasm and in the nucleus divided by the area of the measured cell. Error bars show +/- SD. *P < 0.05.

In other cell lines, HEK293T express virtually no PML protein (Fig. 33B), and when we stain them for FGFRL1 most of the localization is found in the cytoplasm (Fig. 33A). In MCF10a cells, FGFRL1 is primarily localized to the cytoplasm (Fig. 33C). However, in MCF-7 cells we see nuclear expression, but an absence of PML NB punctate. Western blot analysis confirms differential regulation of FGFRL1 in MCF-10a and MCF7 cells (Fig. 33D). It is possible that FGFRL1 may have an alternative role in cells that do not express PML nuclear bodies, such as cancer and other transformed cells. Future studies will help us to understand nuclear FGFRL1 and its function.

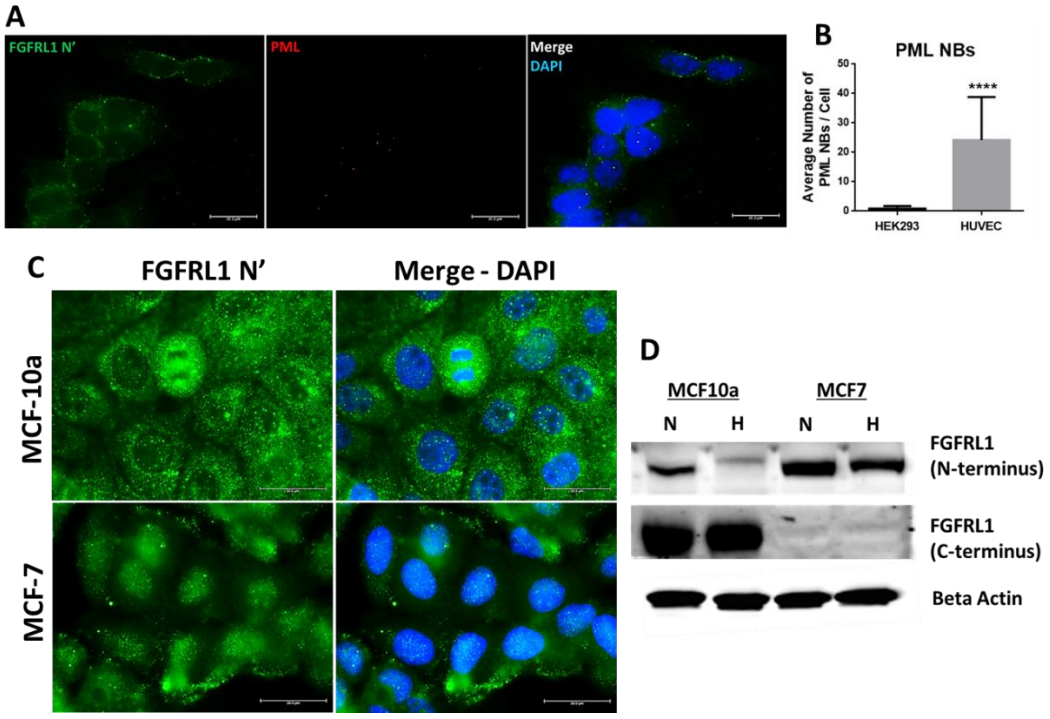

Figure 33 – FGFRL1 localization in non-endothelial cell lines. (A) Representative immunofluorescent images of FGFRL1 N' (green) and PML (red) in HEK 293 cells. (B) The average number of PML bodies per HEK 293 and HUVEC cell was quantified and represented in the histogram. ****P < 0.0001. (C) Representative immunofluorescent images of FGFRL1 N' in mammary epithelial non-tumorigenic cells (MCF10a) and human breast adenocarcinoma cells (MCF7). Images on the right are merged with DAPI nuclear staining. Scales represent 20μm. (D) Representative immunoblots of MCF10a and MCF7 cells in normoxia (N) and hypoxia (H). Blot probed for FGFRL1 N' and C' terminal regions.

Using a construct to overexpress FGFRL1 (FGFRL1-venus or RL1ven) in HUVEC, we further confirmed its role in endothelial cell proliferation. Compared to GFP control cells, RL1ven HUVECs showed decreased proliferation (Fig. 34A).

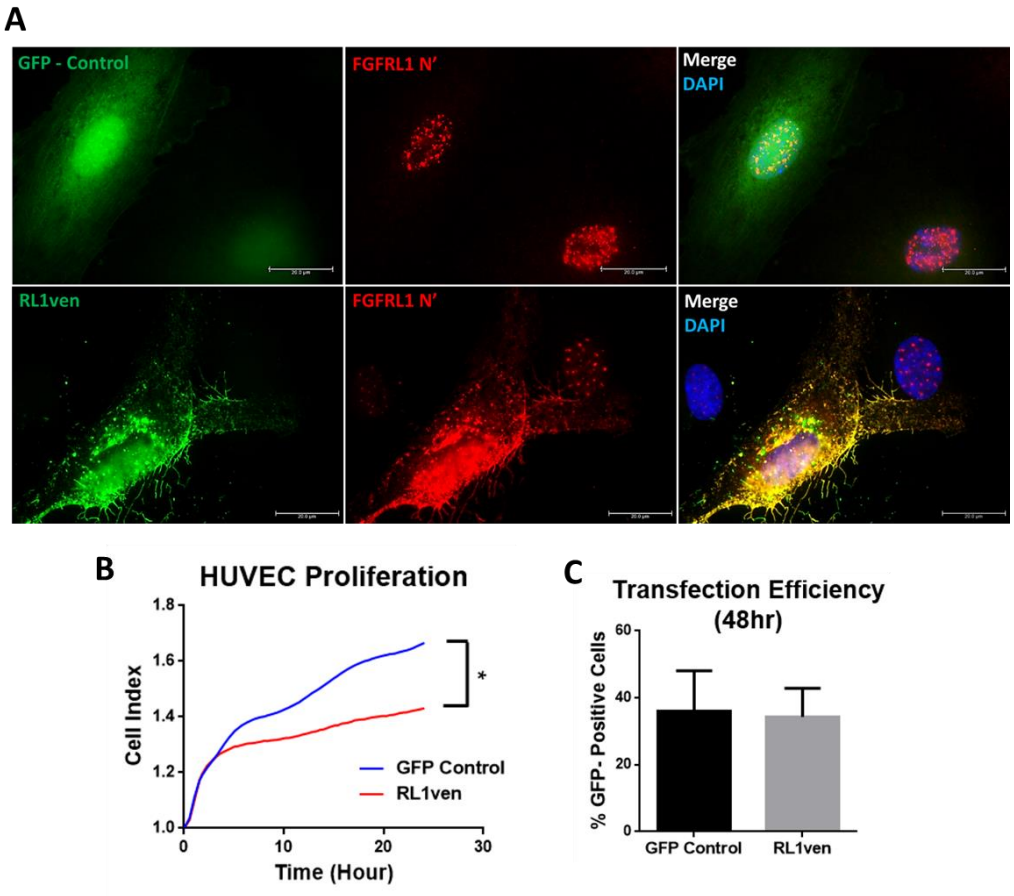

Figure 34 – Overexpression of FGFRL1 decreases EC proliferation. (A) Overexpression of FGFRL1 in HUVECs. Representative images of cells that were transfected with a plasmid construct containing FGFRL1 C-terminal tagged venus fluorescent protein (RL1ven). GFP expression construct used as a control. Cells were fixed 48 hours after transfection followed by immunofluorescent staining for FGFRL1 N' (red). Nuclei were stained with DAPI. Scale bar represents 20um. (B) Real time proliferation assay of HUVEC overexpressing FGFRL1 (RL1ven) or GFP control. After cell recovery from transfection, HUVECs were transferred to an E-plate to proliferate for 24 hours. Cell index indicates electrical impedance measurements. *P< 0.05 at the 24 hour time point. Transfection efficiency (%) is calculated in C. Construct provided by Kilkenny D. (95).

The role of miR-210 in developmental angiogenesis – In order to establish the physiological relevance of our *in vitro* findings, we carried out the next series of experiments to characterize the role of miR-210 and FGFRL1 on angiogenesis was performed using *in vivo* zebrafish (data from Alexey Benumov) and mouse models.

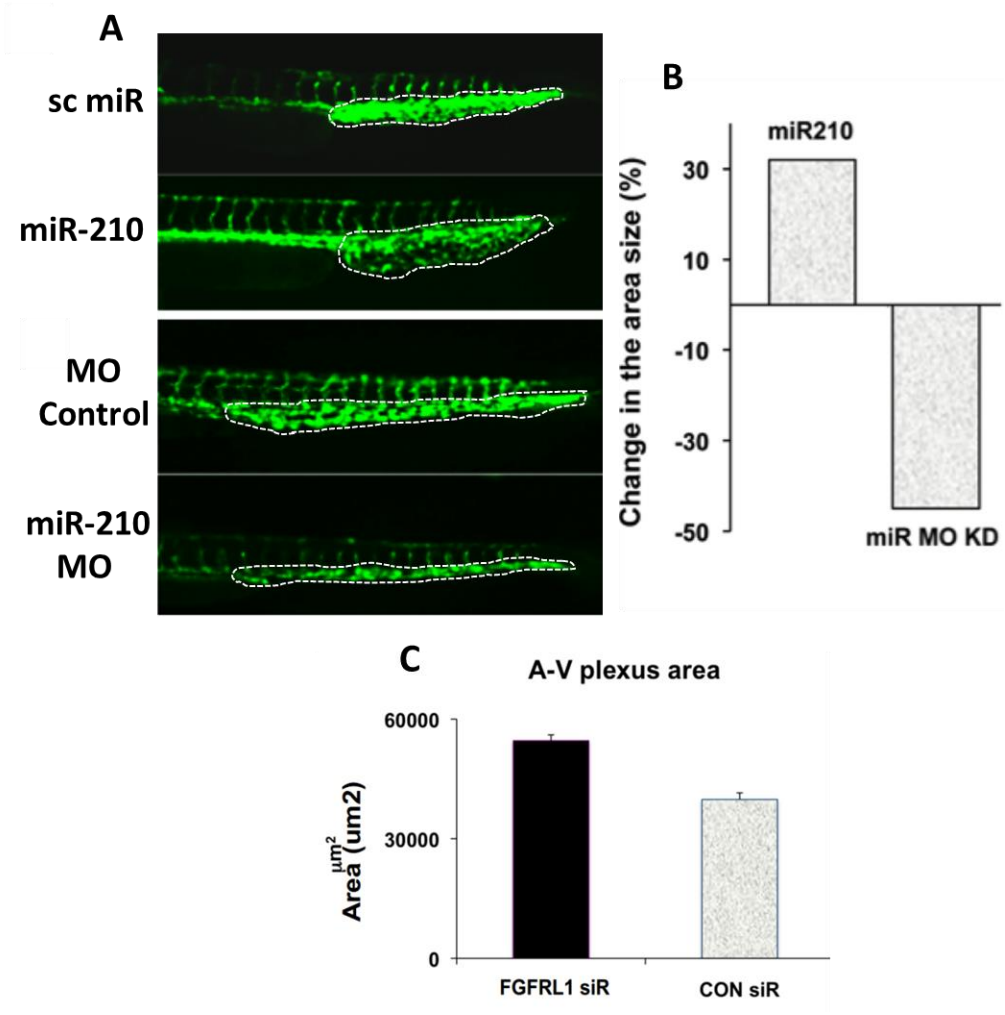

Figure 35 – miR-210 and FGFRL1 regulate developmental angiogenesis in zebrafish. (A) Fluorescence microscopy of Tg(fli-gfp) zebrafish caudal vein plexus (CVP). Embryos were injected with either miR-210 or miR-210 morpholino (MO); miR-control or control MO respectively. CVP area was analyzed 36 hpf (area outlined by white-dashes). (B) Change in the area size (%) was quantified and represented in the top histogram. (C) Tg(fli-gfp) zebrafish embryos were injected with either siFGFRL1 or siControl and the CVP was analyzed 36 hpf. Histogram

represents the average area (um^2) of the CVP in siFGFRL1 (black) and siC (gray) zebrafish. Data from Alexey Benumov.

First, transgenic zebrafish expressing EGFP in vascular endothelium were utilized, and embryos were injected with either miR-210 or miR-210 morpholino. After 36 hours post fertilization the caudal-vein plexus (CVP) was analyzed. Our results show that miR-210 significantly increased the area of the CVP compared to scrambled control (Fig 35A, B). In the reciprocal experiment, miR-210 morpholino caused a decrease in the area of the CVP (Fig. 35A, B). Next, siFGFRL1 was injected into embryos, causing an increase in the CVP area compared to siControl (Fig. 35C). These results confirm that miR-210 and FGFRL1 may play a role in developmental angiogenesis in zebrafish.

miR-210 KO mice were generated by our collaborator, Dr. Yan Zeng as described in the methods section and shown in figure 36A. miR-210 loss was confirmed using both tail-snip genotyping and qPCR analysis (Fig. 36B).

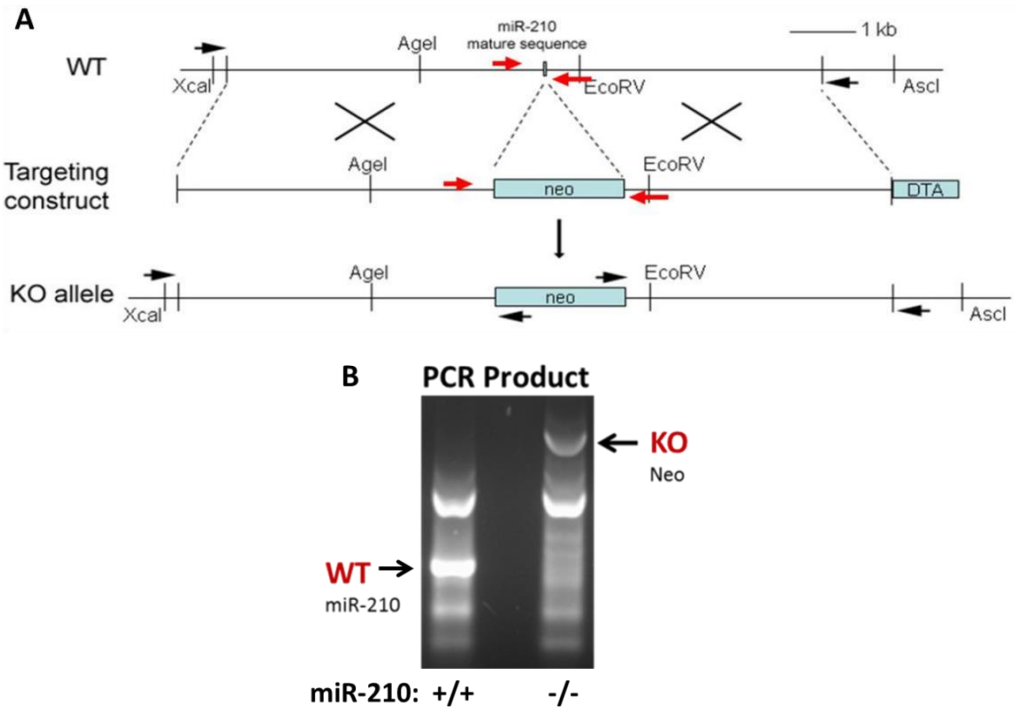

Figure 36 – Generation of miR-210 KO (-/-) mice. (A) Diagram of the targeting construct used in miR-210 KO mice generation. (B) PCR fragments of WT (lane 1) and miR-210 -/- mice (lane 2). Only the mature miR-210 sequence was deleted and replaced by a neomycin resistance gene cassette (designated as “neo”). Mice generated in collaboration with Dr. Yan Zeng.

Loss of miR-210 did not affect development and KO mice did not show any gross phenotype. Next, we examined whether the target for miR-210, FGFRL1 expression levels were changed in the miR-210 KO mice. Results in Figure 37A, B shows q-PCR data confirming the loss of miR-210 in KO mouse endothelial cells isolated from lung tissue. Then we determined the protein levels of FGFRL1 in miR-210 KO endothelium and adipose tissue by westernblots (Fig. 37C). Loss of miR-210 resulted in higher levels of FGFRL1 in both the tissues which was further confirmed by confocal imaging (Fig. 37E). Treatment of miR-210 KO mouse endothelial cells with hypoxia failed to significantly reduce FGFRL1 levels compared to WT mouse endothelium (Fig. 37D).

Developmental angiogenesis was analyzed in the miR-210 KO mice by performing immunofluorescent staining of the vascular endothelium in neonatal mouse retinas. As described in the methods section, mouse retinas were obtained from P5 mice and stained with isolectin GS-IB4. We found no changes in the miR-210 KO vascular network compared to WT mice (Fig. 38). Additionally, we found no differences in length of the vascular plexus (Fig. 39A-B), or in the number of tip cells at the vascular periphery (Fig 39C-D). There was no significant difference in the vessel density, branch points, or empty sleeves in miR-210 KO mice compared to WT control animals (Fig. 39 E-H).

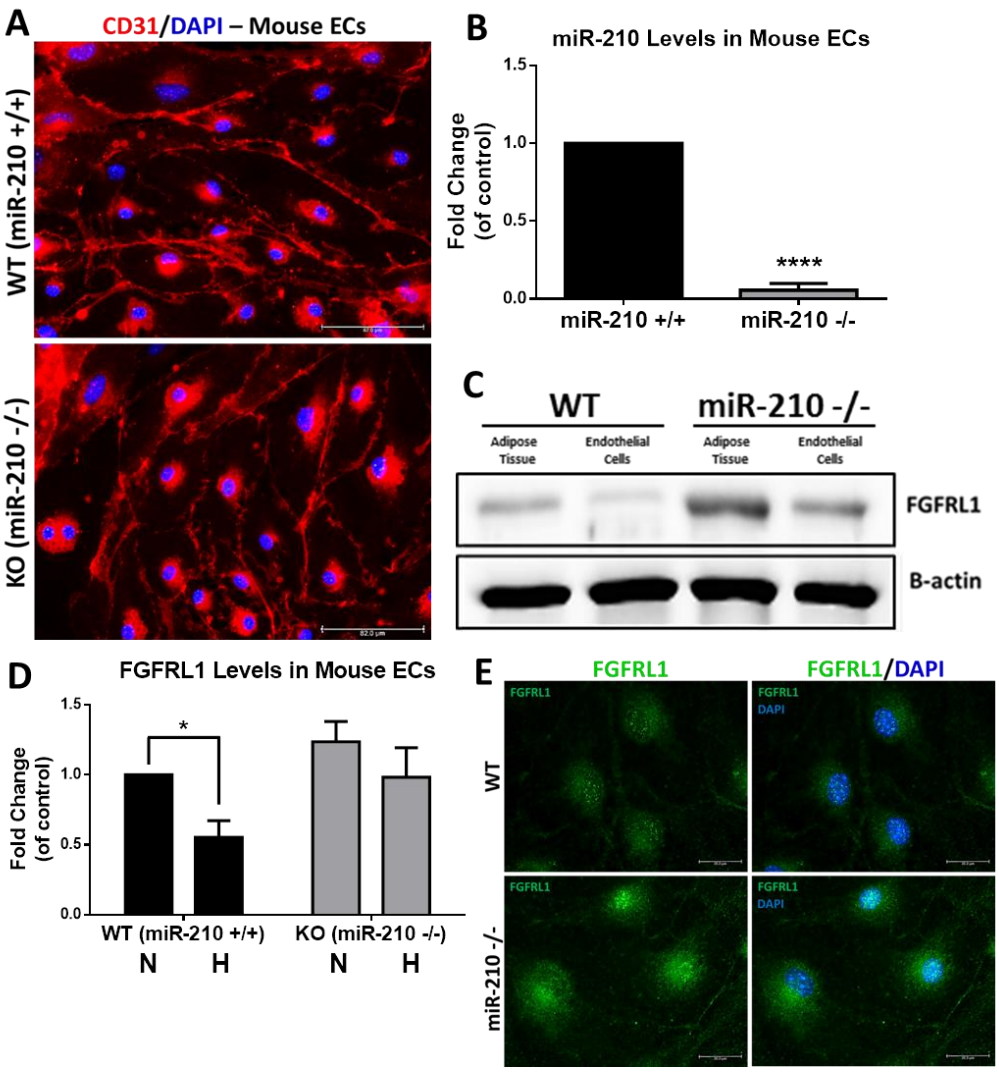

Figure 37 – FGFRL1 levels are increased in miR-210 KO mouse ECs. (A) Mouse endothelial cells harvested from WT and miR-210 KO lungs using magnetic beads as described in the methods section. Cells were plated on gelatin coated coverslips then fixed with 4% PFA and stained with CD31 to confirm endothelial cell populations. (B) Histogram shows qPCR data confirming loss of miR-210 expression in the miR-210 -/- mice compared to WT (miR-210 +/+) mice. RNA was extracted from mouse (n=5) lung endothelial cells as described in the methods section. ****P < .0001. (C) Representative immunoblots of FGFRL1 protein expression in WT compared to miR-210 -/- mouse tissues. Lysates were prepared from adipose tissue and lung endothelial cells. (D) Data represent FGFRL1 levels in endothelial cells from miR-210 KO and WT mice as measured by qPCR. Cells were cultured in normoxia or hypoxia for 24 hours. Bars show fold change +/- SD; *P < 0.05, **P< 0.01. (D) FGFRL1 (green) immunostaining in WT and miR-210 KO endothelial cells.

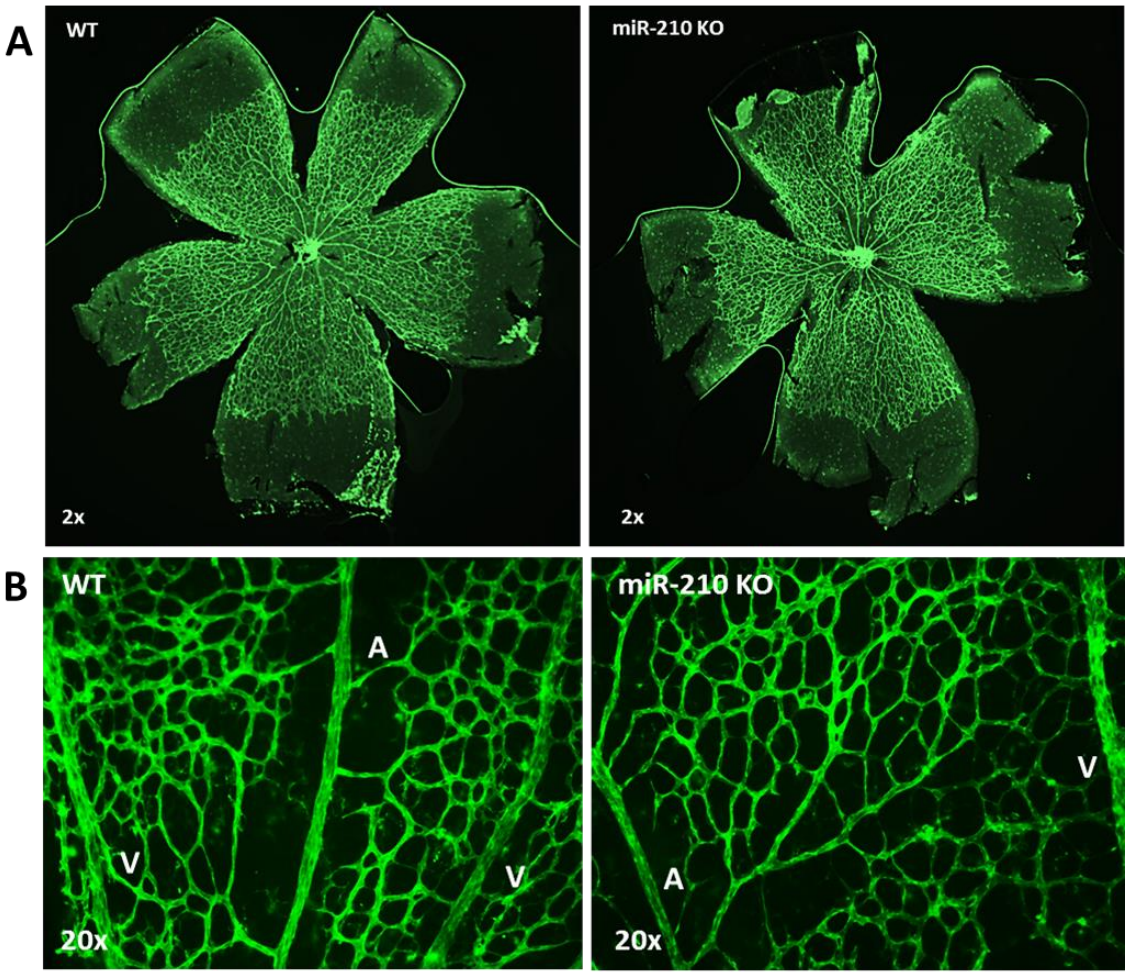

Figure 38 – Developmental angiogenesis is normal in miR-210 KO mice. (A) Visualization of retinal vasculature by CD31 (green) whole-mount immunofluorescence staining in WT and miR-210 -/- (P5) mouse retinas. Images taken at 2X and 4X magnification with the Nikon AZ100M Fluorescence Microscope. (B) Representative images of arterial (A) and venous (V) architecture at 20X magnification.

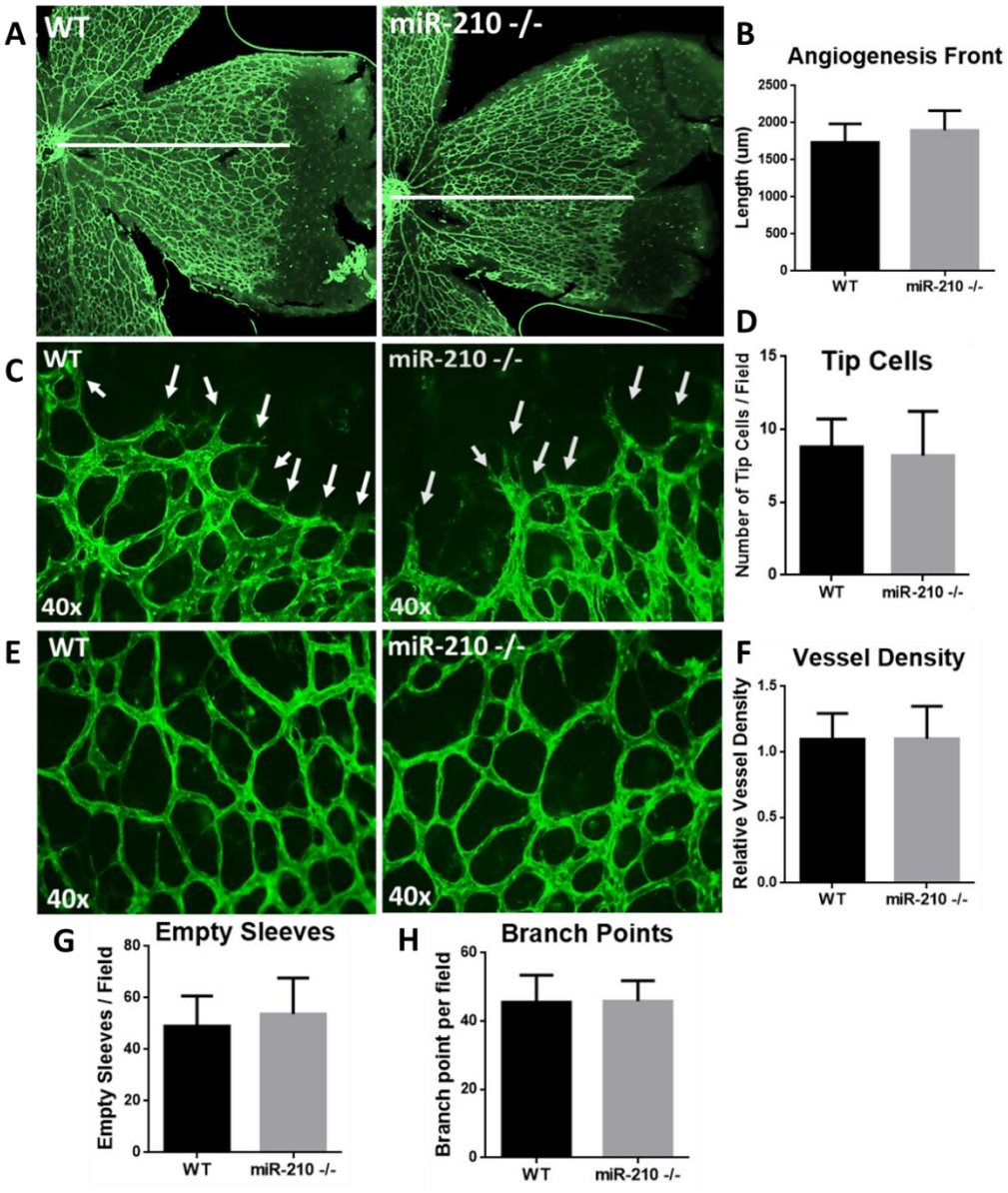

Figure 39 – No developmental angiogenesis defects in miR-210 KO neonatal mouse retinas. (A) Quantitative analysis of miR-210 KO and WT retina vascularization. Data pooled from three litters containing altogether 6 miR-210 -/- and 8 WT pups. Leica DM5500 B microscope was used. (B) Vessel migration toward the retinal periphery was quantified by measuring total length as illustrated by the white line. (B) Data represent mean length of the vascular plexus (from the optic stalk) +/- SD. (C) Tip cells at the retinal periphery. (D) Data represent mean number of tip cells per field +/- SD in WT and KO retinas. (E) Representative images of the vascular plexus at 40X magnification were used to quantify; (G) Empty sleeves per field, (F) Relative vessel density and (H) mean branch points per field. Error bars show SD.

Pathological angiogenesis is impaired in miR-210 KO mice. – In the first series of experiments we determined whether the response to hypoxia is attenuated in the blood vessels of miR-210 KO mice. For this purpose the aortic ring assay was used. Aortas were obtained from age and sex matched mice, placed on Matrigel containing bFGF, and incubated in normoxic and hypoxic conditions. Vessel sprouting was very similar between WT and miR-210 KO mice under normoxia (Fig. 40A). However, when aortas were subjected to hypoxia, miR-210 KO sprout length was significantly decreased compared to WT microvessels in the presence of bFGF, (Fig. 40B).

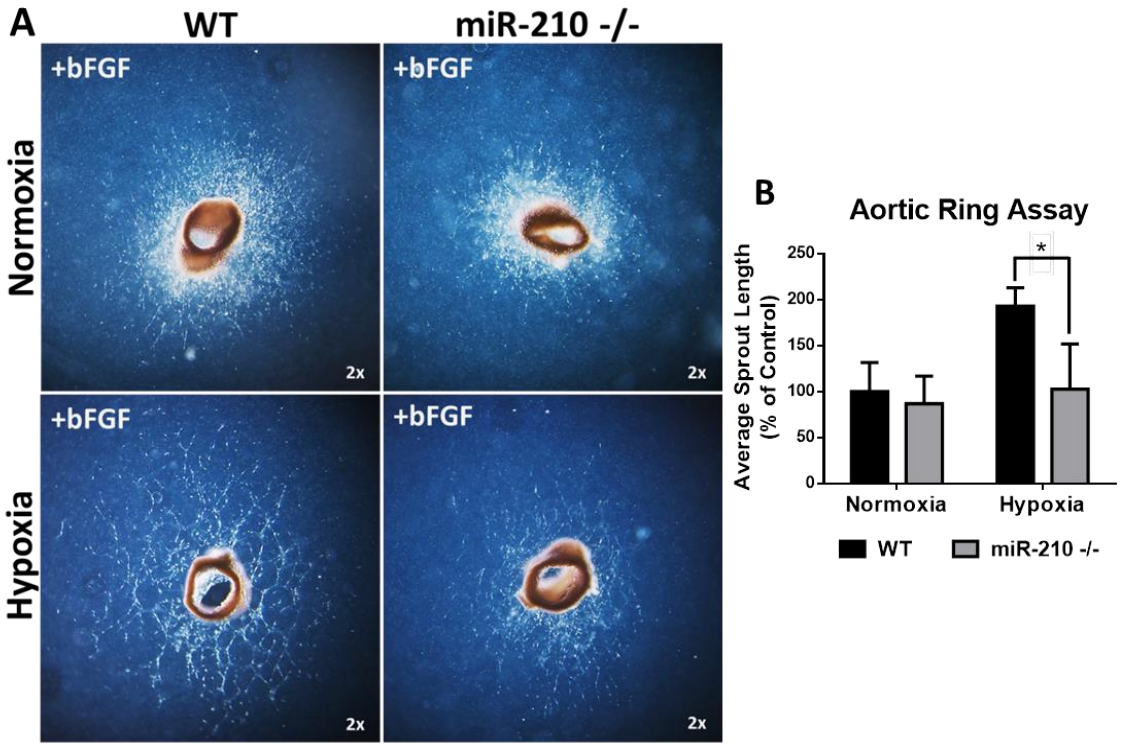

Figure 40 – Microvessel sprout length decreased in miR-210 KO aortas in the presence of hypoxia and bFGF. (A) Representative images of WT and mir-210 -/- aortas in the aortic ring assay taken under a 2X objective on the Nikon AZ100M microscope. Aortas were cultured in the presence of bFGF under normoxic or hypoxic conditions as described in the methods section. (B) Quantitative analysis was performed by measuring sprout length (distance from the aortic ring to the sprout tip). Data pooled from 6 miR-210 -/- mice and 8 WT female mice from at least 3 separate liters. Histogram represents mean sprout length per group +/- SD, *P<0.05.

The next series of experiments focused on FGF-induced angiogenesis in Matrigel plug assays. These data are summarized in Figure 41. Photomicrographs show gross morphology of subcutaneous matrigel plugs. Cellular infiltration induced by FGF was significantly reduced in miR-210 KO mice. Further studies showed CD31 positive blood vessels were significantly reduced in the KO animals. Blood vessel number per field was reduced in miR-210 KO animals when compared to WT (Fig. 41B). Overall, these results suggest that loss of miR-210 attenuated bFGF induced angiogenesis.

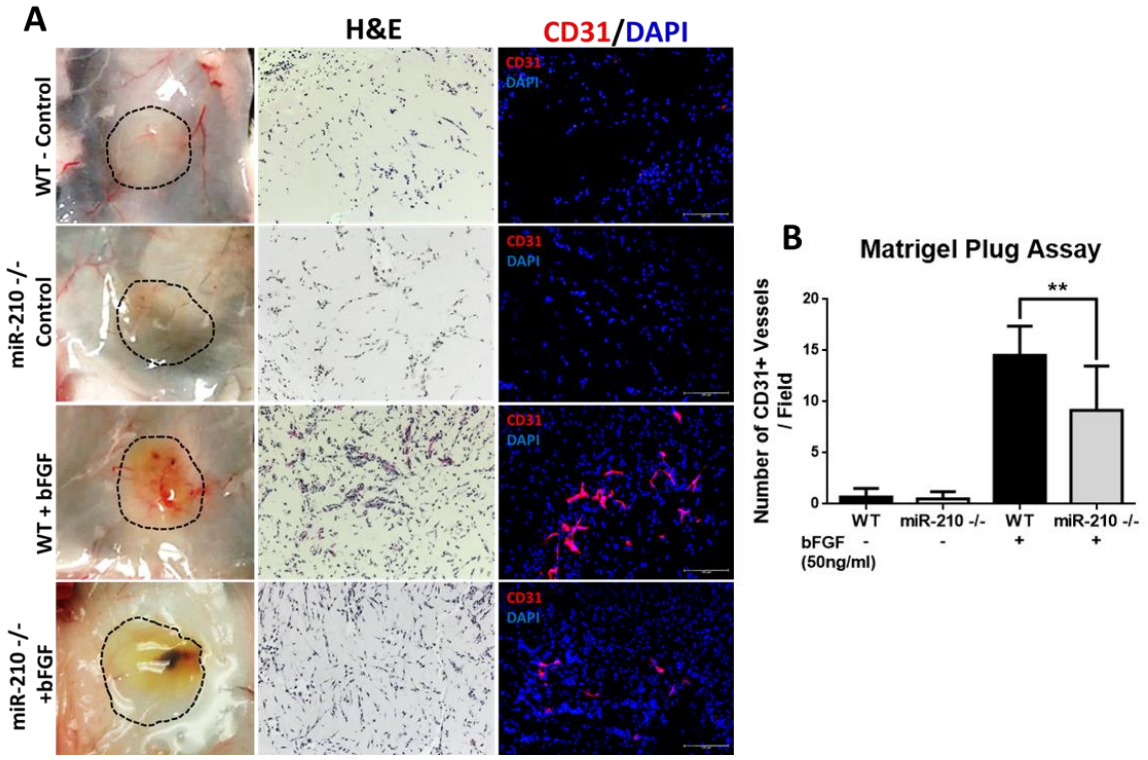

Figure 41 – miR-210 KO mice showed decreased vessel migration toward a bFGF stimulus in the Matrigel plug assay. (A) bFGF-induced angiogenesis in Matrigel (GFR) plugs in WT and miR-210 -/- mice. Representive images of the plugs are shown in the left column. After 10 days, the Matrigel plugs were removed, and either fixed in formalin or flash frozen in OCT. Formalin fixed plugs were paraffin embedded, sectioned, H&E stained (middle column). Flash frozen plugs were sectioned (10um) for staining with DAPI and anti-CD31 (right column). Images taken using Leica DM5500 B microscope. (B) Number of CD31 positive blood vessels per field was quantified and represented in the histogram. Bars represent the mean +/- SD, **P<.01.

Next, we investigated the role of miR-210 on tumor induced angiogenesis. Tumor plugs were implanted on the flanks of miR-210 KO and WT mice and tumor volume was monitored over a 12 day period (Fig. 42B). We noted a significant volume difference on day 10 between the KO and WT mice; however by the end of the study the tumors showed no statistical significance in size. Tumors were next harvested and weighed (Fig. 42A). We found no difference in the overall weight of the tumors (Fig. 42C).

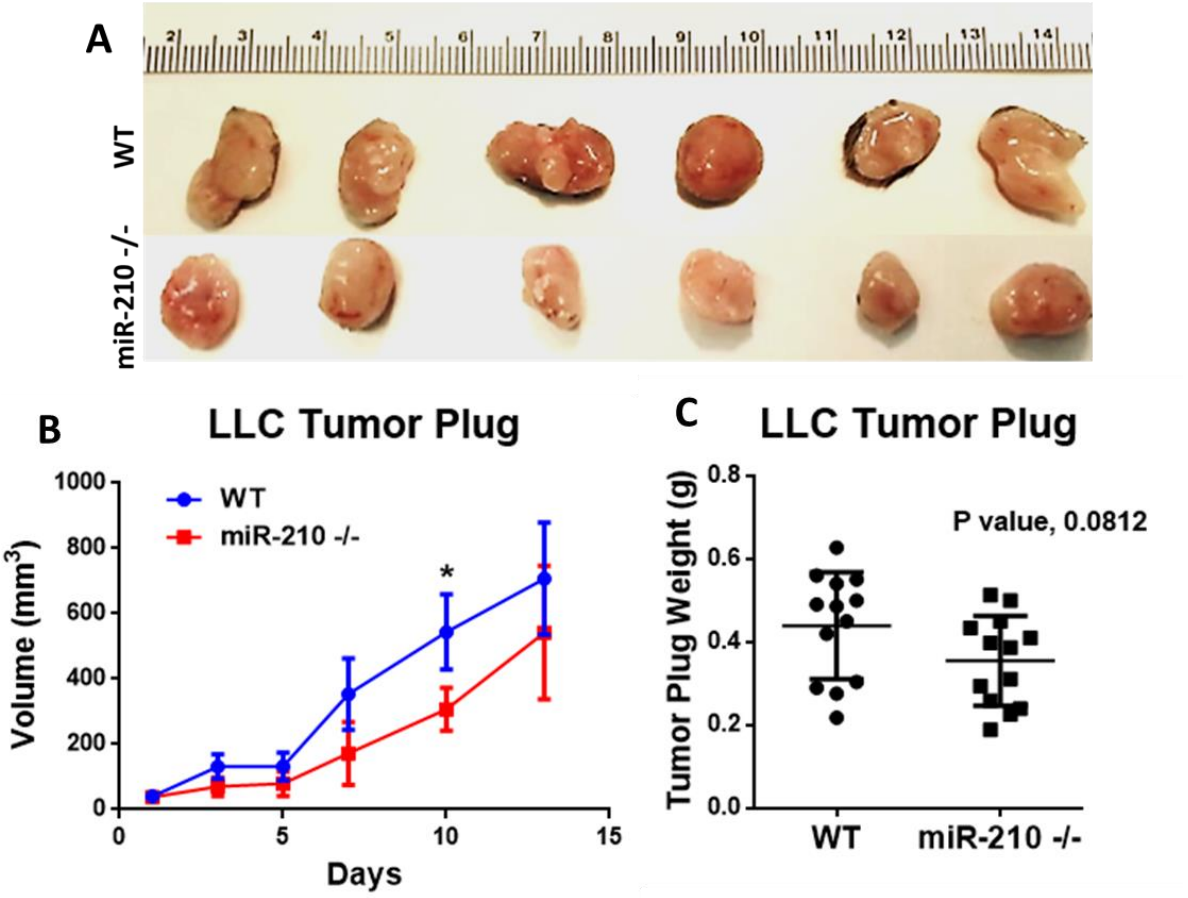

Figure 42 – miR-210 KO mice show a modest decrease in tumor growth. (A) Gross morphology of the tumor plugs. (B) Subcutaneous LLC tumor plug volume in WT and miR-210 -/- mice was measured over a 12 day period and plotted in the graph above. (C) Scatter plot shows the average tumor plug weight in WT and KO mice +/- SD.

However, sectioning revealed a significant increase in the area of tumor necrosis in miR-210 KO tumor plugs (Fig. 43A, B) compared to WT. Tumor blood vessel length (CD31 positive), was also decreased in miR-210 KO mice, indicating that recruitment of new vasculature to the tumor was impaired (Fig. 44A, B). Pericyte coverage (aSMA positive) was measured to evaluate mature tumor vessels (Fig. 44C). Average pericyte coverage was reduced in miR-210 KO mice. Overall, these results suggest that loss of miR-210 results in inhibition of pathological angiogenesis.

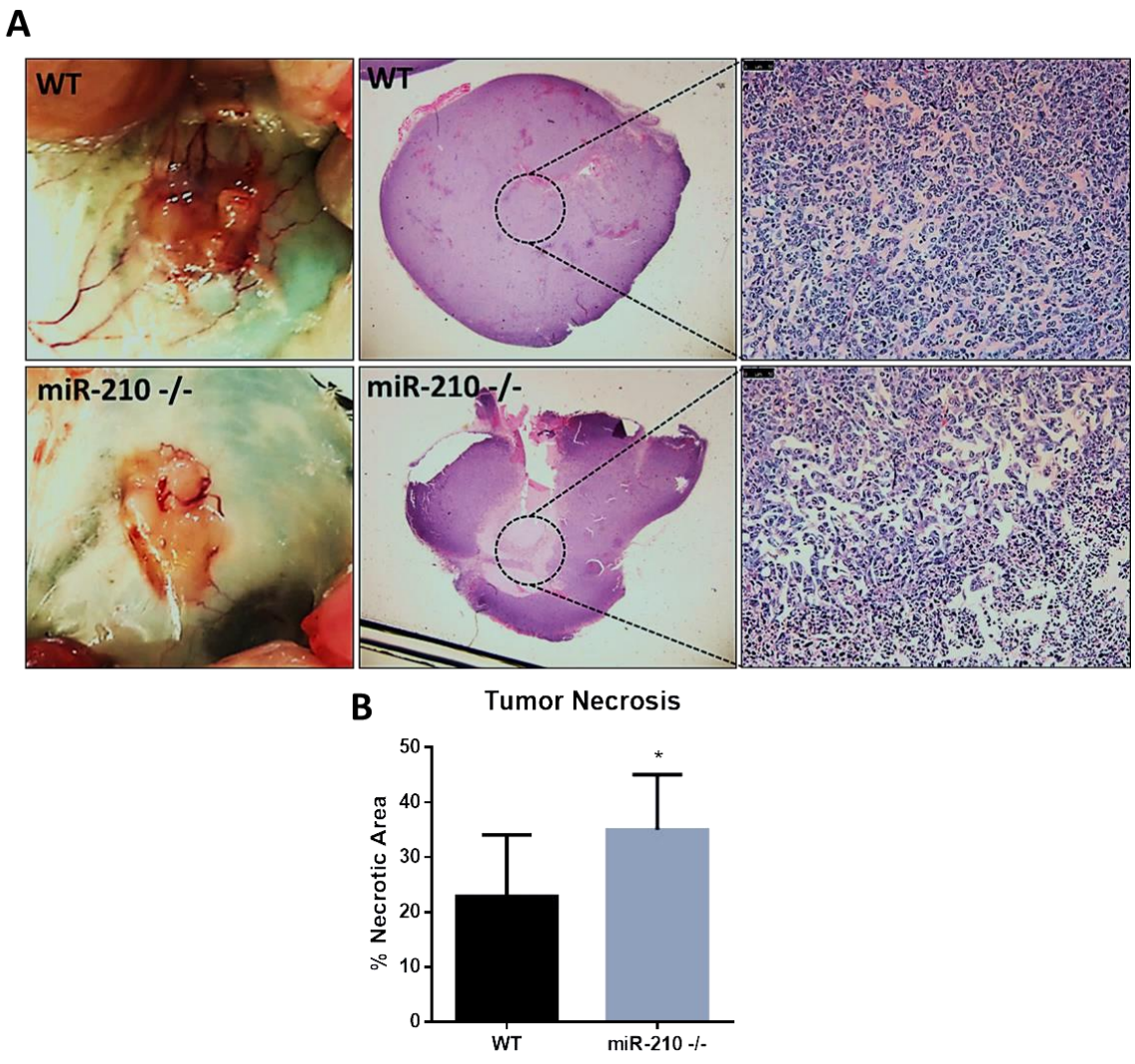

Figure 43 – Tumors in miR-210 KO mice have increased necrotic area. (A) After 12 days, the LLC tumor plugs were removed, and either fixed in formalin or flash frozen in OCT. Formalin fixed plugs were paraffin embedded, sectioned, and H&E stained. H&E stained whole tumor sections were imaged using the Nikon AZ100M microscope. (E) Image J was used to calculate the area of necrosis. The histogram represents quantification of average tumor necrosis in WT and KO tumors as a percent of the total area. Data represent mean +/- SD. *P< 0.05.

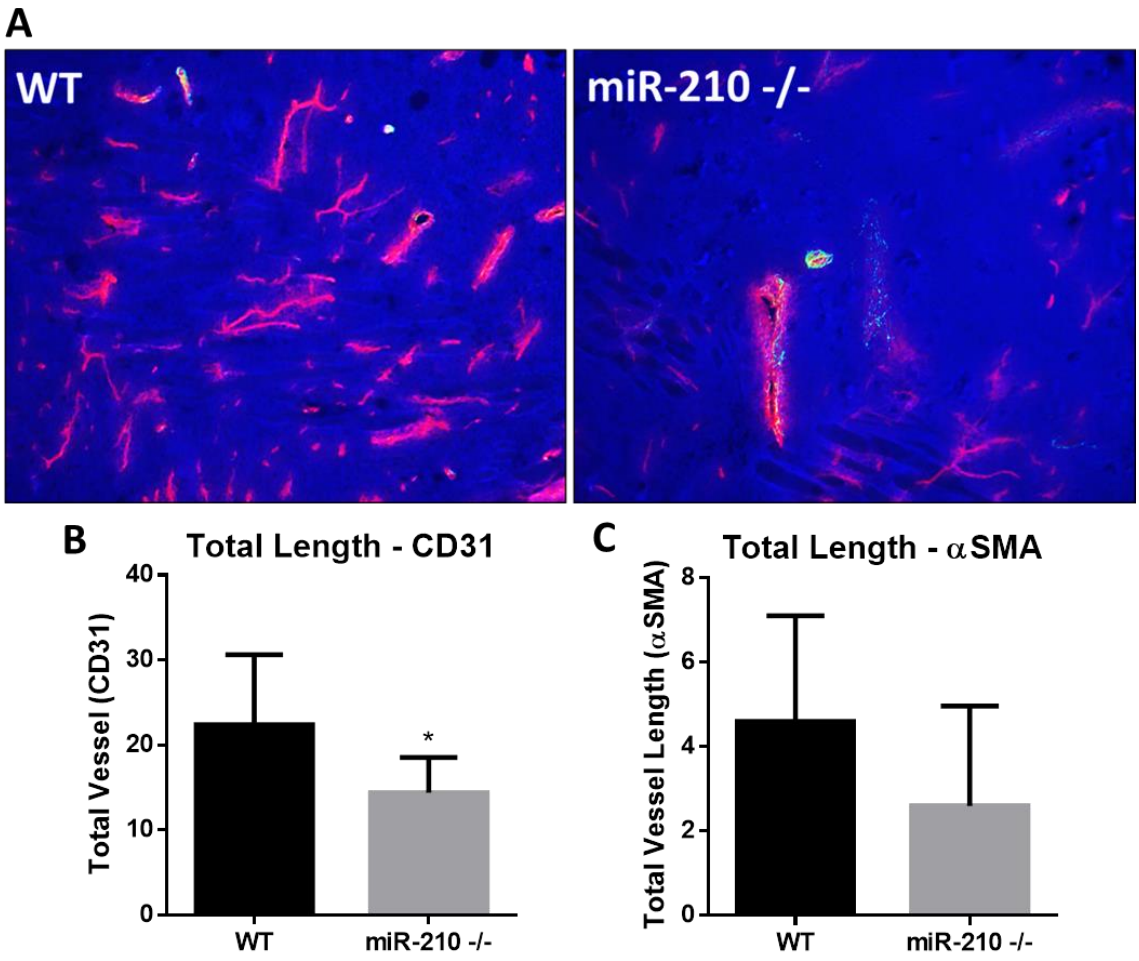

Figure 44 – Tumors in miR-210 KO mice have decreased tumor vasculature. (A) Flash frozen tumor plugs were sectioned (15um) and co-stained with DAPI, anti-CD31 (red), and anti-alphaSMA (green). Images at 20X were taken using Leica DM5500 B microscope. (B) The histogram represents average CD31- positive vessel length +/- SD in the LLC tumor plug sections frozen sections. *P< 0.05. (C) The histogram represents percent pericyte-covered vessel length (α-SMA positive vessels co-staining with CD31) in Matrigel plugs harvested from mice.

Utilizing another more clinically relevant cancer model, ID8 ovarian cancer cells were injected IP into mice to further characterize miR-210's role in malignant disease. At the end of the study, both miR-210 KO and WT mice developed large abdomens due to malignant ascites (Fig. 45A). Ascites collected from both groups contained tumor spheroids (Fig 45 B). There was no difference in ascites volume between WT and miR-210 KO mice (Fig 45C).

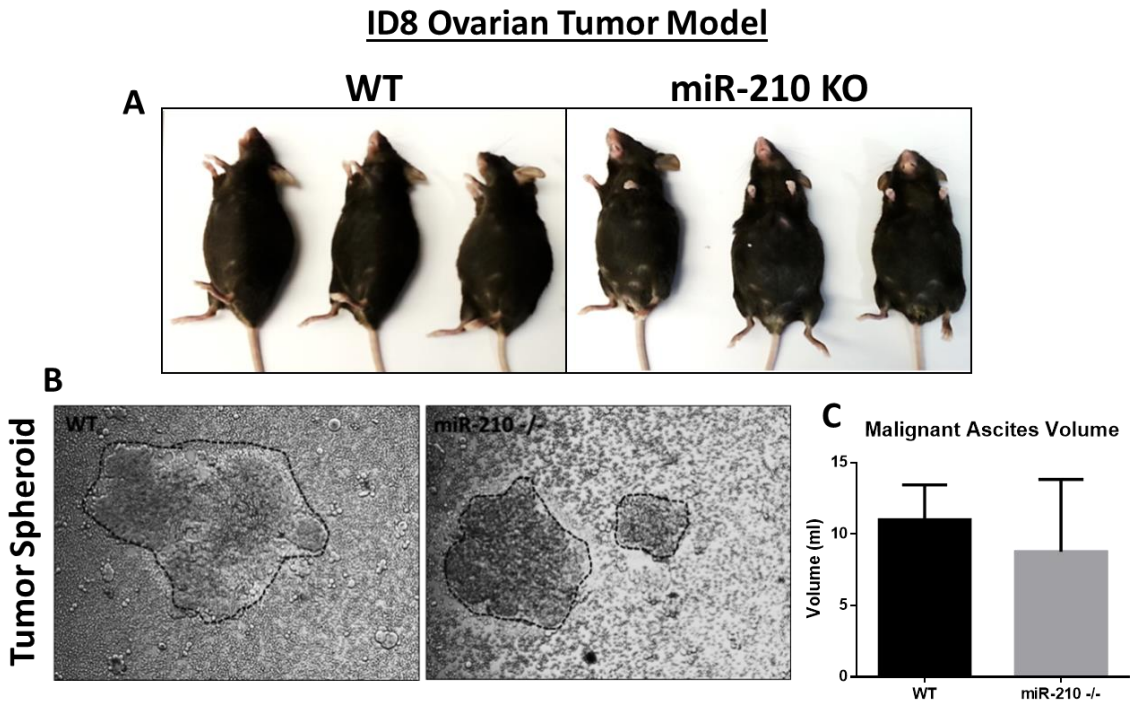

Figure 48 – Both WT and miR-210 KO mice develop malignant ascites in ID8 ovarian cancer model. (A) Gross images of mice with expanded abdomens due to advanced stage ovarian cancer and malignant ascites development. WT and miR-210 KO mice were injected with ID8 cells IP in a long term ovarian cancer study. (B) Representative images of tumor spheroids in WT and miR-210 KO mice. (C) After sacrifice, ascites volume was measured. Data represent average ascites volume (ml) between WT and miR-210 KO mice +/- SD.

Despite developing ascites, miR-210 KO mice did show a significant decrease in omental metastasis and invasion (Fig. 46A, B). As shown in Figure 46, miR-210 KO mice had few metastatic nodules around the omentum and reproductive organs, compared to WT. By measuring the adipocyte area, we found a dramatic decrease in ID8 invasion into the omentum.

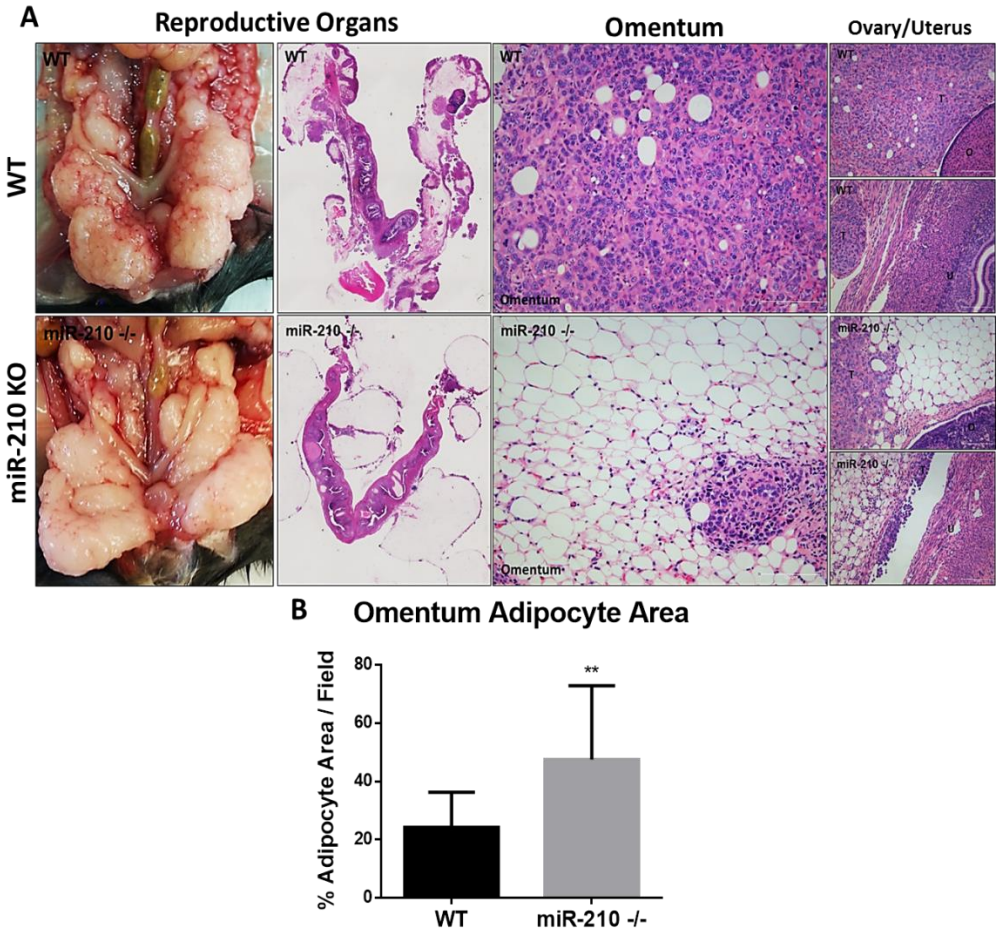

Figure 46 – Decreased ID8 tumor invasion into the omentum of miR-210 KO mice. (A) Gross images of the intraperitoneal cavity and reproductive organs of miR-210 KO and WT mice were taken followed by organ harvest and fixation with 10% formalin. Fixed organs were paraffin embedded, sectioned, and H&E stained. Whole images of the reproductive organs were stitched together using the Nikon AZ100M Microscope at 2X magnification. 10X images of tumor invasion into the omentum, uterus, and ovary were acquired. (B) Graph represents average adipose area (%) in miR-210 KO and WT omentum +/- SD, **P<.01.

We also found a significantly decreased number of metastatic nodules on the peritoneal wall and diaphragm of miR-210 KO mice (Fig. 47B, D). However, the average number of metastatic nodules on peritoneal organs, such as the liver, spleen, pancreas, GI, and kidney was the same between the two groups (Fig. 47A, C, D).

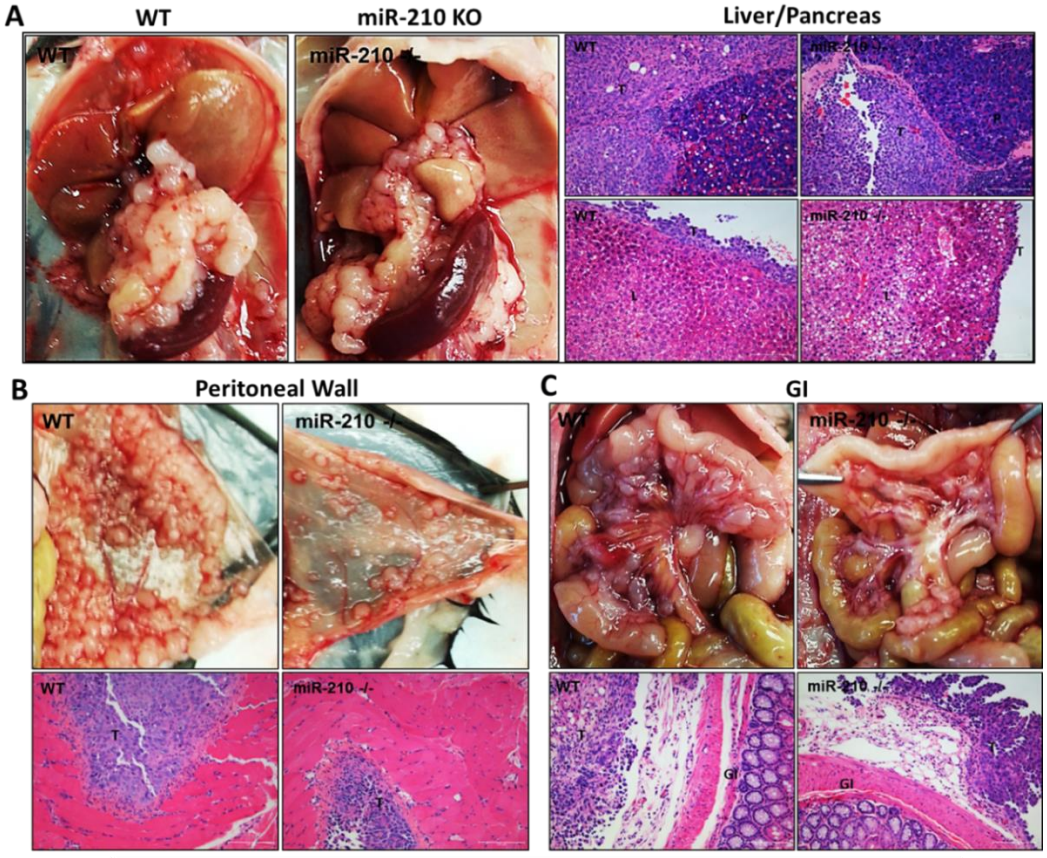

D

Organ	Average Number of Nodules (over 10mm^3)	
	WT	miR-210 KO
Peritoneum	35.6 ± 5.1	22.7 ± 8.2*
Diaphragm	8.2 ± 1.5	4.3 ± 2.6*
Liver	6.1 ± 1.3	7.4 ± 3.2
Spleen/Pancreas	12.8 ± 2.6	13.2 ± 2.4
GI	23.5 ± 5.2	20.6 ± 8.6
Kidney	5.1 ± 1.8	3.9 ± 0.8

Figure 47 – miR-210 KO mice have decreased ID8 tumor nodules on the peritoneal wall and diaphragm. No difference in number of nodules to IP organs in miR-210 KO mice

compared to WT. (A) Gross images and H&E staining of Liver/Pancreas tumor nodules and invasion. (B) Gross images and H&E staining of peritoneal wall tumor nodules and invasion. (C) Gross images and H&E staining of GI tumor nodules and invasion. (D) Table showing the average number of tumor nodules (+/- SD) found within the peritoneal cavity of miR-210 KO and WT mice. Only nodules over $10mm^3$ were counted. *P < 0.05.

Discussion:

Endothelial cells are sensitive to environmental alterations in oxygen level. In a hypoxic microenvironment, response to growth factors is critical for stimulating angiogenesis. As a direct target of HIF1a, VEGF has played a dominant role in angiogenesis research as well as targeted drug design (172). While VEGF targeted therapies hold great promise, their efficacy in the clinic has been modest, likely owing to complementary angiogenic pathways (173, 174). Our work along with several others has helped to define the critical role of FGF signaling in the hypoxic microenvironment and in pathological angiogenesis (102, 107, 153). Endothelial cells for example become highly responsive to FGF when exposed to low oxygen levels by upregulating enzymes involved in the synthesis of heparan sulfate (HS) (30). HS containing proteoglycans facilitates interaction between FGF and FGFR. HS also creates catchment areas for FGF in the extracellular matrix. Our data contributes to the value of developing targeted FGF signaling pathway therapies to either stimulate or suppress angiogenesis. Here, we show mechanistically how ECs may become sensitized to FGF signaling during hypoxia. Our studies identify hypoxia induced miR-210 as regulator of FGF signaling by decreasing FGFRL1 levels.

In human primary endothelial cell studies *in vitro*, FGFRL1 negatively influenced bFGF induced proliferation, but did not have an effect on migration or tube formation. This observation is in contrast to papers that argue FGFRL1 plays a role in cell adhesion, which should arguably influence cell migration and tube formation (97, 175). Additionally, we found that bFGF did not induce calcium signaling in HUVECs, which is critical for endothelial cell migration. For these reasons, we don't think FGFRL1 plays a primary role in endothelial cell adhesion or migration in our *in vitro* studies. Research in cancer cell lines corroborates our findings showing FGFRL1 is a primary influencer of cell proliferation (155, 156). However, in cancer FGFRL1 seems to have the opposite effect, whereby it increases cell proliferation (155, 156).

miR-210 was able to stimulate not only EC proliferation but also migration and tube formation in the presence of bFGF. It is possible that miR-210s ability to enhance migration and tube formation is by downregulating gene targets other than FGFRL1. Ephrin-A3 (EFNA3) and vacuole membrane protein 1 (VMP1) are two targets of miR-210 that have been implicated in cell migration (152, 176). We speculate that these miR-210 targets and others may play a significant role in endothelial cell attachment and migration. Although a many miR-210 targets have been identified, it remains a great challenge to predict the precise mechanisms and cellular functions of this miRNA. On the other hand our work clearly contributes to the growing evidence that miR-210 is a potent angiomiR.

Several studies have gained valuable insight on the function of FGFRL1 by studying its localization and trafficking in various cell lines (88, 90, 95, 177). Therefore, we wanted to take a closer look at FGFRL1 localization in primary endothelial cells. FGFRL1 is found endogenously and in high abundance in HUVECs and other

endothelial cells (108), so we did not have to use of expression vectors. Our results confirm previous findings about FGFRL1 dynamics as well as offer new insights about protein localization and function. First, our immunofluorescent studies confirm that it is unlikely that FGFR1-FGFRL1 heterodimerization is occurring in endothelial cells. Unlike FGFR1, FGFRL1 is not primarily localizing on the membrane. This agrees with studies that show wild-type FGFRL1 is barely located at the cell membrane, but is rather found in vesicular structures and the Golgi complex (87, 177). Likely, FGFRL1 that does reach the membrane is either rapidly released or endocytosed. Secondly, we also find large amounts of FGFRL1 in the culture medium, suggesting that it is either being shed or exported outside the cell (88). Immunoprecipitation studies showed that extracellular FGFRL1 was bFGF bound. It is tempting to speculate that extracellular FGFRL1 may act as a decoy receptor to scavenge FGF molecules. However, additional studies are required to identify the exact mechanisms by which FGFRL1 negatively regulates FGF signaling. Finally, immunofluorescence and western blot studies also support that there is a cleavage event of FGFRL1 in endothelial cells. Likely cleavage is occurring around the transmembrane region. However, the enzyme and location of FGFRL1 cleavage continues to remain a mystery. Inhibitors to various enzymes that associate with the cell membrane, such as MMPs or γ-secretase, can be used to identify by which mechanisms FGFRL1 us getting shed into the culture media.

Our studies are the first to identify nuclear localization of FGFRL1 in endothelial cells. However, multiple studies have previously shown that other members of the FGF receptor family are capable of translocating to the nucleus (178-182). FGFR1 retrograde transport and nuclear localization has been extensively studied in both normal and transformed cell lines (183-188). It is proposed that both endosomal as well as newly

synthesized FGFR1 may traffic to the nucleus. Studies show importin beta plays a role in transporting FGFR1 (189). The interaction between FGFR and importin beta appears to be indirect, as FGFR1 does not have a putative NLS, and it is not currently known which proteins mediate this interaction. Interestingly, bFGF ligands themselves have NLSs making them potentially attractive linker molecules. As a member of the FGFR family, it is conceivable that FGFRL1 may traffic to the nucleus via similar mechanisms as FGFR1.

Using NLS prediction algorithms (190-192), we identified a potential NLS sequence within FGFRL1 at amino acid positions ^{200}RKK^{202}. Additionally, sumoylation site prediction algorithms (193, 194) were used to detect a potential Sumoylation interacting motif (SIM) within FGFRL1 at amino acid positions ^{185}MKDD^{188}. Sumoylation state or presence of SUMO interacting motif (SIM) in protein partners are proposed to be major signals in driving their recruitment into PML NBs (195). Interestingly both of these predicted sequences are located in the Ig2 domain of FGFRL, but are not conserved among other FGFR family members. Using mutant analysis, future studies will determine if the predicted NLS site plays a role in FGFRL1 translocation to the nucleus.

Our studies also provide evidence that FGFRL1 interacts with bFGF in the cytoplasm and nucleus of HUVECs. Interestingly, studies have shown that endogenous bFGF ligands within endothelial cells also primarily localize to the nucleus (196). bFGF lacks the signal peptide sequence for secretion, and yet is still found in the surrounding microenvironment. A number of mechanisms have been put forth to describe how bFGF leaves the cell as reviewed in (197). However, few studies have looked at the trafficking and function of intracellular and nuclear bFGF. We speculate that bFGF and FGFRL1 may play an important role in regulating cell cycle and proliferation internally.

Additionally, FGFRL1 may provide a mechanism by which bFGF molecules are stored and trafficked within the cell. Future studies will focus on clarifying the dynamics between bFGF and FGFRL1 trafficking in ECs. We are curious to discover if FGFRL1 is binding newly synthesized intracellular bFGF or bFGF ligands that have already made it out to the extracellular matrix. Because we find FGFRL1 outside the cell, we would also like to determine if it plays a role in autocrine or paracrine FGF signaling.

Our studies further reveal that FGFRL1 localizes to PML NBs. Interestingly, PML NBs are highly expressed in vascular endothelium and have been reported in the literature as suppressors of neoangiogenesis (157-159). PML NBs are known as tumor suppressors that are involved in regulating cell proliferation, cell cycle, and apoptosis (163, 198, 199). Because of this function they are often lost or downregulated in cancer and transformed cell lines (200). PML NBs are largely regulated by factors known to induce cell stress such as viral infection, DNA-damage, and oxidative stress. It is hypothesized that endothelial cells express high amounts of PML protein to help blood vessels cope with the regular mechanical and chemical stress they are exposed to. Although the precise cell function of PML NBs is not clear, they are believed to be nuclear depots that sequester other factors to control cellular processes such as transcription (160, 162, 201). Our data show that FGFRL1 is sequestering to PML bodies, but we have yet to understand its precise role and whether or not it is involved in any sort of transcription process. As discussed previously, FGFR1 as well as several other transmembrane receptors, such as EGFR and Erb-2, have been identified to regulate transcription directly in the nucleus (202). Therefore, it is not unreasonable to speculate that FGFRL1 may also play a role in some transcription process. Ch-IP seq and proteomics analysis may help us to understand if FGFRL1 is involved in any

transcription complexes or binding directly to DNA. Importantly, we would like to identify and characterize the role of nuclear FGFRL1 in human ischemic disease and cancer.

Due to a likely cleavage event that separates the FGFRL1 intracellular and extracellular domains we are curious to understand the role of these domains individually. Our immunofluorescence data in endothelial cells show a clear difference in the localization of n and c-terminal FGFRL1 in the nucleus. Interestingly, the c-terminal end of human FGFRL1 contains a histidine-rich motif involved in binding zinc ions (154). Given the critical role of zinc in the nucleus and in the formation of PML nuclear bodies (170, 171), we speculate that FGFRL1 may play a role in the protein-protein interactions or even DNA binding within the nucleus. We were able to disrupt PML NB formation and FGFRL1 interaction by using zinc chelator, TPEN. However, despite NB disruption, FGFRL1 was still localized to the nucleus indicating to us that zinc binding may not be important for trafficking to the nucleus. Future studies aim to clarify the precise regulatory roles of the two domains within the nucleus.

In vivo studies

In contrast to our miR-210 KO mouse retina vascularization studies, we show that miR-210 and FGFRL1 play a role in the development angiogenesis of the caudal vein plexus in zebrafish. Although FGFRL1 is conserved among vertebrates, the protein is recently evolved and shows significant sequence alterations among vertebrate species (154). Interestingly bony fish, including zebrafish, possess two genes for FGFRL1, FGFRL1B and FGFRL1B, because they have undergone whole genome duplication (203). The two copies of FGFRL1 display slightly different expression patterns and thus potentially have different functions. We are not sure how miR-210 may

differentially regulate FGFRL1A/B levels, yet our results show that their downregulation inhibits developmental neovascularization. Additionally, studies have found that zebrafish lack several tumor suppressor genes, including PML protein and PML NBs (204). We speculate that variations in downstream targets of miR-210 may provide a reason for why we see different outcomes in developmental angiogenesis between zebrafish and mice. Additionally, our developmental angiogenesis studies were limited by location. It is possible we missed alterations in developmental angiogenesis in compartments other than the mouse retina or zebrafish CVP. Finally, studies have shown the timing and location of miRNA expression during development is not strictly conserved across vertebrate species (205). In mice, it is also possible that another miRNA is compensating for the loss of miR-210 during developmental angiogenesis.

Although we did not see any major differences in developmental angiogenesis between WT and miR-210 KO mice, we were interested in characterizing the mice using pathological angiogenesis models. Interestingly, PML KO mice also show no developmental defects (161). However, when adult mice were challenged with ischemia in pathological angiogenesis models, the mice showed an accelerated rate of revascularization (157). These results indicate that PML may play a more direct role in regulating pathological angiogenesis, and may not be necessary for developmental angiogenesis. Similar studies have demonstrated that mouse endothelial FGFR1 and FGFR2 and are not required for embryonic development or for vascular homeostasis (206, 207). However, endothelial FGFR1 and FGFR2 are essential for neovascularization after skin or eye injury or following retinal ischemia. Overall, these studies have identified key pathways and factors that are critical for disease associated neovascularization, yet are dispensable for developmental angiogenesis. Taking these

results into account, we speculate that miR-210 may play a more dominant role in pathological angiogenesis. Interestingly, other studies utilizing miR-210 KO mice also reveal that miR-210s effects are largely age or disease associated (208, 209). For these reasons we were very interested in understanding miR-210's role in pathological angiogenesis.

Importantly, we also showed that miR-210 KO mouse endothelial cells expressed an increased level of FGFRL1, confirming *in vitro* studies that miR-210 regulates FGFRL1. In the aortic ring assay, WT and miR-210 KO aortas cultured in bFGF showed similar microvessel sprouting in normoxic conditions. However, when aortas were challenged with hypoxia we noted a significant decrease in the length of sprouting vessels in miR-210 KO aortas. In the subcutaneous Matrigel plug assay, WT mice recruited more endothelial cells in the presence of bFGF compared to miR-210 KO mice. In subcutaneous LLC tumor plug studies, miR-210 KO mice exhibited decreased blood vessel recruitment to the tumor compared to WT. Larger areas of necrosis were also found in KO tumors, indicating that fast growing cancer cells were dying, likely due to the significantly decreased vasculature in the miR-210 KO mice. However, by the end of the 12-day study KO and WT tumors showed no statistical difference in volume or weight. Several recent studies have identified that miR-210 can be leaked into the tumor microenvironment via exosomes secreted by the tumor cells (210-212). It is possible that exosomes containing miR-210 may have confounded our studies by introducing tumor associated miR-210 into cellular components of the tumor microenvironment, such as endothelial cells. Genetic deletion of miR-210 in both the host and the tumor cells may help answering this question. Overall, our work suggests that miR-210 KO endothelium has decreased sensitivity to bFGF which will lead to decreased angiogenesis. However

in the context of the tumor microenvironment there are likely other growth factors and compensatory mechanisms that will make up for the decreased response to bFGF.

By adding the ID8 ovarian cancer study to our experiments, we introduced an element of clinical relevance to our model. While we saw no major difference in the development of advanced stage disease in both the WT and miR-210 KO mice, there was a striking difference in tumor invasion into the omentum. In mouse ovarian cancer models, studies have shown that adipocytes from the omentum secrete adipokines to attract tumor cells (213). These adipocytes also supply the cancer cells with fatty acids for fuel. We speculate that miR-210 adipocytes may have altered secretion of adipokines or possibly changes in the cellular machinery required for the transfer of fatty acids to the tumor. Future studies are needed to understand more about miR-210's role in adipocytes and omental invasion.

Overall, these studies have helped to define the critical role of FGF signaling in the hypoxic microenvironment and in pathological angiogenesis. Our data contributes to the value of developing targeted FGF signaling pathway therapies to either stimulate or suppress angiogenesis. We further identify miR-210 as a potent angiomiR that may be targeted to suppress tumor angiogenesis. Furthermore, as a negative regulator of endothelial cell proliferation, we propose that FGFRL1 could be a potential target to inhibit in order to stimulate angiogenesis in ischemic disease. Overall, these studies will generate more research interest in understanding the biological role of FGFRL1 and that our findings could translate towards the treatment of human diseases.

CHAPTER III:

CONCLUSIONS & FUTURE DIRECTIONS

Conclusions:

Hypoxia induced miR-210 downregulates FGFRL1 in ECs – Bioinformatics analysis predicted that FGFRL1 was a strong target for repression by miR-210. Using a luciferase construct in which expression of the reporter is under the control of the FGFRL1 3'UTR, we showed that miR-210 directly targets the predicted sites within the FGFRL1 3'UTR. In complementary studies, we found that overexpression of miR-210 in endothelial cells downregulates FGFRL1 at both the transcript and protein level. We also demonstrated that miR-210 KO mice had increased levels of FGFRL1 in mouse endothelial cells. This confirms miR-210 regulation of miR-210 *in vivo*.

miR-210 sensitizes ECs to bFGF induced proliferation, migration, and tube formation – Due to the critical role that both hypoxia and FGF signaling play in angiogenesis we investigated if miR-210 had any effect on sensitizing primary endothelial cells to bFGF induced proliferation, cell migration, and tube formation. Furthermore, we were interested in identifying if these effects were mediated through the downregulation of FGFRL1. In human primary endothelial cells we found that increase of miR-210 expression sensitized cells to bFGF proliferation, migration, and tube formation. Additionally, we found that miR-210 increased levels of phosphorylated FGFR1 and downstream targets MAPK and AKT after treatment of bFGF. We believe that these effects are mediated by miR-210's downregulation of FGFRL1. However, due to the known synergism in endothelial cells between VEGF/FGF pathways (105), and miR-210's ability to also regulate VEGFR, some of the effects we are seeing may be due to crosstalk between the two pathways. Additional experiments may be required to identify how miR-210 orchestrates these two pathways in hypoxia.

FGFRL1 negatively regulates bFGF induced proliferation and intracellular signaling – In order to corroborate our miR-210 studies in endothelial cells we utilized siRNA to decrease levels of FGFRL1. Like FGFR1, FGFRL1 is highly expressed in endothelial cells. We hypothesized that as a negative regulator of FGF signaling, knock down (KD) of FGFRL1 in endothelial cells would sensitize then to bFGF. Our results suggest that this was the case in the context of proliferation. KD of FGFRL1 increased endothelial cell response to bFGF induced proliferation. However we did not see that FGFRL1 had any effect on migration or tube formation. This is contrary to what we found in treating HUVEC with miR-210 and bFGF. Likely the bFGF induced migration we see in cells treated with miR-210 may be a result of another gene target or pathway. Future studies will clarify this point. In agreement with our miR-210 studies we found that FGFRL1 KD also increased bFGF induced FGFR1 phosphorylation and activation of downstream targets MAPK and AKT. These results show that FGFRL1 regulation by miR-210 plays a strong role endothelial cells response to bFGF. However, the precise molecular mechanisms by which FGFRL1 may decrease FGF sensitivity will require further investigation. We performed several immunofluorescence studies to help uncover this question as described in the next section.

FGFRL1 is shed from endothelial cells and is also found in the nucleus – In order to gain more insight about the function of FGFRL1 we performed several immunofluorescence, immunoblotting, and immunoprecipitation studies to identify where the protein was localizing in HUVEC. We found large amount of soluble FGFRL1 in the culture medium, as well as populations in the cytoplasm and nucleus. As speculated in a previous study (88), we think that the secreted form of FGFRL1 may act to scavenge FGF molecules in the matrix which may reduce the available amount of FGF that

reaches the cell surface to activate FGF receptors. However further studies are needed to corroborate this hypothesis. Overall, it is important to characterize why FGFRL1 is being excreted, and how it interacts with FGF ligands and also heparin sulfates outside the cell. Our studies also suggest that it is unlikely heterodimerization is occurring between FGFRL1/FGFR1 based on cellular localization. To date, there is no evidence that such an interaction occurs.

Our studies also agree with research that shows FGFRL1 is cleaved around the transmembrane region. The enzyme involved in FGFRL1 cleavage has yet to be identified. We find both FGFRL1 N' and C' cleavage products in the cytoplasm and nucleus. However, there is a stark difference in the nuclear localization of FGFRL1 N' and C'. We find FGFRL1 N' in discrete nuclear punctate, while FGFRL1 C' is more diffuse throughout the nucleus. We currently do not know how FGFRL1 is getting into the nucleus. Multiple prediction algorithms identified a potential NLS sequence in the Ig2 domain of FGFRL1, but we will need to conduct mutant protein analysis to identify if this site is responsible for nuclear localization. Because FGFRL1 C' is capable of binding zinc molecules, it is possible that it may function in DNA binding or in some nuclear protein-protein interaction. Finally we have identified that FGFRL1 localizes to PML NBs. Future studies aim to identify whether or not nuclear FGFRL1 plays a role in transcription, or is merely being sequestered to NBs for storage. Overall, based on these studies we think it is possible that FGFRL1 may have multiple functions within the cell and could potentially regulate FGF signaling both extracellularly and at the nuclear level.

Pathological angiogenesis is impaired in miR-210 KO mice – Importantly, we also showed that miR-210 KO mouse endothelial cells expressed an increased level of FGFRL1, confirming *in vitro* studies that miR-210 regulates FGFRL1. Absence of miR-

210 dampened hypoxia/bFGF-induced vessel sprouting in both the aortic ring and Matrigel plug assays. We plan on corroborating these observations with more clinically relevant mouse models such as myocardial ischemia and stroke experiments. These studies will help us to better understand miR-210's role in disease. Additionally, while our work focused on endothelial cells, we also hope to utilize miR-210 KO mice to study other important cell types of the tumor microenvironment such as adipocytes, and other miR-210 targets such as IGF-II.

In subcutaneous LLC tumor plug studies, miR-210 KO mice exhibited decreased blood vessel recruitment to the tumor compared to WT. Larger areas of necrosis were also found in KO tumors, indicating that fast growing cancer cells were dying, likely due to the significantly decreased vasculature in the miR-210 KO mice. However, by the end of the 12-day study KO and WT tumors showed no statistical difference in volume or weight. Several recent studies have identified that miR-210 can be leaked into the tumor microenvironment via exosomes secreted by the tumor cells (210-212). It is possible that exosomes containing miR-210 may have confounded our studies by introducing tumor associated miR-210 into cellular components of the tumor microenvironment, such as endothelial cells. Knocking out miR-210 in both the host and the tumor cells may help us answer this question. Overall, our work suggests that miR-210 KO endothelium has decreased sensitivity to bFGF which will lead to decreased angiogenesis. However in the context of the tumor microenvironment there are likely other growth factors and compensatory mechanisms that will make up for the decreased response to bFGF.

Long-Term Prospects

Cancer is a complex disease and will require a treatment regimen that not only targets the tumor cells, but also the tumor microenvironment, such as blocking angiogenesis or stimulating immune response. Understanding the mechanisms of hypoxia induced angiogenesis leading to tumor progression and survival is important as these insights may lead to improved response to therapy, and eventually to better biology-based disease management, thereby improving prognosis and quality of life. In addition to cancer, hypoxia plays a central role in the pathogenesis of major ischemic disorders, such as stroke and cardiovascular diseases. Therefore, a deeper understanding of cellular adaptation to oxygen deprivation has broad implications for translational medicine.

Our work contributes to the growing evidence that miR-210 acts as a potent angiomiR. We find that hypoxia induced miR-210 can regulate endothelial cell response to FGF signaling by regulating the levels of FGFRL1. In the context of cancer, it may be possible to use RNAi therapies to inhibit miR-210. As summarized in (141), several types of inhibitory RNAs, such as AntagomiRs, miR-sponge, and miR-Mask can be used to therapeutically inhibit miRNAs. However, the successful delivery of these therapeutic RNAi agents to the tumor remains a great challenge. Our studies also suggest that FGFRL1 plays a role as a negative regulator of endothelial cell proliferation and angiogenesis. An interesting approach to stimulate angiogenesis for the use in ischemic diseases is to develop strategies to inhibit this molecule. Overall, we hope that the findings presented in this work will translate to the treatment of human diseases.

CHAPTER IV:

BILIOGRAPHY

1. Hanahan D, Weinberg RA. The hallmarks of cancer. Cell. 2000;100(1):57-70.
2. Hanahan D, Weinberg RA. Hallmarks of cancer: the next generation. Cell. 2011;144(5):646-74.
3. Balkwill FR, Capasso M, Hagemann T. The tumor microenvironment at a glance. Journal of cell science. 2012;125(Pt 23):5591-6.
4. Albini A, Sporn MB. The tumour microenvironment as a target for chemoprevention. Nature reviews Cancer. 2007;7(2):139-47.
5. Folkman J. Tumor angiogenesis: therapeutic implications. N Engl J Med. 1971;285(21):1182-6.
6. Leung DW, Cachianes G, Kuang WJ, Goeddel DV, Ferrara N. Vascular endothelial growth factor is a secreted angiogenic mitogen. Science. 1989;246(4935):1306-9.
7. Vasudev NS, Reynolds AR. Anti-angiogenic therapy for cancer: current progress, unresolved questions and future directions. Angiogenesis. 2014;17(3):471-94.
8. Welti J, Loges S, Dimmeler S, Carmeliet P. Recent molecular discoveries in angiogenesis and antiangiogenic therapies in cancer. The Journal of clinical investigation. 2013;123(8):3190-200.
9. Chung AS, Lee J, Ferrara N. Targeting the tumour vasculature: insights from physiological angiogenesis. Nature reviews Cancer. 2010;10(7):505-14.
10. Witz IP. The tumor microenvironment: the making of a paradigm. Cancer microenvironment : official journal of the International Cancer Microenvironment Society. 2009;2 Suppl 1:9-17.
11. Cui Y, Guo G. Immunomodulatory Function of the Tumor Suppressor p53 in Host Immune Response and the Tumor Microenvironment. International journal of molecular sciences. 2016;17(11).
12. Frantz C, Stewart KM, Weaver VM. The extracellular matrix at a glance. Journal of cell science. 2010;123(Pt 24):4195-200.
13. Quail DF, Joyce JA. Microenvironmental regulation of tumor progression and metastasis. Nature medicine. 2013;19(11):1423-37.
14. Pietras K, Ostman A. Hallmarks of cancer: interactions with the tumor stroma. Experimental cell research. 2010;316(8):1324-31.
15. Dvorak HF. Tumors: wounds that do not heal-redux. Cancer immunology research. 2015;3(1):1-11.
16. Kalluri R, Zeisberg M. Fibroblasts in cancer. Nature reviews Cancer. 2006;6(5):392-401.
17. Lamouille S, Xu J, Derynck R. Molecular mechanisms of epithelial-mesenchymal transition. Nature reviews Molecular cell biology. 2014;15(3):178-96.
18. Gilkes DM, Semenza GL, Wirtz D. Hypoxia and the extracellular matrix: drivers of tumour metastasis. Nature reviews Cancer. 2014;14(6):430-9.
19. Harris AL. Hypoxia--a key regulatory factor in tumour growth. Nature reviews Cancer. 2002;2(1):38-47.
20. Casazza A, Di Conza G, Wenes M, Finisguerra V, Deschoemaeker S, Mazzone M. Tumor stroma: a complexity dictated by the hypoxic tumor microenvironment. Oncogene. 2014;33(14):1743-54.
21. Masoud GN, Li W. HIF-1alpha pathway: role, regulation and intervention for cancer therapy. Acta pharmaceutica Sinica B. 2015;5(5):378-89.
22. Tredan O, Galmarini CM, Patel K, Tannock IF. Drug resistance and the solid tumor microenvironment. Journal of the National Cancer Institute. 2007;99(19):1441-54.

23. Azzi S, Hebda JK, Gavard J. Vascular permeability and drug delivery in cancers. Frontiers in oncology. 2013;3:211.
24. Karakashev SV, Reginato MJ. Progress toward overcoming hypoxia-induced resistance to solid tumor therapy. Cancer management and research. 2015;7:253-64.
25. Kato Y, Ozawa S, Miyamoto C, Maehata Y, Suzuki A, Maeda T, et al. Acidic extracellular microenvironment and cancer. Cancer cell international. 2013;13(1):89.
26. Stacker SA, Williams SP, Karnezis T, Shayan R, Fox SB, Achen MG. Lymphangiogenesis and lymphatic vessel remodelling in cancer. Nature reviews Cancer. 2014;14(3):159-72.
27. Junttila MR, de Sauvage FJ. Influence of tumour micro-environment heterogeneity on therapeutic response. Nature. 2013;501(7467):346-54.
28. Bae YH, Park K. Targeted drug delivery to tumors: myths, reality and possibility. Journal of controlled release : official journal of the Controlled Release Society. 2011;153(3):198-205.
29. Joyce JA. Therapeutic targeting of the tumor microenvironment. Cancer cell. 2005;7(6):513-20.
30. Scott AM, Wolchok JD, Old LJ. Antibody therapy of cancer. Nature reviews Cancer. 2012;12(4):278-87.
31. Weber J. Review: anti-CTLA-4 antibody ipilimumab: case studies of clinical response and immune-related adverse events. The oncologist. 2007;12(7):864-72.
32. Regad T. Targeting RTK Signaling Pathways in Cancer. Cancers. 2015;7(3):1758-84.
33. Torchilin VP. Multifunctional, stimuli-sensitive nanoparticulate systems for drug delivery. Nature reviews Drug discovery. 2014;13(11):813-27.
34. Lao J, Madani J, Puertolas T, Alvarez M, Hernandez A, Pazo-Cid R, et al. Liposomal Doxorubicin in the treatment of breast cancer patients: a review. Journal of drug delivery. 2013;2013:456409.
35. Michiels C. Physiological and pathological responses to hypoxia. The American journal of pathology. 2004;164(6):1875-82.
36. Kiaer T, Kristensen KD. Intracompartmental pressure, PO2, PCO2 and blood flow in the human skeletal muscle. Archives of orthopaedic and traumatic surgery Archiv fur orthopadische und Unfall-Chirurgie. 1988;107(2):114-6.
37. Ndubuizu O, LaManna JC. Brain tissue oxygen concentration measurements. Antioxidants & redox signaling. 2007;9(8):1207-19.
38. Semenza GL. Surviving ischemia: adaptive responses mediated by hypoxia-inducible factor 1. The Journal of clinical investigation. 2000;106(7):809-12.
39. Semenza GL. Regulation of mammalian O2 homeostasis by hypoxia-inducible factor 1. Annual review of cell and developmental biology. 1999;15:551-78.
40. Dengler VL, Galbraith MD, Espinosa JM. Transcriptional regulation by hypoxia inducible factors. Critical reviews in biochemistry and molecular biology. 2014;49(1):1-15.
41. Kuschel A, Simon P, Tug S. Functional regulation of HIF-1alpha under normoxia--is there more than post-translational regulation? Journal of cellular physiology. 2012;227(2):514-24.
42. Semenza GL. HIF-1, O(2), and the 3 PHDs: how animal cells signal hypoxia to the nucleus. Cell. 2001;107(1):1-3.
43. Ghosh G, Subramanian IV, Adhikari N, Zhang X, Joshi HP, Basi D, et al. Hypoxia-induced microRNA-424 expression in human endothelial cells regulates HIF-alpha isoforms and promotes angiogenesis. The Journal of clinical investigation. 2010;120(11):4141-54.
44. Semenza GL. HIF-1 and mechanisms of hypoxia sensing. Current opinion in cell biology. 2001;13(2):167-71.

45. Semenza GL, Jiang BH, Leung SW, Passantino R, Concordet JP, Maire P, et al. Hypoxia response elements in the aldolase A, enolase 1, and lactate dehydrogenase A gene promoters contain essential binding sites for hypoxia-inducible factor 1. The Journal of biological chemistry. 1996;271(51):32529-37.
46. Hong SS, Lee H, Kim KW. HIF-1alpha: a valid therapeutic target for tumor therapy. Cancer research and treatment : official journal of Korean Cancer Association. 2004;36(6):343-53.
47. Semenza GL. Hypoxia-inducible factor 1 and cardiovascular disease. Annual review of physiology. 2014;76:39-56.
48. Chen SM, Li YG, Zhang HX, Zhang GH, Long JR, Tan CJ, et al. Hypoxia-inducible factor-1alpha induces the coronary collaterals for coronary artery disease. Coronary artery disease. 2008;19(3):173-9.
49. Bardos JI, Ashcroft M. Hypoxia-inducible factor-1 and oncogenic signalling. BioEssays : news and reviews in molecular, cellular and developmental biology. 2004;26(3):262-9.
50. LaGory EL, Giaccia AJ. The ever-expanding role of HIF in tumour and stromal biology. Nature cell biology. 2016;18(4):356-65.
51. Brahimi-Horn C, Pouyssegur J. The role of the hypoxia-inducible factor in tumor metabolism growth and invasion. Bulletin du cancer. 2006;93(8):E73-80.
52. Krock BL, Skuli N, Simon MC. Hypoxia-induced angiogenesis: good and evil. Genes & cancer. 2011;2(12):1117-33.
53. Zellmer VR, Zhang S. Evolving concepts of tumor heterogeneity. Cell & bioscience. 2014;4:69.
54. Ruoslahti E. Specialization of tumour vasculature. Nature reviews Cancer. 2002;2(2):83-90.
55. Vander Heiden MG, Cantley LC, Thompson CB. Understanding the Warburg effect: the metabolic requirements of cell proliferation. Science. 2009;324(5930):1029-33.
56. Hirschhaeuser F, Sattler UG, Mueller-Klieser W. Lactate: a metabolic key player in cancer. Cancer research. 2011;71(22):6921-5.
57. Raghunand N, Gillies RJ. pH and drug resistance in tumors. Drug resistance updates : reviews and commentaries in antimicrobial and anticancer chemotherapy. 2000;3(1):39-47.
58. Luoto KR, Kumareswaran R, Bristow RG. Tumor hypoxia as a driving force in genetic instability. Genome integrity. 2013;4(1):5.
59. Nishi H, Nakada T, Kyo S, Inoue M, Shay JW, Isaka K. Hypoxia-inducible factor 1 mediates upregulation of telomerase (hTERT). Molecular and cellular biology. 2004;24(13):6076-83.
60. Peinado H, Cano A. A hypoxic twist in metastasis. Nature cell biology. 2008;10(3):253-4.
61. Semenza GL. HIF-1 and tumor progression: pathophysiology and therapeutics. Trends in molecular medicine. 2002;8(4 Suppl):S62-7.
62. Vaupel P, Hockel M. [Hypoxia in cervical cancer: pathogenesis, characterization, and biological/clinical consequences]. Zentralblatt fur Gynakologie. 2001;123(4):192-7.
63. Zhong H, De Marzo AM, Laughner E, Lim M, Hilton DA, Zagzag D, et al. Overexpression of hypoxia-inducible factor 1alpha in common human cancers and their metastases. Cancer research. 1999;59(22):5830-5.
64. Nishikawa SI, Hirashima M, Nishikawa S, Ogawa M. Cell biology of vascular endothelial cells. Annals of the New York Academy of Sciences. 2001;947:35-40; discussion 1.
65. Bergers G, Song S. The role of pericytes in blood-vessel formation and maintenance. Neuro-oncology. 2005;7(4):452-64.

66. Papetti M, Herman IM. Mechanisms of normal and tumor-derived angiogenesis. American journal of physiology Cell physiology. 2002;282(5):C947-70.
67. Carmeliet P, Jain RK. Molecular mechanisms and clinical applications of angiogenesis. Nature. 2011;473(7347):298-307.
68. Ehling M, Adams S, Benedito R, Adams RH. Notch controls retinal blood vessel maturation and quiescence. Development. 2013;140(14):3051-61.
69. Adams RH, Alitalo K. Molecular regulation of angiogenesis and lymphangiogenesis. Nature reviews Molecular cell biology. 2007;8(6):464-78.
70. Baeriswyl V, Christofori G. The angiogenic switch in carcinogenesis. Seminars in cancer biology. 2009;19(5):329-37.
71. Bergers G, Brekken R, McMahon G, Vu TH, Itoh T, Tamaki K, et al. Matrix metalloproteinase-9 triggers the angiogenic switch during carcinogenesis. Nature cell biology. 2000;2(10):737-44.
72. Carmeliet P, Jain RK. Principles and mechanisms of vessel normalization for cancer and other angiogenic diseases. Nature reviews Drug discovery. 2011;10(6):417-27.
73. Siemann DW. The unique characteristics of tumor vasculature and preclinical evidence for its selective disruption by Tumor-Vascular Disrupting Agents. Cancer treatment reviews. 2011;37(1):63-74.
74. Jain RK, Duda DG, Clark JW, Loeffler JS. Lessons from phase III clinical trials on anti-VEGF therapy for cancer. Nature clinical practice Oncology. 2006;3(1):24-40.
75. Ellis LM, Hicklin DJ. VEGF-targeted therapy: mechanisms of anti-tumour activity. Nature reviews Cancer. 2008;8(8):579-91.
76. Medina MA, Munoz-Chapuli R, Quesada AR. Challenges of antiangiogenic cancer therapy: trials and errors, and renewed hope. Journal of cellular and molecular medicine. 2007;11(3):374-82.
77. Jain RK. Normalizing tumor vasculature with anti-angiogenic therapy: a new paradigm for combination therapy. Nature medicine. 2001;7(9):987-9.
78. Arjaans M, Oude Munnink TH, Oosting SF, Terwisscha van Scheltinga AG, Gietema JA, Garbacik ET, et al. Bevacizumab-induced normalization of blood vessels in tumors hampers antibody uptake. Cancer research. 2013;73(11):3347-55.
79. Baird A, Esch F, Mormede P, Ueno N, Ling N, Bohlen P, et al. Molecular characterization of fibroblast growth factor: distribution and biological activities in various tissues. Recent progress in hormone research. 1986;42:143-205.
80. Ornitz DM, Itoh N. The Fibroblast Growth Factor signaling pathway. Wiley interdisciplinary reviews Developmental biology. 2015;4(3):215-66.
81. Itoh N, Ornitz DM. Evolution of the Fgf and Fgfr gene families. Trends in genetics : TIG. 2004;20(11):563-9.
82. Schlessinger J, Plotnikov AN, Ibrahimi OA, Eliseenkova AV, Yeh BK, Yayon A, et al. Crystal structure of a ternary FGF-FGFR-heparin complex reveals a dual role for heparin in FGFR binding and dimerization. Molecular cell. 2000;6(3):743-50.
83. Zhang X, Ibrahimi OA, Olsen SK, Umemori H, Mohammadi M, Ornitz DM. Receptor specificity of the fibroblast growth factor family. The complete mammalian FGF family. The Journal of biological chemistry. 2006;281(23):15694-700.
84. Turner N, Grose R. Fibroblast growth factor signalling: from development to cancer. Nature reviews Cancer. 2010;10(2):116-29.

85. Thisse B, Thisse C. Functions and regulations of fibroblast growth factor signaling during embryonic development. Developmental biology. 2005;287(2):390-402.
86. Givol D, Yayon A. Complexity of FGF receptors: genetic basis for structural diversity and functional specificity. FASEB journal : official publication of the Federation of American Societies for Experimental Biology. 1992;6(15):3362-9.
87. Trueb B. Biology of FGFRL1, the fifth fibroblast growth factor receptor. Cellular and molecular life sciences : CMLS. 2011;68(6):951-64.
88. Steinberg F, Zhuang L, Beyeler M, Kalin RE, Mullis PE, Brandli AW, et al. The FGFRL1 receptor is shed from cell membranes, binds fibroblast growth factors (FGFs), and antagonizes FGF signaling in Xenopus embryos. The Journal of biological chemistry. 2010;285(3):2193-202.
89. Trueb B, Zhuang L, Taeschler S, Wiedemann M. Characterization of FGFRL1, a novel fibroblast growth factor (FGF) receptor preferentially expressed in skeletal tissues. The Journal of biological chemistry. 2003;278(36):33857-65.
90. Trueb B, Steinberg F. A net-like structure with pores is observed during cell fusion induced by the receptor FGFRL1. Communicative & integrative biology. 2011;4(3):287-90.
91. Steinberg F, Gerber SD, Rieckmann T, Trueb B. Rapid fusion and syncytium formation of heterologous cells upon expression of the FGFRL1 receptor. The Journal of biological chemistry. 2010;285(48):37704-15.
92. Zhuang L, Falquet L, Trueb B. Genome-wide comparison of FGFRL1 with structurally related surface receptors. Experimental and therapeutic medicine. 2010;1(1):161-8.
93. Zhuang L, Villiger P, Trueb B. Interaction of the receptor FGFRL1 with the negative regulator Spred1. Cellular signalling. 2011;23(9):1496-504.
94. Amann R, Trueb B. Evidence that the novel receptor FGFRL1 signals indirectly via FGFR1. International journal of molecular medicine. 2013;32(5):983-8.
95. Silva PN, Altamentova SM, Kilkenny DM, Rocheleau JV. Fibroblast growth factor receptor like-1 (FGFRL1) interacts with SHP-1 phosphatase at insulin secretory granules and induces beta-cell ERK1/2 protein activation. The Journal of biological chemistry. 2013;288(24):17859-70.
96. Zhuang L, Pandey AV, Villiger PM, Trueb B. Cell-cell fusion induced by the Ig3 domain of receptor FGFRL1 in CHO cells. Biochimica et biophysica acta. 2015;1853(10 Pt A):2273-85.
97. Yang X, Steinberg F, Zhuang L, Bessey R, Trueb B. Receptor FGFRL1 does not promote cell proliferation but induces cell adhesion. International journal of molecular medicine. 2016;38(1):30-8.
98. Bluteau G, Zhuang L, Amann R, Trueb B. Targeted disruption of the intracellular domain of receptor FgfrL1 in mice. PloS one. 2014;9(8):e105210.
99. Baertschi S, Zhuang L, Trueb B. Mice with a targeted disruption of the Fgfrl1 gene die at birth due to alterations in the diaphragm. The FEBS journal. 2007;274(23):6241-53.
100. Zhuang L, Bluteau G, Trueb B. Phylogenetic analysis of receptor FgfrL1 shows divergence of the C-terminal end in rodents. Comparative biochemistry and physiology Part B, Biochemistry & molecular biology. 2015;186:43-50.
101. Lanner F, Rossant J. The role of FGF/Erk signaling in pluripotent cells. Development. 2010;137(20):3351-60.
102. Lieu C, Heymach J, Overman M, Tran H, Kopetz S. Beyond VEGF: inhibition of the fibroblast growth factor pathway and antiangiogenesis. Clinical cancer research : an official journal of the American Association for Cancer Research. 2011;17(19):6130-9.
103. Werner S, Grose R. Regulation of wound healing by growth factors and cytokines. Physiological reviews. 2003;83(3):835-70.

104. Risau W. Angiogenic growth factors. Progress in growth factor research. 1990;2(1):71-9.
105. Pepper MS, Ferrara N, Orci L, Montesano R. Potent synergism between vascular endothelial growth factor and basic fibroblast growth factor in the induction of angiogenesis in vitro. Biochemical and biophysical research communications. 1992;189(2):824-31.
106. Javerzat S, Auguste P, Bikfalvi A. The role of fibroblast growth factors in vascular development. Trends in molecular medicine. 2002;8(10):483-9.
107. Presta M, Dell'Era P, Mitola S, Moroni E, Ronca R, Rusnati M. Fibroblast growth factor/fibroblast growth factor receptor system in angiogenesis. Cytokine & growth factor reviews. 2005;16(2):159-78.
108. Antoine M, Wirz W, Tag CG, Mavituna M, Emans N, Korff T, et al. Expression pattern of fibroblast growth factors (FGFs), their receptors and antagonists in primary endothelial cells and vascular smooth muscle cells. Growth factors. 2005;23(2):87-95.
109. Kopetz S, Hoff PM, Morris JS, Wolff RA, Eng C, Glover KY, et al. Phase II trial of infusional fluorouracil, irinotecan, and bevacizumab for metastatic colorectal cancer: efficacy and circulating angiogenic biomarkers associated with therapeutic resistance. Journal of clinical oncology : official journal of the American Society of Clinical Oncology. 2010;28(3):453-9.
110. Batchelor TT, Sorensen AG, di Tomaso E, Zhang WT, Duda DG, Cohen KS, et al. AZD2171, a pan-VEGF receptor tyrosine kinase inhibitor, normalizes tumor vasculature and alleviates edema in glioblastoma patients. Cancer cell. 2007;11(1):83-95.
111. Dieci MV, Arnedos M, Andre F, Soria JC. Fibroblast growth factor receptor inhibitors as a cancer treatment: from a biologic rationale to medical perspectives. Cancer discovery. 2013;3(3):264-79.
112. Ha M, Kim VN. Regulation of microRNA biogenesis. Nature reviews Molecular cell biology. 2014;15(8):509-24.
113. Berezikov E. Evolution of microRNA diversity and regulation in animals. Nature reviews Genetics. 2011;12(12):846-60.
114. Friedman RC, Farh KK, Burge CB, Bartel DP. Most mammalian mRNAs are conserved targets of microRNAs. Genome research. 2009;19(1):92-105.
115. Ludwig N, Leidinger P, Becker K, Backes C, Fehlmann T, Pallasch C, et al. Distribution of miRNA expression across human tissues. Nucleic acids research. 2016;44(8):3865-77.
116. Jansson MD, Lund AH. MicroRNA and cancer. Molecular oncology. 2012;6(6):590-610.
117. Christopher AF, Kaur RP, Kaur G, Kaur A, Gupta V, Bansal P. MicroRNA therapeutics: Discovering novel targets and developing specific therapy. Perspectives in clinical research. 2016;7(2):68-74.
118. Wahid F, Shehzad A, Khan T, Kim YY. MicroRNAs: synthesis, mechanism, function, and recent clinical trials. Biochimica et biophysica acta. 2010;1803(11):1231-43.
119. Martin HC, Wani S, Steptoe AL, Krishnan K, Nones K, Nourbakhsh E, et al. Imperfect centered miRNA binding sites are common and can mediate repression of target mRNAs. Genome biology. 2014;15(3):R51.
120. Filipowicz W, Bhattacharyya SN, Sonenberg N. Mechanisms of post-transcriptional regulation by microRNAs: are the answers in sight? Nature reviews Genetics. 2008;9(2):102-14.
121. Wilczynska A, Bushell M. The complexity of miRNA-mediated repression. Cell death and differentiation. 2015;22(1):22-33.
122. Zinovyev A, Morozova N, Gorban AN, Harel-Belan A. Mathematical modeling of microRNA-mediated mechanisms of translation repression. Advances in experimental medicine and biology. 2013;774:189-224.

123. Crosby ME, Devlin CM, Glazer PM, Calin GA, Ivan M. Emerging roles of microRNAs in the molecular responses to hypoxia. Curr Pharm Des. 2009;15(33):3861-6.
124. Nallamshetty S, Chan SY, Loscalzo J. Hypoxia: a master regulator of microRNA biogenesis and activity. Free Radic Biol Med. 2013;64:20-30.
125. Suzuki HI, Katsura A, Matsuyama H, Miyazono K. MicroRNA regulons in tumor microenvironment. Oncogene. 2015;34(24):3085-94.
126. Yang W, Lee DY, Ben-David Y. The roles of microRNAs in tumorigenesis and angiogenesis. Int J Physiol Pathophysiol Pharmacol. 2011;3(2):140-55.
127. Shen G, Li X, Jia YF, Piazza GA, Xi Y. Hypoxia-regulated microRNAs in human cancer. Acta pharmacologica Sinica. 2013;34(3):336-41.
128. Giles KM, Barker A, Zhang PM, Epis MR, Leedman PJ. MicroRNA regulation of growth factor receptor signaling in human cancer cells. Methods in molecular biology. 2011;676:147-63.
129. Rutnam ZJ, Wight TN, Yang BB. miRNAs regulate expression and function of extracellular matrix molecules. Matrix biology : journal of the International Society for Matrix Biology. 2013;32(2):74-85.
130. Wang S, Olson EN. AngiomiRs--key regulators of angiogenesis. Current opinion in genetics & development. 2009;19(3):205-11.
131. Hoff PM, Machado KK. Role of angiogenesis in the pathogenesis of cancer. Cancer treatment reviews. 2012;38(7):825-33.
132. Kerbel RS. Tumor angiogenesis. N Engl J Med. 2008;358(19):2039-49.
133. Losordo DW, Dimmeler S. Therapeutic angiogenesis and vasculogenesis for ischemic disease. Part I: angiogenic cytokines. Circulation. 2004;109(21):2487-91.
134. Losordo DW, Dimmeler S. Therapeutic angiogenesis and vasculogenesis for ischemic disease: part II: cell-based therapies. Circulation. 2004;109(22):2692-7.
135. Khurana R, Simons M, Martin JF, Zachary IC. Role of angiogenesis in cardiovascular disease: a critical appraisal. Circulation. 2005;112(12):1813-24.
136. Joshi HP, Subramanian IV, Schnettler EK, Ghosh G, Rupaimoole R, Evans C, et al. Dynamin 2 along with microRNA-199a reciprocally regulate hypoxia-inducible factors and ovarian cancer metastasis. Proceedings of the National Academy of Sciences of the United States of America. 2014;111(14):5331-6.
137. Greco S, Martelli F. MicroRNAs in Hypoxia Response. Antioxidants & redox signaling. 2014;21(8):1164-6.
138. Loscalzo J. The cellular response to hypoxia: tuning the system with microRNAs. The Journal of clinical investigation. 2010;120(11):3815-7.
139. Chan SY, Loscalzo J. MicroRNA-210: a unique and pleiotropic hypoxamir. Cell cycle. 2010;9(6):1072-83.
140. Chan YC, Banerjee J, Choi SY, Sen CK. miR-210: the master hypoxamir. Microcirculation. 2012;19(3):215-23.
141. Dang K, Myers KA. The role of hypoxia-induced miR-210 in cancer progression. International journal of molecular sciences. 2015;16(3):6353-72.
142. Devlin C, Greco S, Martelli F, Ivan M. miR-210: More than a silent player in hypoxia. IUBMB life. 2011;63(2):94-100.
143. Suarez Y, Sessa WC. MicroRNAs as novel regulators of angiogenesis. Circulation research. 2009;104(4):442-54.

144. Zeng L, He X, Wang Y, Tang Y, Zheng C, Cai H, et al. MicroRNA-210 overexpression induces angiogenesis and neurogenesis in the normal adult mouse brain. Gene therapy. 2014;21(1):37-43.
145. Liu F, Lou YL, Wu J, Ruan QF, Xie A, Guo F, et al. Upregulation of microRNA-210 regulates renal angiogenesis mediated by activation of VEGF signaling pathway under ischemia/perfusion injury in vivo and in vitro. Kidney & blood pressure research. 2012;35(3):182-91.
146. Hong L, Han Y, Zhang H, Zhao Q, Qiao Y. miR-210: a therapeutic target in cancer. Expert opinion on therapeutic targets. 2013;17(1):21-8.
147. Wang Y, Wang Y, Yang GY. MicroRNAs in Cerebral Ischemia. Stroke research and treatment. 2013;2013:276540.
148. Greco S, Gaetano C, Martelli F. HypoxamiR regulation and function in ischemic cardiovascular diseases. Antioxidants & redox signaling. 2014;21(8):1202-19.
149. Chan SY, Zhang YY, Hemann C, Mahoney CE, Zweier JL, Loscalzo J. MicroRNA-210 controls mitochondrial metabolism during hypoxia by repressing the iron-sulfur cluster assembly proteins ISCU1/2. Cell metabolism. 2009;10(4):273-84.
150. He M, Lu Y, Xu S, Mao L, Zhang L, Duan W, et al. MiRNA-210 modulates a nickel-induced cellular energy metabolism shift by repressing the iron-sulfur cluster assembly proteins ISCU1/2 in Neuro-2a cells. Cell death & disease. 2014;5:e1090.
151. Hu S, Huang M, Li Z, Jia F, Ghosh Z, Lijkwan MA, et al. MicroRNA-210 as a novel therapy for treatment of ischemic heart disease. Circulation. 2010;122(11 Suppl):S124-31.
152. Fasanaro P, D'Alessandra Y, Di Stefano V, Melchionna R, Romani S, Pompilio G, et al. MicroRNA-210 modulates endothelial cell response to hypoxia and inhibits the receptor tyrosine kinase ligand Ephrin-A3. The Journal of biological chemistry. 2008;283(23):15878-83.
153. Cross MJ, Claesson-Welsh L. FGF and VEGF function in angiogenesis: signalling pathways, biological responses and therapeutic inhibition. Trends in pharmacological sciences. 2001;22(4):201-7.
154. Zhuang L, Karotki AV, Bruecker P, Trueb B. Comparison of the receptor FGFRL1 from sea urchins and humans illustrates evolution of a zinc binding motif in the intracellular domain. BMC biochemistry. 2009;10:33.
155. Tsuchiya S, Fujiwara T, Sato F, Shimada Y, Tanaka E, Sakai Y, et al. MicroRNA-210 regulates cancer cell proliferation through targeting fibroblast growth factor receptor-like 1 (FGFRL1). The Journal of biological chemistry. 2011;286(1):420-8.
156. Zuo J, Wen M, Lei M, Peng X, Yang X, Liu Z. MiR-210 links hypoxia with cell proliferation regulation in human Laryngocarcinoma cancer. Journal of cellular biochemistry. 2015;116(6):1039-49.
157. Bernardi R, Guernah I, Jin D, Grisendi S, Alimonti A, Teruya-Feldstein J, et al. PML inhibits HIF-1alpha translation and neoangiogenesis through repression of mTOR. Nature. 2006;442(7104):779-85.
158. Cheng X, Liu Y, Chu H, Kao HY. Promyelocytic leukemia protein (PML) regulates endothelial cell network formation and migration in response to tumor necrosis factor alpha (TNFalpha) and interferon alpha (IFNalpha). The Journal of biological chemistry. 2012;287(28):23356-67.
159. Cheng X, Kao HY. Microarray analysis revealing common and distinct functions of promyelocytic leukemia protein (PML) and tumor necrosis factor alpha (TNFalpha) signaling in endothelial cells. BMC genomics. 2012;13:453.

160. Zhong S, Salomoni P, Pandolfi PP. The transcriptional role of PML and the nuclear body. Nature cell biology. 2000;2(5):E85-90.
161. Bernardi R, Pandolfi PP. Structure, dynamics and functions of promyelocytic leukaemia nuclear bodies. Nature reviews Molecular cell biology. 2007;8(12):1006-16.
162. Negorev D, Maul GG. Cellular proteins localized at and interacting within ND10/PML nuclear bodies/PODs suggest functions of a nuclear depot. Oncogene. 2001;20(49):7234-42.
163. Lallemand-Breitenbach V, de The H. PML nuclear bodies. Cold Spring Harbor perspectives in biology. 2010;2(5):a000661.
164. Chanakira A, Kir D, Barke RA, Santilli SM, Ramakrishnan S, Roy S. Hypoxia Differentially Regulates Arterial and Venous Smooth Muscle Cell Migration. PloS one. 2015;10(9):e0138587.
165. Tual-Chalot S, Allinson KR, Fruttiger M, Arthur HM. Whole mount immunofluorescent staining of the neonatal mouse retina to investigate angiogenesis in vivo. Journal of visualized experiments : JoVE. 2013(77):e50546.
166. Bellacen K, Lewis EC. Aortic ring assay. Journal of visualized experiments : JoVE. 2009(33).
167. Wild R, Ramakrishnan S, Sedgewick J, Griffioen AW. Quantitative assessment of angiogenesis and tumor vessel architecture by computer-assisted digital image analysis: effects of VEGF-toxin conjugate on tumor microvessel density. Microvascular research. 2000;59(3):368-76.
168. Ziche M, Morbidelli L, Choudhuri R, Zhang HT, Donnini S, Granger HJ, et al. Nitric oxide synthase lies downstream from vascular endothelial growth factor-induced but not basic fibroblast growth factor-induced angiogenesis. The Journal of clinical investigation. 1997;99(11):2625-34.
169. Yuan WC, Lee YR, Huang SF, Lin YM, Chen TY, Chung HC, et al. A Cullin3-KLHL20 Ubiquitin ligase-dependent pathway targets PML to potentiate HIF-1 signaling and prostate cancer progression. Cancer cell. 2011;20(2):214-28.
170. Boddy MN, Duprez E, Borden KL, Freemont PS. Surface residue mutations of the PML RING finger domain alter the formation of nuclear matrix-associated PML bodies. Journal of cell science. 1997;110 (Pt 18):2197-205.
171. Grant K, Grant L, Tong L, Boutell C. Depletion of intracellular zinc inhibits the ubiquitin ligase activity of viral regulatory protein ICP0 and restricts herpes simplex virus 1 replication in cell culture. Journal of virology. 2012;86(7):4029-33.
172. Ferrara N, Adamis AP. Ten years of anti-vascular endothelial growth factor therapy. Nature reviews Drug discovery. 2016;15(6):385-403.
173. Meadows KL, Hurwitz HI. Anti-VEGF therapies in the clinic. Cold Spring Harbor perspectives in medicine. 2012;2(10).
174. Choi HJ, Armaiz Pena GN, Pradeep S, Cho MS, Coleman RL, Sood AK. Anti-vascular therapies in ovarian cancer: moving beyond anti-VEGF approaches. Cancer metastasis reviews. 2015;34(1):19-40.
175. Rieckmann T, Kotevic I, Trueb B. The cell surface receptor FGFRL1 forms constitutive dimers that promote cell adhesion. Experimental cell research. 2008;314(5):1071-81.
176. Liu T, Zhao L, Chen W, Li Z, Hou H, Ding L, et al. Inactivation of von Hippel-Lindau increases ovarian cancer cell aggressiveness through the HIF1alpha/miR-210/VMP1 signaling pathway. International journal of molecular medicine. 2014;33(5):1236-42.
177. Rieckmann T, Zhuang L, Fluck CE, Trueb B. Characterization of the first FGFRL1 mutation identified in a craniosynostosis patient. Biochimica et biophysica acta. 2009;1792(2):112-21.

178. Coleman SJ, Chioni AM, Ghallab M, Anderson RK, Lemoine NR, Kocher HM, et al. Nuclear translocation of FGFR1 and FGF2 in pancreatic stellate cells facilitates pancreatic cancer cell invasion. EMBO molecular medicine. 2014;6(4):467-81.
179. Stachowiak MK, Maher PA, Stachowiak EK. Integrative nuclear signaling in cell development--a role for FGF receptor-1. DNA and cell biology. 2007;26(12):811-26.
180. Zhou L, Yao LT, Liang ZY, Zhou WX, You L, Shao QQ, et al. Nuclear translocation of fibroblast growth factor receptor 3 and its significance in pancreatic cancer. International journal of clinical and experimental pathology. 2015;8(11):14640-8.
181. Martin AJ, Grant A, Ashfield AM, Palmer CN, Baker L, Quinlan PR, et al. FGFR2 protein expression in breast cancer: nuclear localisation and correlation with patient genotype. BMC research notes. 2011;4:72.
182. Chioni AM, Grose R. FGFR1 cleavage and nuclear translocation regulates breast cancer cell behavior. The Journal of cell biology. 2012;197(6):801-17.
183. Bryant DM, Wylie FG, Stow JL. Regulation of endocytosis, nuclear translocation, and signaling of fibroblast growth factor receptor 1 by E-cadherin. Molecular biology of the cell. 2005;16(1):14-23.
184. Coleman SJ, Bruce C, Chioni AM, Kocher HM, Grose RP. The ins and outs of fibroblast growth factor receptor signalling. Clinical science. 2014;127(4):217-31.
185. Mukherjee S, Tessema M, Wandinger-Ness A. Vesicular trafficking of tyrosine kinase receptors and associated proteins in the regulation of signaling and vascular function. Circulation research. 2006;98(6):743-56.
186. Myers JM, Martins GG, Ostrowski J, Stachowiak MK. Nuclear trafficking of FGFR1: a role for the transmembrane domain. Journal of cellular biochemistry. 2003;88(6):1273-91.
187. Stachowiak MK, Fang X, Myers JM, Dunham SM, Berezney R, Maher PA, et al. Integrative nuclear FGFR1 signaling (INFS) as a part of a universal "feed-forward-and-gate" signaling module that controls cell growth and differentiation. Journal of cellular biochemistry. 2003;90(4):662-91.
188. Wang YN, Lee HH, Lee HJ, Du Y, Yamaguchi H, Hung MC. Membrane-bound trafficking regulates nuclear transport of integral epidermal growth factor receptor (EGFR) and ErbB-2. The Journal of biological chemistry. 2012;287(20):16869-79.
189. Reilly JF, Maher PA. Importin beta-mediated nuclear import of fibroblast growth factor receptor: role in cell proliferation. The Journal of cell biology. 2001;152(6):1307-12.
190. Kosugi S, Hasebe M, Tomita M, Yanagawa H. Systematic identification of cell cycle-dependent yeast nucleocytoplasmic shuttling proteins by prediction of composite motifs. Proceedings of the National Academy of Sciences of the United States of America. 2009;106(25):10171-6.
191. Brameier M, Krings A, MacCallum RM. NucPred--predicting nuclear localization of proteins. Bioinformatics. 2007;23(9):1159-60.
192. Nguyen Ba AN, Pogoutse A, Provart N, Moses AM. NLStradamus: a simple Hidden Markov Model for nuclear localization signal prediction. BMC bioinformatics. 2009;10:202.
193. Zhao Q, Xie Y, Zheng Y, Jiang S, Liu W, Mu W, et al. GPS-SUMO: a tool for the prediction of sumoylation sites and SUMO-interaction motifs. Nucleic acids research. 2014;42(Web Server issue):W325-30.
194. Beauclair G, Bridier-Nahmias A, Zagury JF, Saib A, Zamborlini A. JASSA: a comprehensive tool for prediction of SUMOylation sites and SIMs. Bioinformatics. 2015;31(21):3483-91.

195. Ivanschitz L, De The H, Le Bras M. PML, SUMOylation, and Senescence. Frontiers in oncology. 2013;3:171.
196. Aktas RG, Kayton RJ. Ultrastructural immunolocalization of basic fibroblast growth factor in endothelial cells: morphologic evidence for unconventional secretion of a novel protein. Journal of molecular histology. 2011;42(5):417-25.
197. Steringer JP, Muller HM, Nickel W. Unconventional secretion of fibroblast growth factor 2--a novel type of protein translocation across membranes? Journal of molecular biology. 2015;427(6 Pt A):1202-10.
198. Salomoni P, Pandolfi PP. The role of PML in tumor suppression. Cell. 2002;108(2):165-70.
199. Terris B, Baldin V, Dubois S, Degott C, Flejou JF, Henin D, et al. PML nuclear bodies are general targets for inflammation and cell proliferation. Cancer research. 1995;55(7):1590-7.
200. Gurrieri C, Capodieci P, Bernardi R, Scaglioni PP, Nafa K, Rush LJ, et al. Loss of the tumor suppressor PML in human cancers of multiple histologic origins. Journal of the National Cancer Institute. 2004;96(4):269-79.
201. Borden KL. Pondering the promyelocytic leukemia protein (PML) puzzle: possible functions for PML nuclear bodies. Molecular and cellular biology. 2002;22(15):5259-69.
202. Wang SC, Hung MC. Nuclear translocation of the epidermal growth factor receptor family membrane tyrosine kinase receptors. Clinical cancer research : an official journal of the American Association for Cancer Research. 2009;15(21):6484-9.
203. Trueb B, Neuhauss SC, Baertschi S, Rieckmann T, Schild C, Taeschler S. Fish possess multiple copies of fgfrl1, the gene for a novel FGF receptor. Biochimica et biophysica acta. 2005;1727(1):65-74.
204. Veinotte CJ, Dellaire G, Berman JN. Hooking the big one: the potential of zebrafish xenotransplantation to reform cancer drug screening in the genomic era. Disease models & mechanisms. 2014;7(7):745-54.
205. Ason B, Darnell DK, Wittbrodt B, Berezikov E, Kloosterman WP, Wittbrodt J, et al. Differences in vertebrate microRNA expression. Proceedings of the National Academy of Sciences of the United States of America. 2006;103(39):14385-9.
206. House SL, Castro AM, Lupu TS, Weinheimer C, Smith C, Kovacs A, et al. Endothelial fibroblast growth factor receptor signaling is required for vascular remodeling following cardiac ischemia-reperfusion injury. American journal of physiology Heart and circulatory physiology. 2016;310(5):H559-71.
207. Oladipupo SS, Smith C, Santeford A, Park C, Sene A, Wiley LA, et al. Endothelial cell FGF signaling is required for injury response but not for vascular homeostasis. Proceedings of the National Academy of Sciences of the United States of America. 2014;111(37):13379-84.
208. Mok Y, Schwierzeck V, Thomas DC, Vigorito E, Rayner TF, Jarvis LB, et al. MiR-210 is induced by Oct-2, regulates B cells, and inhibits autoantibody production. Journal of immunology. 2013;191(6):3037-48.
209. Wang H, Flach H, Onizawa M, Wei L, McManus MT, Weiss A. Negative regulation of Hif1a expression and TH17 differentiation by the hypoxia-regulated microRNA miR-210. Nature immunology. 2014;15(4):393-401.
210. King HW, Michael MZ, Gleadle JM. Hypoxic enhancement of exosome release by breast cancer cells. BMC cancer. 2012;12:421.

211. Tadokoro H, Umezu T, Ohyashiki K, Hirano T, Ohyashiki JH. Exosomes derived from hypoxic leukemia cells enhance tube formation in endothelial cells. The Journal of biological chemistry. 2013;288(48):34343-51.
212. Cui H, Seubert B, Stahl E, Dietz H, Reuning U, Moreno-Leon L, et al. Tissue inhibitor of metalloproteinases-1 induces a pro-tumourigenic increase of miR-210 in lung adenocarcinoma cells and their exosomes. Oncogene. 2015;34(28):3640-50.
213. Nieman KM, Kenny HA, Penicka CV, Ladanyi A, Buell-Gutbrod R, Zillhardt MR, et al. Adipocytes promote ovarian cancer metastasis and provide energy for rapid tumor growth. Nature medicine. 2011;17(11):1498-503.